RELAXATION AND CHAOTIC BEHAVIOR IN TIME VARYING PHENOMENA

by
Ali Cihan Keleş

Submitted to Graduate School of Natural and Applied Sciences
in Partial Fulfillment of the Requirements
for the Degree of Doctor of Philosophy in
Physics

Yeditepe University
2019

RELAXATION AND CHAOTIC BEHAVIOR IN TIME VARYING PHENOMENA
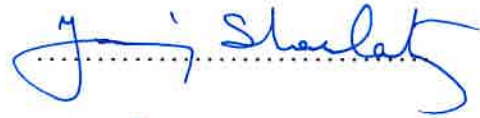
APPROVED BY:

Prof. Dr. Avadis Simon Hacınlıyan
(Thesis Supervisor)
(Yeditepe University)

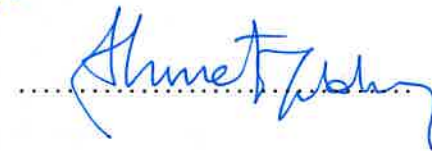Prof. Dr. Şerife İpek Karaaslan
(Yeditepe University)

Prof. Dr. Yani Skarlatos
(Boğaziçi University)

Assist. Prof. Dr. Gökhan Şahin
(Yeditepe University)

Assist. Prof. Dr. Hacı Ahmet Yıldırım
(Sakarya University)

DATE OF APPROVAL: ..../..../2019

ACKNOWLEDGEMENTS

ABSTRACT

RELAXATION AND CHAOTIC BEHAVIOR IN TIME VARYING PHENOMENA

The time evolutions of transient current data for $As_2Te_3(In)$ thin films were measured at different electric fields for the dc voltages of 0.001 V, 0.002 V, 0.005 V, 0.01 V, 0.1 V, 0.5 V and 1 V at room temperature (296 K – 23 °C) and also for the dc voltages of 0.001 V, 0.002 V, 0.005 V, 0.01 V and 0.1 V at temperatures of 313 K (40 °C), 333 K (60 °C) and 353 K (80 °C). Transient current was analyzed by means of time series analysis in order to identify different conduction regimes. The maximal Lyapunov exponents for the transient currents were calculated. Positive maximal Lyapunov exponents reflected electric field and temperature dependencies with positive Lyapunov exponents. Existence of a positive Lyapunov exponent means sensitive dependence on initial conditions and $As_2Te_3(In)$ is known to have memory effects hence different initial conditions for each dc current measurement. Detrended Fluctuation Analysis was utilized to characterize the behavior of dc current time series which is invariant to initial conditions. Detrended Fluctuation Analysis identified three different conduction regimes with multiple conduction mechanisms in terms of applied electric fields. Moreover, crossovers based on current behaviors of $As_2Te_3(In)$ thin films at two different conduction regimes were observed for different temperatures by Detrended Fluctuation Analysis method. Possible conduction mechanisms were decided and extensively discussed with respect to results of scaling exponents which depend on crossover phenomena. On the other hand, it was determined that both the artificial data as current versus time which was simulated by *Mackey-Glass equation* and the empirical data which includes current values varying with time had similar maximal Lyapunov exponents. Hence, delay differential equations such as the *Mackey-Glass equation* can be used as suitable simulation methods to analyze and predict transient current mechanism of $As_2Te_3(In)$ glass substrates at micro-scale concept. As final step, *Stretched exponential parametrization* was used for fitting the modified function of stretched exponential behavior to first 4000 data points of our empirical data sets under 0.1 V at macro-scale concept. Thereupon, it was observed that both relaxation times and stretched exponent values increase with temperature.

ÖZET

ZAMANLA DEĞİŞEN FENOMENLERDE GEVŞEME VE KAOTİK DAVRANIŞ

$As_2Te_3(In)$ ince filmler için geçici akım verilerinin zaman evrimleri, oda sıcaklığında (296 K – 23 °C); 0.001 V, 0.002 V, 0.005 V, 0.01 V, 0.1 V, 0.5 V ve 1 V olan dc gerilimlerine göre ve ayrıca 313 K (40 °C), 333 K (60 °C) ve 353 K (80 °C) değerlerindeki sıcaklıklarda; 0.001 V, 0.002 V, 0.005 V, 0.01 V ve 0.1 V olan dc gerilimlerine göre farklı elektrik alanlarında ölçülmüştür. Geçici akım, farklı iletim rejimlerini tanımlamak için zaman serileri analizi yoluyla analiz edilmiştir. Geçici akımlar için maksimal Lyapunov üstelleri hesaplanmıştır. Pozitif maksimal Lyapunov üstelleri, pozitif Lyapunov üstellerinin elektrik alanı ve sıcaklık ile olan bağımlılıklarını yansıtmıştır. Pozitif bir Lyapunov üstelinin varlığı, başlangıç koşullarına hassas bağlılık anlamına gelir ve $As_2Te_3(In)$'un her bir dc akım ölçümü için farklı başlangıç koşullarından dolayı bellek etkilerine sahip olduğu bilinmektedir. Dc akımlı zaman serilerinin davranışını karakterize etmek için başlangıç koşullarına göre değişmeyen Eğilimlerden Arındırılmış Dalgalanma Analizi kullanılmıştır. Eğilimlerden Arındırılmış Dalgalanma Analizi, uygulanan elektrik alanları açısından çoklu iletim mekanizmalarına sahip üç farklı iletim rejimi belirlemiştir. Ayrıca; $As_2Te_3(In)$ ince filmlerinin iki farklı iletim rejimindeki akım davranışlarına dayanan geçişler, Eğilimlerden Arındırılmış Dalgalanma Analizi yöntemi tarafından farklı sıcaklıklar için gözlenmiştir. Olası iletim mekanizmaları, geçiş fenomenine bağlı olan ölçeklendirme üstellerinin sonuçlarına göre kararlaştırılmış ve kapsamlı bir şekilde tartışılmıştır. Diğer yandan; *Mackey-Glass denklemi* ile simüle edilen akıma karşı zamana göre yapay verilerin ve de zamana göre değişen akım değerlerini içeren deneysel verilerin, benzer maksimal Lyapunov üstellerine sahip oldukları saptanmıştır. Dolayısıyla; *Mackey-Glass denklemi* gibi gecikmeli diferansiyel denklemler, mikro ölçekli konseptte $As_2Te_3(In)$ cam substratların geçici akım mekanizmasını analiz etmek ve tahmin etmek için uygun simülasyon yöntemleri olarak kullanılabilirler. Son adım olarak; gerilmiş üstel davranışın modifiye edilmiş fonksiyonunu, makro ölçekli konseptte 0.1 V altındaki deneysel veri setlerimizin ilk 4000 veri noktasına uyarlamak için *gerilmiş üstel parametrizasyon* kullanılmıştır. Bunun üzerine, hem gevşeme sürelerinin hem de gerilmiş üstel değerlerin sıcaklıkla birlikte arttığı görülmüştür.

TABLE OF CONTENTS

LIST OF FIGURES

LIST OF TABLES

LIST OF SYMBOLS/ABBREVIATIONS

α	Scaling exponent
α	Electron localization radius
α	Stretched exponent
β	Numerical factor (~ 1)
β	Parameter in Mackey-Glass equation
γ	Parameter in Mackey-Glass equation
δ	Width parameter
ε	Neighborhood
ε	Dielectric permitivity (dielectric constant)
η	Numerical coefficient
λ	Hopping transport pathways
λ	Lyapunov exponent
μA	Microampere
ν	Frequency
ξ	Random parameter
π	Pi constant
ρ	Charge density
σ	Conductivity
σ_∞	Bulk conductivity
τ	Parameter in Mackey-Glass equation
τ	Delay time
Φ	Interfacial barrier height
°C	Degree centigrade
A	Ampere
A	Area
A_1	Constant parameter in Stretched Exponential function
A_2	Constant parameter in Stretched Exponential function
a	Intercenter distance
$C_1(\tau)$	Linear Autocorrelation Function

cm	Centimeter
d	Embedding dimension
E	Ionization energy
E	Characteristic decay of the density of tail states
E	Energy of localized states
E_a	Activation energy
E_D	Characteristic delocalization energy
E_F	Fermi energy
eV	Electron-Volt
F	Electric field
F_0	Pre-exponential factor of electric field
$F(n)$	The average fluctuation to box size n
G	Mobility gap
g_0	Density of localized states
g_F	Density of localized states at fermi energy level (E_F)
$g(E)$	Density of tail states
h	Planck constant
I	Current
I_0	Pre-exponential factor of current
$I(t)$	Current varying time
$I(\tau)$	Average Mutual Information function
$i(s)$	The value of the current at the sth time step
j	Current density
K	Kelvin
k	Boltzmann constant
kT_{ph}	Characteristic phonon energy
L	Glass thickness
L_c	Percolation cluster correlation radius
m	Embedding dimension in stretching factor function
m	Effective mass of localized charge carrier
mA	Miliampere
N	Length of time series
n	Parameter in Mackey-Glass equation

n	Size of boxes
nm	Nanometer
$P(i(s))$	The probability of observing $i(s)$ at the time s
$P(i(s), i(s+\tau))$	Joint probability
pA	Picoampere
q	Electron charge (elementary charge)
R	Resistance
R	Inter-center distance
r_0	Radius
r_c	Order parameter
$S(\Delta n)$	Stretching factor
s	Second
$\vec{s}_{n_0}$	Constructed phase space vector
T	Temperature
t_0	Relaxation time
$U(x)$	Electron energy along x axis
V	Porential difference (Voltage – Volt)
V_c	Percolation cluster voltage
V_{max}	Maximum transport barrier
W	Polaron shift
x	Distance
x_τ	The value of the variable x at time $(t-\tau)$ in Mackey-Glass equation
$y(k)$	The integrated time series
$y_n(k)$	The y coordinate of the fitted straight-line in each box
$\vec{y}(s)$	Time dependent vector
As-Se	Arsenic Selenide
As_2Te_3	Arsenic (III) Telluride (Arsenic Tritelluride – Diarsenic Tritelluride)
CORR	Linear Autocorrelation Function
DC	Direct Current
DFA	Detrended Fluctuation Analysis
FNN	False Nearest Neighbors
$Ge_2Sb_2Te_5$	Germanium-Antimony-Telluride composition

In	Indium
Max.	Maximum
MUT	Average Mutual Information
PCM	Phase change materials
PEG-Si	Polyethylene glycol silane
PF	Poole-Frenkel
PMMA	Polymethylmethacrylate
TISEAN	Time Series Analysis

1. INTRODUCTION

Chaos and fractals are pieces of a greater subject that commonly known as *dynamics*. This subject of dynamics takes notice of change such as the systems varying in time. There may be some different behaviors of the system: it can settle down to equilibrium, it can keep repeating in cycles, or it can perform something more complicated. This is the dynamics that we use to analyze the behavior. At the present time, *Dynamics* is an interdisciplinary subject that has been essentially a branch of physics [1].

This subject just began in the mid-1600s, when Newton invented differential equations, explored his laws of motion and universal gravitation, and combined them to explain Kepler's laws of planetary motion. Especially, Newton firstly solved the two-body problem which calculates the motion of the earth around the sun, given the inverse-square law of gravitational attraction between them [1]. Latter mathematicians and physicists attempted to broaden Newton's analytical methods to the three-body problem that includes the relations of sun, earth, and moon. However this problem turned out to be much more difficult to solve. After decades, it was eventually realized that the three-body problem was essentially impossible to solve, in the sense of obtaining explicit formulas for the motions of the three bodies [1].

The breakthrough came with the work of Poincare in the late 1800s. He introduced a new point of view that emphasized *qualitative* rather than *quantitative* questions. Henri Poincare developed a powerful geometric approach to analyzing such questions. That approach has enlarged upon the modern subject of dynamics, with applications reaching beyond celestial mechanics. Henri Poincare was also the first person to take a glance at the possibility of chaos. He discovered that a deterministic system exhibits aperiodic behavior that depends *sensitively on the initial conditions*. Thus it is impossible to state long-term prediction [1]. However, chaos remained in the background in the first half of this century; instead *dynamics* was extensively concerned with nonlinear oscillators and their applications in physics and engineering. Nonlinear oscillators provided incentives to develop such technologies as radio, radar, phase-locked loops, and lasers. Nonlinear oscillators also raised the invention of new mathematical techniques-pioneers in the theoretical area including van der Pol, Andronov, Littlewood, Cartwright, Levinson, and Smale. In the meantime, Poincare's geometric methods were being extended to provide a

much deeper understanding of classical mechanics such as the work of Birkhoff and later Kolmogorov, Arnol'd, and Moser [1].

The high-speed computers were invented in the 1950s, and consequently it was a milestone in the history of *dynamics*. The computer made it possible to investigate the equations that were impossible before. Thus, it ensured development of some approaches to the nonlinear systems. Edward Lorenz [2] discovered the chaotic motion on a strange attractor in 1963 under favor of these experiments and developments. He studied a simplified model of conduction layer versus convection rolls in the atmosphere and he gained insight into the notorious unpredictability of the weather. Lorenz found that the solutions of his equations never settled down to equilibrium or to a periodic state. They continued to oscillate in an irregular, aperiodic trend. Furthermore, he realized that if he began with two slightly different initial conditions at his simulative equations, the system would behave recently totally different depending upon the results [1]. Edward Lorenz made an argument that the system had instinctively very small and unpredictable errors when the current state of the atmosphere was measured. In this case, these unpredictable errors would be enhanced swiftly, consequently leading to inconvenient forecasts. But Lorenz also showed the butterfly-shaped structure which the solutions of his equations corresponded to set of points on three dimensional plot. He argued that this set had to be *"an infinite complex of surfaces"*. But today it would be accepted as an example of an attractor with fractal properties [1].

Edward Lorenz's work had little impact until the 1970s. In 1971 David Ruelle and Floris Takens proposed a new theory for the onset of turbulence in fluids, based on abstract considerations about strange attractors. Mitchell J. Feigenbaum discovered that there are certain universal laws leading the transition from regular to chaotic behavior. This means that completely different systems can behave chaotically in the same way [1]. His work demonstrated a link between chaos and phase transitions, and influenced a generation of physicists to the study of dynamics. Finally, the new ideas about chaos were tested by experimentalists in experiments on fluids, chemical reactions, electronic circuits, mechanical oscillators, and semiconductors. Then, Benoit Mandelbrot codified and popularized fractals, produced magnificent computer graphics of them, and showed how they could be applied in a variety of subjects [1].

In pursuit of these developments, one can see that there are many practices of chaos since chaos get involved in various areas of physics. One of these studies includes the tests and applications on semiconductors. There is much attention on amorphous materials in the last few decades. They are suitable materials for fabricating devices so they have more potential of industrial applications [3]. Also, one of the reasons of this attention is the lack of understanding of many properties of these materials which differ from crystalline materials. Further, some of their properties differs from one sample to another one of the same material. An ideal crystal has an atomic arrangement that can be defined as infinite translational symmetry in all three dimensions. However, we can not assign an explicit definition for an ideal amorphous solid. Amorphous solid is usually defined as one that it does not sustain the long ranged translational symmetry, it has only short-range order [3]. But amorphous solid does not have the same precision indicated as its definition because of the lack of exact definition of long and short-range order. On the other hand, a real crystal does not have infinitely long-range translational symmetry because it has a finite size, but it does not mean that it is amorphous [3]. A crystal has surface atoms that break the translational symmetry, eventually that is the real definition of a finite size. Beside the surface atoms in amorphous materials, amorphous materials have also other structural disorders since they have individually different bond lengths, bond angles and coordination numbers at atomic sites. Although it seems that there are numerous differences between them, amorphous materials have properties similar to crystalline solids [3].

Amorphous semiconductors and amorphous insulators are used to manufacture thin film solar cells, thin film transistors and other opto-electronic devices. In addition to all of these, amorphous chalcogenides are commonly used in producing memory storage discs. There are significant differences between amorphous semiconductors and crystalline semiconductors in manufacturing these mentioned devices here, in fact the devices produced by using crystalline semiconductors are usually more efficient, stable and expensive than the devices produced by amorphous semiconductors [3].

Glasses are well known and used by mankind throughout the centuries. They are typically solids in amorphous phase. However, amorphous semiconductors started to be used in the early 1960s. But the technological innovations and theoretical developments through the instrument of crystalline materials and substances occurred earlier [3]. Consequently, these methods and experiences are applied to penetrate amorphous solids and their properties,

since the relevant theories of the crystalline structures are considerably advanced. Also these elementary techniques are more adaptive to obtain analytical results and calculations for crystalline materials but they cannot be implemented to the amorphous structures [3]. The main reason of this is that the amorphous systems have a more diffucult theoretical background. So, the numerical simulations should be used to compute more efficient results.

Chalcogenide glasses (chalcogenides) that are in the class of non-crystalline materials also have disordered structures. They have a tendency of linking their atoms together in order to form a chain of linking atoms. Amorphous chalcogenides can be prepared by combining the chalcogen elements of S, Se and Te with the elements like As, Ga, In, Si, Ge, Sn, Sb, Bi, Ag, Cd, Zn etc [4]. These combined glasses have covalent bonds that are strong in magnitude and highly directional as short range inter atomic order. On the other hand, they have weak van der Waals' forces which lead to the medium range order. Therefore, their atomic bond structures are commonly harder than the bonding structures of organic polymers but they are more flexible than the bonding structures of oxide glasses [4]. Correspondingly, their glass transition temperatures and elastic properties rank between the organic polymers and oxide glasses. Some chalcogenides include metallic elements and these type of chalcogenides are known as super ionic conductors. Otherwise, chalcogenide glasses can be treated like semiconductors and they are exactly a kind of amorphous semiconductors. H. Fritzsche [5] observed the amorphous chalcogenides that have band gap energies of 1 ± 0.3 eV. In addition, the mechanical strength and thermal stability of the chalcogenide glasses are weaker than that of oxide glasses when one compares them with each other. However, they have higher thermal expansion, greater refractive index, wider range of infrared transparency and higher order of nonlinear optical and electrical properties [4].

The electrical transport of amorphous chalcogenides has nonlinear dependencies of electric field and temperature. Depending upon these theoretical and experimental backgrounds of the amorphous materials, one can see that the relation between the *dynamics* of the amorphous chalcogenides and chaos. Deterministic dynamical systems comprise only a few variables like a dynamical system of chalcogenides. Over the past decades, it was noticed that the deterministic dynamical systems can reveal *complexity* evocative of many particle systems [6]. So, if the dynamics of the system behave chaotically, it means that a

positive Lyapunov exponent exists. The fundamental relations that describes the non-equilibrium transport in terms of microscopic chaos. Microscopic chaos contains the formulas which indicate the Lyapunov exponent coefficients of transport and dynamical entropies [6]. At this point, if we just need to clarify, dynamical entropies consist relative equations of fluctuation theorems that are nowadays extremely studied. These fluctuation theorems are known as a fundamental feature of non-equilibrium processes [6].

In addition to all of these, many scientists have realized that the evolution varying in time and space can behave like a random process. That type of evolution happens under states. They have a weak positive Lyapunov exponent. There are many systems that present zero Lyapunov exponents. Indicating zero Lyapunov exponents means that the dispersion of nearby trajectories is weaker than exponential. In this case, such dynamical systems are referred to as weakly chaotic systems [6].

Weakly chaotic systems (systems with Lyapunov exponents close to zero) and random walks driven by a mildly hyperbolic dynamic exhibit anomalous dynamics, which show characteristic properties like the non-equivalence of time and ensemble averages (metastability), the existence of Levy type probability distributions and ageing (relaxation towards equilibrium with many time scales) [7–10]. All of these phenomena were investigated in many systems such as anomalous statistics of blinking quantum dots, in anomalous diffusion of atoms in optical lattices, in plasma physics and also in cells and animal migrations [7–12]. *Detrended Fluctuation Analysis* (DFA) has been performed to the data of the experimental time series and long range correlations have been inherently observed in many complex signals [13].

Kleges [10] states that weakly chaotic systems are non-stationary due to the weak chaos by which they are generated. The main challenge is to find and identify measurable observables for weakly chaotic systems such as fluctuation relations [10]. Weak chaos has been observed in dc currents in amorphous polymer thin films (namely PMMA thin films [14], PEG-Si thin films [15], and As-Se thin films [16]). In thin films experiments, the first problem encountered was the difficulty of obtaining the same results under nearly identical conditions (challenge of finding a measurable observable): the same dc current versus voltage data were never identical, which is explained by the materials' sensitivity to thermal, mechanical, and electrical history [17–20]. In spite of the reproducibility problem, reproducible chaotic behaviour indicated by a positive Lyapunov exponent in the transient

current of polymer thin films was reported [14–16]. Moreover, fluctuation analysis (*Detrended Fluctuation Analysis*) happened to be another measurable and reproducible observable [14,15] as well as confirmatory test for agreement with observation where the transient current in thin PMMA films were simulated via "one-dimensional model of randomly pinned charge density waves" [21].

In this thesis, we investigated the dc current in amorphous $As_2Te_3(In)$ thin films. $As_2Te_3(In)$ is a chalcogenide which is known to have electrical threshold and memory switching properties via the application of an electric field, heating or radiation [22–25]. The dc conductivity of $As_2Te_3(In)$ is known to be temperature and electric field dependent and also exhibits dependence on the thickness of the thin film [26,27]. In the amorphous state, electrical transport of chalcogenides is nonlinearly dependent on the electric field and temperature as well as compositional structure [28–32]. The electric field dependence is non-ohmic [33]. Despite multitude of scientific activities (theoretical studies, experimental studies and computer simulations) on the transport properties of amorphous materials, no consensus exists on a universally agreed model or a coherent view of the problem [3,34,35]. For a review of possible transport mechanisms with conductivities, we refer the reader to [35] (where 12 different transport mechanisms are described and argued by including the conflicting experimental results which are reported as to the nature of non-ohmic and non-linear I-V characteristics). It is also possible that some of the mechanisms that are mentioned in the above reference might be competing among each other which makes the problem of identifying the relevant mechanisms much more challenging.

Moreover, the amorphous phase is in an unstable state and undergoes structural relaxation (also called resistance drift) [28]. The resistance drift causes the electrical resistance of the amorphous phase to increase with time on the scale of months at room temperature [36]. The time dependence of resistance is a common feature of amorphous materials (like PMMA thin films [14], PEG-Si thin films [15], and As-Se thin films [16]) and is result of the aging effects of the metastable amorphous state. The time dependence of transport properties causes a continuous temporal evolution.

Continuous temporal evolution dictates that one cannot replicate practically the initial conditions of complex systems. In case that the underlying mechanism(s) is (are) chaotic, every measurement is sensitively dependent on initial conditions. If this is the case; then, it is almost impossible to replicate temporal evolution of the system exactly which might

manifest itself in seemingly conflicting results and forces the researchers to rely on the logarithmic fits of the observables (hence loss of information). In the case of a chaotic mechanism, Lyapunov exponents are repeatable observables as well as the scaling exponents of *Detrended Fluctuation Analysis* (moreover DFA is invariant to initial conditions [37]).

Figure 2.1 exhibits two data sets which are measured under the same conditions at different times (under the dc voltage of 0.01 V at 296 K) which are clearly different. In experimental studies, the nonlinear properties of the materials are seen as obstacles to be avoided most of the time. In this thesis, dc currents in *As$_2$Te$_3$(In)* thin films in the non-ohmic regime are investigated to find a measurable repeatable observable and to identify the change in conduction regimes. The irregularity of conductivity in the amorphous materials force the use of a statistical observable which identifies common features between seemingly different outcomes under the same conditions. *Detrended Fluctuation Analysis* and maximal Lyapunov exponents are used to overcome this problem. The dc current was recorded for the voltages in the range of 0.001 V – 1 V at temperatures of 296 K (23 °C – room temperature) and also in the range of 0.001 V – 0.1 V at temperatures of 313 K (40 °C), 333 K (60 °C) and 353 K (80 °C). In characterizing the current, we relied on two reproducible observables: i) maximal Lyapunov exponents that are close to zero ii) *Detrended Fluctuation Analysis*.

Thesis plan is summarized in different sections and each section describes a certain part of the studies. Section 2 contains details of the applied analyses and presented observations. The data show two different time scales. These scales (delay times) were obtained by using the methods of *Autocorrelation Function* (as linear approach) and *Mutual Information* (as non-linear approach). After that, *False Nearest Neighbors* method has been used to find optimal embedding dimension for phase space reconstruction. Chaotic behavior has been seen in the transient data. This section also clarifies how to estimate *Lyapunov exponent* values and how to implement *Detrended Fluctuation Analysis* (DFA).

In section 3, the electric field dependence of current behaviors in varying time is determined to show long-range power-law correlation exponents. In section 4, the temperature dependency is examined to find correlation exponents (scaling exponents of DFA) and determine its effect to transient current behaviors of *As$_2$Te$_3$(In)* thin films. On the other hand, in section 5, the conduction mechanisms are briefly defined in terms of

their both theoretical and experimental backgrounds. Furthermore, the possible conduction mechanisms in *As₂Te₃(In)* thin films are extensively discussed in regard to the results of scaling exponents calculated by using the method of DFA.

In section 6, the *Mackey-Glass equation* has been performed to a part of an empirical dataset. However, the *Mackey-Glass equation* has been simulated as an artificial data which is generated by using a tool of MATLAB named as NAR (nonlinear autoregressive) Neural Network Analysis. The *Mackey-Glass equation* is the nonlinear time delay differential equation which is defined by Mackey and Glass [38]

$$\frac{dx}{dt} = \beta \frac{x_\tau}{1+x_\tau{}^n} - \gamma x \quad \text{where} \quad \gamma, \beta, n > 0. \tag{1.1}$$

where β, γ, τ, n are real numbers and x_τ represents the value of the variable *x* at time $(t - \tau)$. Depending on the values of the parameters, this equation displays a range of periodic and chaotic dynamics. Section 6 also contains the observations and results of the *Stretched exponential parametrization* to describe the relaxation mechanism of glassy systems when a constant electric field is applied and to see how the transient current behavior changes with different temperature ranges. Finally, the conclusions of all studies are clearly defined and summarized in section 7.

2. EXPERIMENTAL DETAILS AND ANALYSES

The samples under investigation were set up as sandwiched metal-glass-metal structures. The films were manufactured by vacuum evaporation using an Edwards Coating System, E306A. The samples were kept at 10^{-6} mbar during the thermal evaporation. Afterwards, indium (In) was evaporated onto the films to form coplanar contacts. The I-V characteristics were measured by a programmable picoammeter/voltage source (Keithley, model 4200-SCS, accuracy of the measure as $0.050\% \pm 600\,pA$) and the temperature was kept at 296 K (23 °C – room temperature), 313 K (40 °C), 333 K (60 °C) and 353 K (80 °C) via a Hart-Scientific, model 9150, Portable Furnace. First the dc current time series (gathering time varying between 0.075 s and 0.081 s) was measured for the dc voltages of 0.001 V, 0.002 V, 0.005 V, 0.01 V, 0.1 V, 0.5 V and 1 V at 296 K (23 °C – room temperature) and also for the dc voltages of 0.001 V, 0.002 V, 0.005 V, 0.01 V and 0.1 V at temperatures of 313 K (40 °C), 333 K (60 °C) and 353 K (80 °C). Figure 2.1 shows two data sets which are measured under the same conditions at different times (under the dc voltage of 0.01 V at 296 K) which are clearly different. The transient current behavior of $As_2Te_3(In)$ thin films were exemplarily shown in Figures 2.2, 2.3 and 2.4 (under the dc voltage of 0.1 V). All data sets were taken individually as cycles (4000 data for each cycle – the source has maximum limit as 4000 steps for obtaining data) which have holding times (elapsed time from one cycle to another one) that is approximately 0.05 s. The holding times were observed to be very close to the varying time scale of gathering data when the electric field was applied by the source. The existence of a positive *Lyapunov exponent* was checked to ensure the sensitive dependence on initial conditions to explain the non-repeatability in the time series. The TISEAN software package was utilized to find the maximal *Lyapunov exponent* for the time series of the current which uses the embedding theorem and phase space reconstruction [39–42]. In order to reconstruct the phase space, two parameters were found first: an appropriate delay time and an embedding dimension (any dimension that is greater than $2d + 1$ is valid where d is the "real" dimension of the system [43,44]). In this thesis, delay times were calculated by using the methods of *Linear Autocorrelation Function* and *Average Mutual Information* [45], and minimal embedding dimension was determined using the method of *False Nearest Neighbors* [46]. The maximal *Lyapunov exponent* for each time series were calculated for the reconstructed embedding space (see next subsection for a brief explanation).
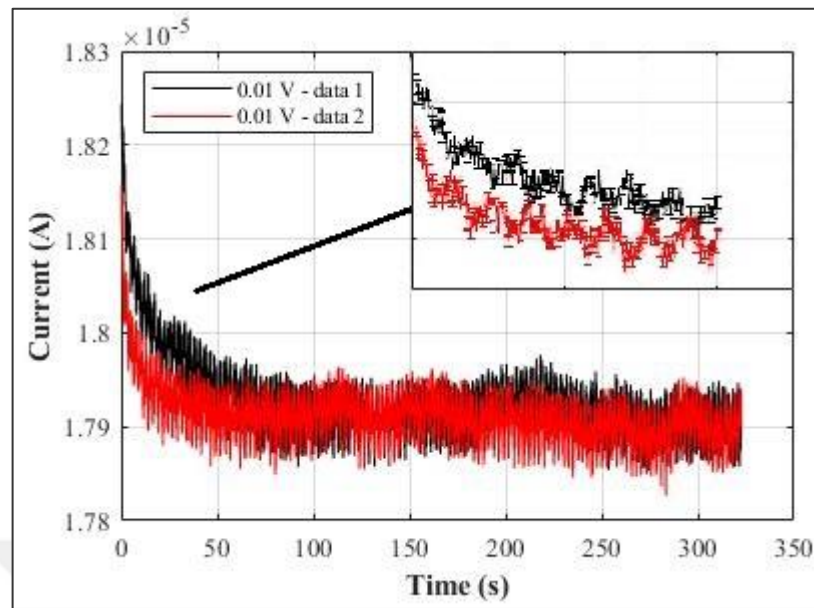
Figure 2.1. Two current vs. time graphs of the same *As₂Te₃(In)* sample at 0.01 V and 296 K measured at different times are overlaid. The inset shows the data recorded for the first 20 seconds with error bars where the accuracy is 0.050 % $\pm$ 600 pA.
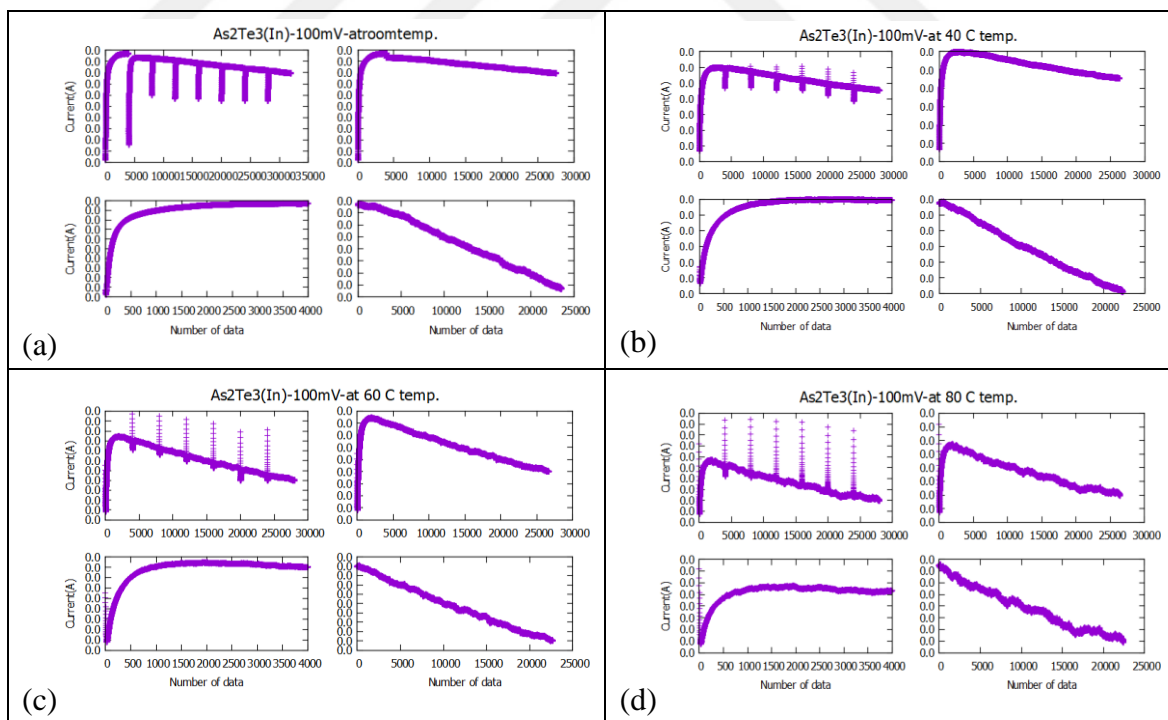
Figure 2.2. The current change in *As₂Te₃(In)* under a constant applied voltage of 0.1 V at temperatures: (a) 296 K (23 °C), (b) 313 K (40 °C), (c) 333 K (60 °C), (d) 353 K (80 °C).
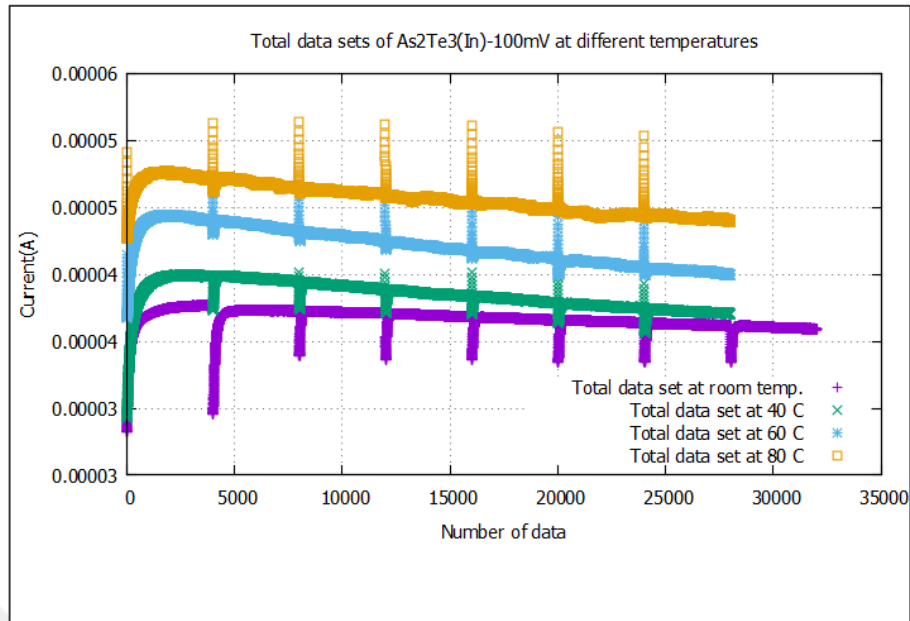
Figure 2.3. The total parts of data sets with increasing temperature under 0.1 V which have artifacts and noise.
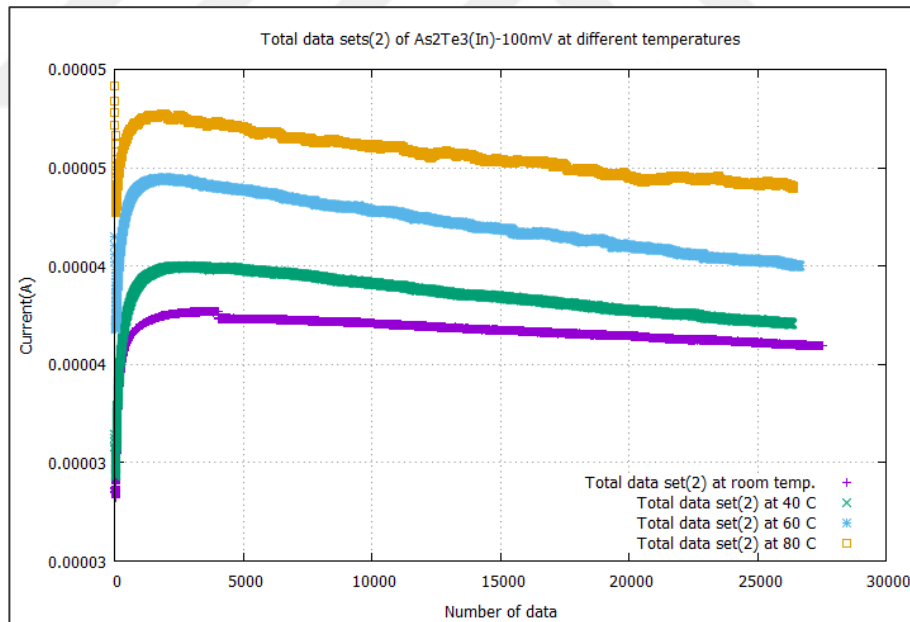
Figure 2.4. The total parts of data sets with increasing temperature under 0.1 V which are purified from artifacts.

In Figure 2.3 and Figure 2.4, the transient current behavior of *As₂Te₃(In)* thin films under the dc voltage of 0.1 V were presented for different temperatures. All data sets were taken individually as cycles which have holding times that is approximately 0.05 s. The holding times were remarked to be very close to prevent the information loss depending on the

varying time scale of gathering data points. Despite this process, artifacts and noise arised on the system and they are eliminated by using the noise reduction tool of TISEAN software package and the method of Fast Fourier Transform (see Figure 2.4). Some artifacts arising from the source were manually reduced.

The data sets were originally obtained to find a steady state value for the current at different temperatures in an experiment prepared to study mechanisms of conductivity in $As_2Te_3(In)$ thin film samples. The current was expected to settle down to a steady state value in a couple of minutes. On the other hand, during this process, it was observed that the current against time (gathering time varying between 0.075 s and 0.081 s) plots show a transient behavior characteristic of chaotic dynamical systems.

As an example, Figure 2.5 and Figure 2.6 show us how the transient current mechanism changes with temperature values under 0.1 V. The data sets were separated in two parts to present clearly variances of underlying current mechanism at different temperatures when the electric field was applied to the thin films. When the data sets were examined piece by piece, one can see that the first parts have shorter peak ranges with increasing temperature as shown in Figure 2.5. The current quickly reached the steady state point when temperature increased. On the other hand, second parts of the data sets indicate the relaxation of the current mechanism depending upon applied stable electric field and temperature. But at the second parts of the data sets as shown in Figure 2.6, one can see that the tails have wider range with respect to increasing temperature to reach the first current points at the time of applied electric field. At that point, the electron traps in thin films due to the structural defects and the impurities of their structural networks can increase depending upon relevant impacts which have transitions between the created new traps and the annihilated existing traps because of the applied DC electric field. For this reason, it can be considered that the system was impressed by the applied electric field for damping and tending of these impacts. Also, changing temperature can speed up the process of these impacts and increase transitions between the creation and the annihilation of traps.

However, the data sets of $As_2Te_3(In)$ thin films have similar behavior of the transient current data for PMMA thin films [14], PEG-Si thin films [15], and As-Se thin films [16]. Nonlinear systems based on chaos have a feature of forced damped motion. The observed signal which has non-periodicity indicates chaos. Consequently, these features prompt us

to analyze the transient current data of *As₂Te₃(In)* thin films by applying the methods of nonlinear time series analysis.
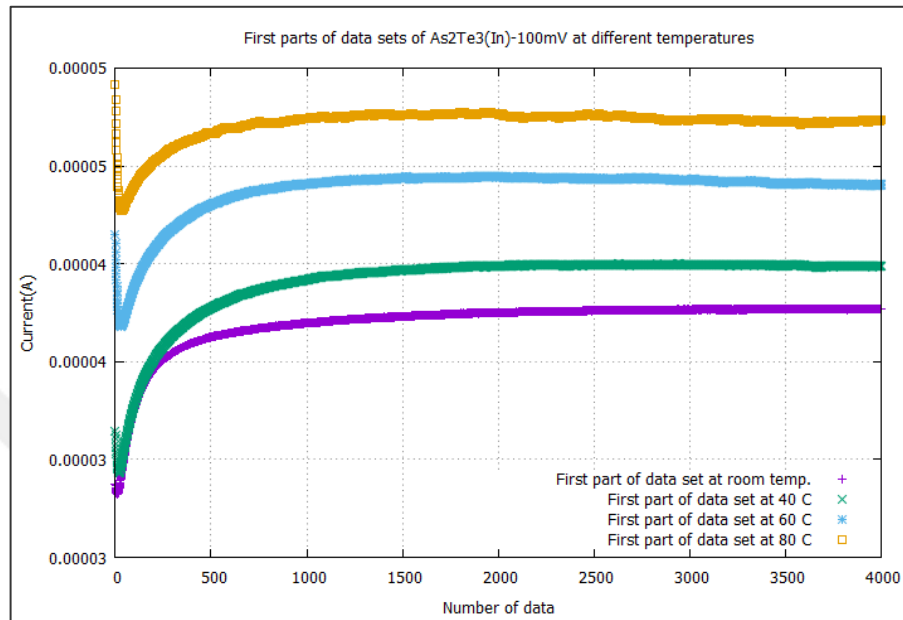
Figure 2.5. The first parts of data sets with increasing temperature under 0.1 V.
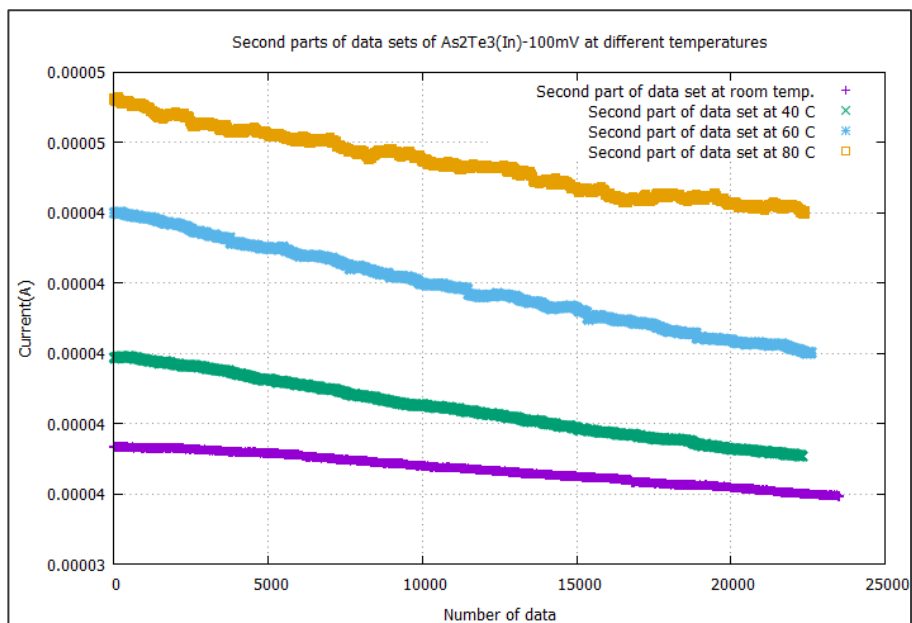
Figure 2.6. The second parts of data sets with increasing temperature under 0.1 V.

2.1. NONLINEAR TIME SERIES ANALYSIS

Time series analysis is used for analyzing the data of $As_2Te_3(In)$ using the TISEAN [39,40] software package. In order to reconstruct the phase space from scalar current measurements (denoted as $i(s)$, where $i(s)$ is the value of the current at the sth time step) we need to construct time dependent vectors, $\vec{y}(s)$ which are defined as

$$\vec{y}(s) = [i(s), i(s+\tau), ..., i(s+(d-1)\tau)] \qquad \vec{y} \in R^d \qquad (2.1)$$

where τ and d denote the delay time and the embedding dimension, respectively [43,44]. The delay time τ must be a multiple of the sampling time s of the scalar $i(s)$. The choice of delay time is subject to two constraints: i) It should not be too small (if $i(s)$ and $i(s+\tau)$ are too close to each other; then, the two observations will not be independent enough to reveal a distinguishable tangent jet [45,47]). ii) It should not be too large (hence the correlations between the two observations are not lost).

The significant values of delay time (τ) and embedding dimension (d) are obtained to generate time delay vectors. Nonetheless, these values detect the number of parameters which are corresponding to the dimensionality of the system. The delay time is found by using the methods of *Linear Autocorrelation Function (CORR)* and *Average Mutual Information (MUT)*. The linear autocorrelation function that determines the delay time which corresponds to the first zero of the function is proposed by Abarbanel [48]

$$C_1(\tau) = \frac{\frac{1}{N}\sum_{s=1}^{N}[i(s+\tau)-\bar{\imath}]\,[i(s)-\bar{\imath}]}{\frac{1}{N}\sum_{s=1}^{N}[i(s)-\bar{\imath}]} \qquad (2.2)$$

where $\bar{\imath} = \frac{1}{N}\sum_{s=1}^{N}i(s)$. The autocorrelation functions, which are the Fourier transforms of the power spectrums, are exemplarily presented in Figure 2.7 for data sets under 0.1 V at different temperatures. One can see that the autocorrelation functions, shown as graphs of $C_1(\tau)$ versus τ, have first zeros at different times. Also, these values are briefly shown in Table 2.1 for different voltages ranging from 0.001 V to 1 V at room temperature and in Table 2.2 – 2.6 for different temperatures under different voltages ranging from 0.001 V to 0.1 V.
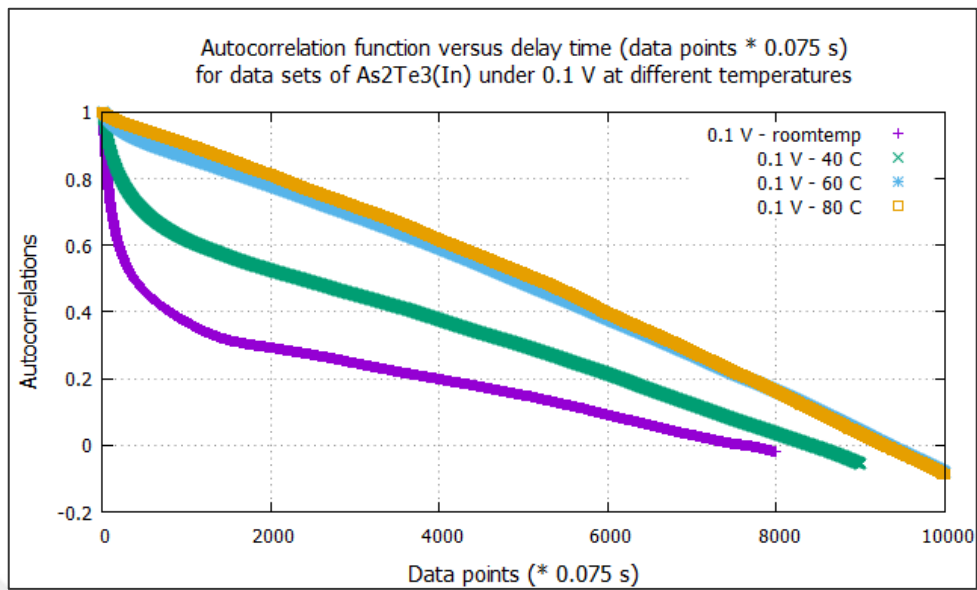
Figure 2.7. Autocorrelation function vs. delay time for data sets under 0.1 V at different temperatures of 296 K (23 °C), 313 K (40 °C), 333 K (60 °C) and 353 K (80 °C).

Table 2.1. Correlation lengths and delay times for different voltages at 296 K (23 °C – room temperature).

Voltage (V)	Temperature (°C)	Correlation Length (steps) (Data points)	Delay time (s) (Data points*sampling time)
0.001	23.0 ± 0.5	5010 steps	404 s = (5010 steps * 0.081 s)
0.002	23.0 ± 0.5	4402 steps	355 s = (4402 steps * 0.081 s)
0.005	23.0 ± 0.5	4028 steps	325 s = (4028 steps * 0.081 s)
0.01	23.0 ± 0.5	4602 steps	371 s = (4602 steps * 0.081 s)
0.1	23.0 ± 0.5	7615 steps	571 s = (7615 steps * 0.075 s)
0.5	23.0 ± 0.5	4901 steps	392 s = (4901 steps * 0.080 s)
1	23.0 ± 0.5	5133 steps	411 s = (5133 steps * 0.080 s)

Table 2.2. Correlation lengths and delay times for different temperatures under 0.001 V.

Voltage (V)	Temperature (°C)	Correlation Length (steps) (Data points)	Delay time (s) (Data points*sampling time)
0.001	23.0 ± 0.5	5010 steps	404 s = (5010 steps * 0.081 s)
0.001	40.0 ± 0.3	4028 steps	325 s = (4028 steps * 0.081 s)
0.001	60.0 ± 0.3	4618 steps	372 s = (4618 steps * 0.081 s)
0.001	80.0 ± 0.7	5849 steps	472 s = (5849 steps * 0.081 s)

Table 2.3. Correlation lengths and delay times for different temperatures under 0.002 V.

Voltage (V)	Temperature (°C)	Correlation Length (steps) (Data points)	Delay time (s) (Data points*sampling time)
0.002	23.0 ± 0.5	4402 steps	355 s = (4402 steps * 0.081 s)
0.002	40.0 ± 0.3	3388 steps	273 s = (3388 steps * 0.081 s)
0.002	60.0 ± 0.3	3893 steps	314 s = (3893 steps * 0.081 s)
0.002	80.0 ± 0.7	4066 steps	328 s = (4066 steps * 0.081 s)

Table 2.4. Correlation lengths and delay times for different temperatures under 0.005 V.

Voltage (V)	Temperature (°C)	Correlation Length (steps) (Data points)	Delay time (s) (Data points*sampling time)
0.005	23.0 ± 0.5	4028 steps	325 s = (4028 steps * 0.081 s)
0.005	40.0 ± 0.3	4927 steps	397 s = (4927 steps * 0.081 s)
0.005	60.0 ± 0.3	3402 steps	274 s = (3402 steps * 0.081 s)
0.005	80.0 ± 0.7	4161 steps	335 s = (4161 steps * 0.081 s)

Table 2.5. Correlation lengths and delay times for different temperatures under 0.01 V.

Voltage (V)	Temperature (°C)	Correlation Length (steps) (Data points)	Delay time (s) (Data points*sampling time)
0.01	23.0 ± 0.5	4602 steps	371 s = (4602 steps * 0.081 s)
0.01	40.0 ± 0.3	4423 steps	356 s = (4423 steps * 0.081 s)
0.01	60.0 ± 0.3	5215 steps	420 s = (5215 steps * 0.081 s)
0.01	80.0 ± 0.7	4400 steps	355 s = (4400 steps * 0.081 s)

Table 2.6. Correlation lengths and delay times for different temperatures under 0.1 V.

Voltage (V)	Temperature (°C)	Correlation Length (steps) (Data points)	Delay time (s) (Data points*sampling time)
0.1	23.0 ± 0.5	7615 steps	571 s = (7615 steps * 0.075 s)
0.1	40.0 ± 0.3	8413 steps	631 s = (8413 steps * 0.075 s)
0.1	60.0 ± 0.3	9325 steps	699 s = (9325 steps * 0.075 s)
0.1	80.0 ± 0.7	9283 steps	696 s = (9283 steps * 0.075 s)

Systems can involve multiple time scales. Therefore, a fundamental selection should be decided between the first zero of the autocorrelation function and the first minimum of the average mutual information to determine a meaningful delay time. One can see that the delay times which are obtained by using the autocorrelation function do not have more consistent results to be able to understand transient current behavior of $As_2Te_3(In)$ thin films and understand how the conduction mechanisms change. However, a coherent approximation needs to be clearly indicated. Just because of this reason, second method is mostly favored [49]. As narrated above, delay time has an important role for the construction of the phase space step by step. If the delay time is chosen as too small, the iterated current values will be to close to each other. Then, this causes to lose information about the system behavior. The observations will not be independent to reveal a definable tangent jet – frames will position on the diagonal line. If the delay time is chosen as too large, the correlations between the two observations will be lost.

In order to find a reasonable delay time τ, *Average Mutual Information (MUT)* is used as proposed in [39–41,47]. Once a suitable delay time is chosen, the embedding dimension is determined by using *False Nearest Neighbors (FNN)* [39–41,46]. Delay time is chosen as the first minimum of the average mutual information ($I(\tau)$) as proposed by Fraser and Swinney [47]

$$I(\tau) = I_{AB} = \sum_{a_i, b_j} P\big(i(s + \tau), i(s)\big) \log_2 \left[\frac{P(i(s), i(s+\tau))}{P(i(s+\tau))P(i(s))} \right] \qquad (2.3)$$

$P\big(i(s), i(s + \tau)\big)$ is the joint probability of measuring $i(s)$ at time s and measuring $i(s + \tau)$ at time $s + \tau$. $P(i(s))$ is the probability of observing $i(s)$ at the time s [40,45].

For the current through *As₂Te₃(In)* thin films, one of the phase space reconstruction parameters - delay time (τ) - is determined by using the *Mutual Information Analysis* (see Figure 2.8) (where the first minima is accepted as a good delay time estimate). Figure 2.9 (is exemplarily presented) shows mutual information of data sets under 0.1 V at different temperatures. Subsequently, these values – extensively presented for indicating the results of analysis – are shown in Table 2.7 for different voltages ranging from 0.001 V to 1 V at room temperature and in Table 2.8 – 2.12 for different temperatures under different voltages ranging from 0.001 V to 0.1 V.
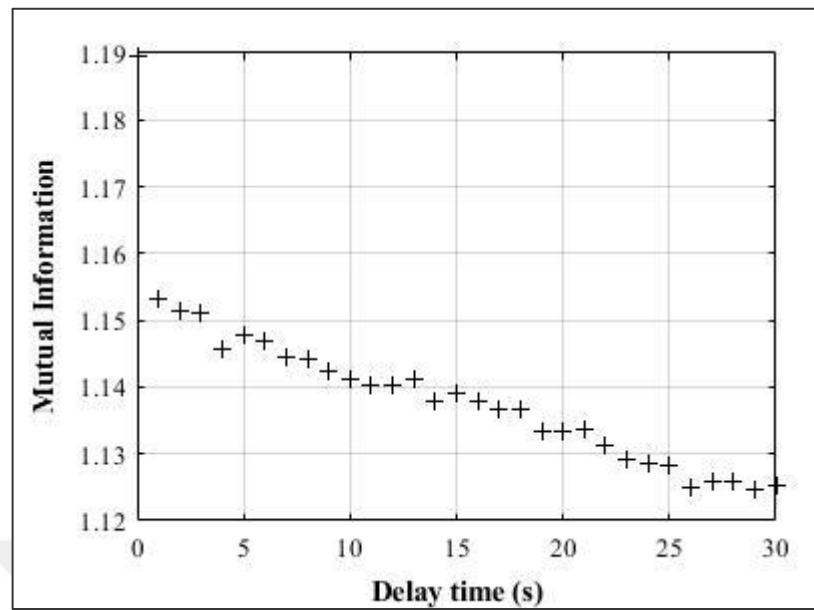
Figure 2.8. Average mutual information vs. delay time for data set under 0.1 V at room temperature.
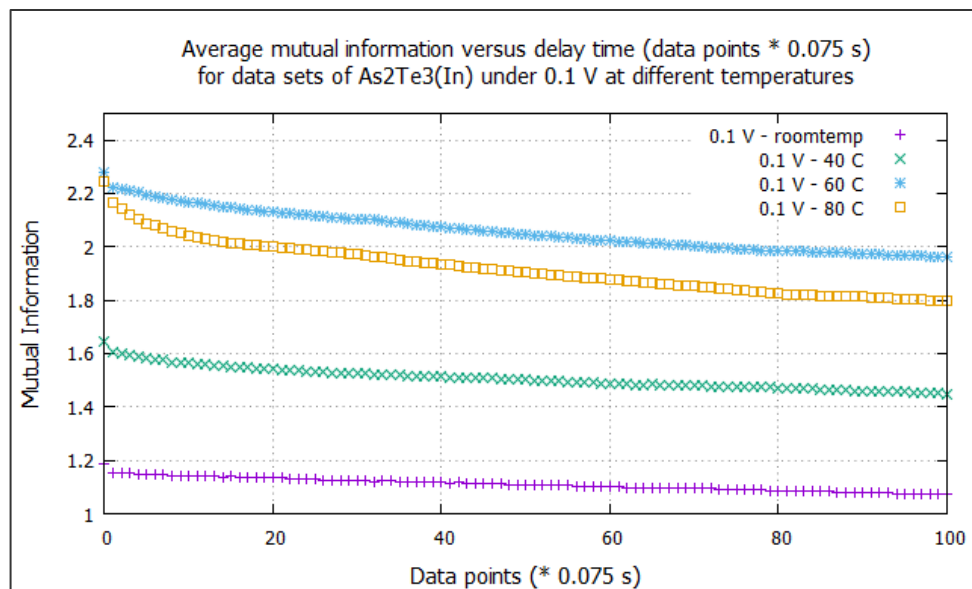
Figure 2.9. Average mutual information vs. delay time for data sets under 0.1 V at different temperatures of 296 K (23 °C), 313 K (40 °C), 333 K (60 °C) and 353 K (80 °C).

Table 2.7. Mutual information lengths and delay times for different voltages at 296 K (23 °C – room temperature).

Voltage (V)	Temperature (°C)	Mutual Information Length (steps) (Data points)	Delay time (s) (Data points*sampling time)
0.001	23.0 ± 0.5	4 steps	0.31 s = (4 steps * 0.081 s)
		10 steps	0.81 s = (10 steps * 0.081 s)
		21 steps	1.69 s = (21 steps * 0.081 s)
0.002	23.0 ± 0.5	4 steps	0.32 s = (4 steps * 0.081 s)
		13 steps	1.05 s = (13 steps * 0.081 s)
		16 steps	1.30 s = (16 steps * 0.081 s)
0.005	23.0 ± 0.5	4 steps	0.32 s = (4 steps * 0.081 s)
		13 steps	1.05 s = (13 steps * 0.081 s)
		19 steps	1.53 s = (16 steps * 0.081 s)
0.01	23.0 ± 0.5	4 steps	0.32 s = (4 steps * 0.081 s)
		13 steps	1.05 s = (13 steps * 0.081 s)
		20 steps	1.61 s = (20 steps * 0.081 s)
0.1	23.0 ± 0.5	4 steps	0.30 s = (4 steps * 0.075 s)
		14 steps	1.05 s = (14 steps * 0.075 s)
		26 steps	1.95 s = (26 steps * 0.075 s)
0.5	23.0 ± 0.5	5 steps	0.40 s = (5 steps * 0.080 s)
		16 steps	1.28 s = (16 steps * 0.080 s)
		29 steps	2.32 s = (29 steps * 0.080 s)
1	23.0 ± 0.5	5 steps	0.40 s = (5 steps * 0.080 s)
		18 steps	1.44 s = (18 steps * 0.080 s)
		29 steps	2.32 s = (29 steps * 0.080 s)

Table 2.8. Mutual information lengths and delay times for different temperatures under 0.001 V.

Voltage (V)	Temperature (°C)	Mutual Information Length (steps) (Data points)	Delay time (s) (Data points*sampling time)
0.001	23.0 ± 0.5	4 steps	0.31 s = (4 steps * 0.081 s)
		10 steps	0.81 s = (10 steps * 0.081 s)
		21 steps	1.69 s = (21 steps * 0.081 s)
0.001	40.0 ± 0.3	7 steps	0.56 s = (7 steps * 0.081 s)
		18 steps	1.45 s = (18 steps * 0.081 s)
		41 steps	3.31 s = (41 steps * 0.081 s)
0.001	60.0 ± 0.3	11 steps	0.89 s = (11 steps * 0.081 s)
		18 steps	1.45 s = (18 steps * 0.081 s)
		50 steps	4.03 s = (50 steps * 0.081 s)
0.001	80.0 ± 0.7	15 steps	1.21 s = (15 steps * 0.081 s)
		46 steps	3.71 s = (46 steps * 0.081 s)
		73 steps	5.89 s = (73 steps * 0.081 s)

Table 2.9. Mutual information lengths and delay times for different temperatures under 0.002 V.

Voltage (V)	Temperature (°C)	Mutual Information Length (steps) (Data points)	Delay time (s) (Data points*sampling time)
0.002	23.0 ± 0.5	4 steps	0.32 s = (4 steps * 0.081 s)
		13 steps	1.05 s = (13 steps * 0.081 s)
		16 steps	1.30 s = (16 steps * 0.081 s)
0.002	40.0 ± 0.3	8 steps	0.64 s = (7 steps * 0.081 s)
		19 steps	1.53 s = (18 steps * 0.081 s)
		44 steps	3.55 s = (44 steps * 0.081 s)
0.002	60.0 ± 0.3	10 steps	0.81 s = (10 steps * 0.081 s)
		15 steps	1.21 s = (15 steps * 0.081 s)
		45 steps	3.63 s = (45 steps * 0.081 s)
0.002	80.0 ± 0.7	15 steps	1.21 s = (15 steps * 0.081 s)
		46 steps	3.71 s = (46 steps * 0.081 s)
		76 steps	6.13 s = (76 steps * 0.081 s)

Table 2.10. Mutual information lengths and delay times for different temperatures under 0.005 V.

Voltage (V)	Temperature (°C)	Mutual Information Length (steps) (Data points)	Delay time (s) (Data points*sampling time)
0.005	23.0 ± 0.5	4 steps	0.32 s = (4 steps * 0.081 s)
		13 steps	1.05 s = (13 steps * 0.081 s)
		19 steps	1.53 s = (16 steps * 0.081 s)
0.005	40.0 ± 0.3	5 steps	0.40 s = (5 steps * 0.081 s)
		16 steps	1.29 s = (16 steps * 0.081 s)
		43 steps	3.47 s = (43 steps * 0.081 s)
0.005	60.0 ± 0.3	7 steps	0.56 s = (7 steps * 0.081 s)
		16 steps	1.29 s = (16 steps * 0.081 s)
		49 steps	3.95 s = (49 steps * 0.081 s)
0.005	80.0 ± 0.7	17 steps	1.37 s = (17 steps * 0.081 s)
		44 steps	3.55 s = (44 steps * 0.081 s)
		64 steps	5.16 s = (64 steps * 0.081 s)

Table 2.11. Mutual information lengths and delay times for different temperatures under 0.01 V.

Voltage (V)	Temperature (°C)	Mutual Information Length (steps) (Data points)	Delay time (s) (Data points*sampling time)
0.01	23.0 ± 0.5	4 steps	0.32 s = (4 steps * 0.081 s)
		13 steps	1.05 s = (13 steps * 0.081 s)
		20 steps	1.61 s = (20 steps * 0.081 s)
0.01	40.0 ± 0.3	7 steps	0.56 s = (7 steps * 0.081 s)
		18 steps	1.45 s = (18 steps * 0.081 s)
		48 steps	3.87 s = (48 steps * 0.081 s)
0.01	60.0 ± 0.3	14 steps	1.13 s = (14 steps * 0.081 s)
		31 steps	2.50 s = (31 steps * 0.081 s)
		48 steps	3.87 s = (48 steps * 0.081 s)
0.01	80.0 ± 0.7	15 steps	1.21 s = (15 steps * 0.081 s)
		45 steps	3.63 s = (45 steps * 0.081 s)
		77 steps	6.21 s = (77 steps * 0.081 s)

Table 2.12. Mutual information lengths and delay times for different temperatures under 0.1 V.

Voltage (V)	Temperature (°C)	Mutual Information Length (steps) (Data points)	Delay time (s) (Data points*sampling time)
0.1	23.0 ± 0.5	4 steps	0.30 s = (4 steps * 0.075 s)
		14 steps	1.05 s = (14 steps * 0.075 s)
		26 steps	1.95 s = (26 steps * 0.075 s)
0.1	40.0 ± 0.3	15 steps	1.12 s = (15 steps * 0.075 s)
		29 steps	2.17 s = (29 steps * 0.075 s)
0.1	60.0 ± 0.3	27 steps	2.02 s = (27 steps * 0.075 s)
		79 steps	5.92 s = (79 steps * 0.075 s)
0.1	80.0 ± 0.7	26 steps	1.95 s = (26 steps * 0.075 s)
		85 steps	6.37 s = (85 steps * 0.075 s)

These estimated delay times are more reliable values which include nonlinear effects than the delay time values of linear autocorrelation function. When the methods of average mutual information and linear autocorrelation function are compared, one can see that two different time scales are observed. The transient current signals leave their states when nonlinearity is considered, but they also have linear correlations. In that case, it can be expressed that system may have two different time mechanisms that progress with two different timing scales.

The other phase space reconstruction parameter – the minimal embedding dimension (see Figure 2.10) – is determined by using the method of *False Nearest Neighbors* [45,46]. The fractions of false neighbors for different temperatures are exemplarily presented against the embedding dimensions for different delay times respectively correlation lengths of autocorrelation function (in Figure 2.11 for data sets under 0.1 V at different temperatures) and mutual information lengths for average mutual information (in Figure 2.12 for data sets under 0.1 V at different temperatures).
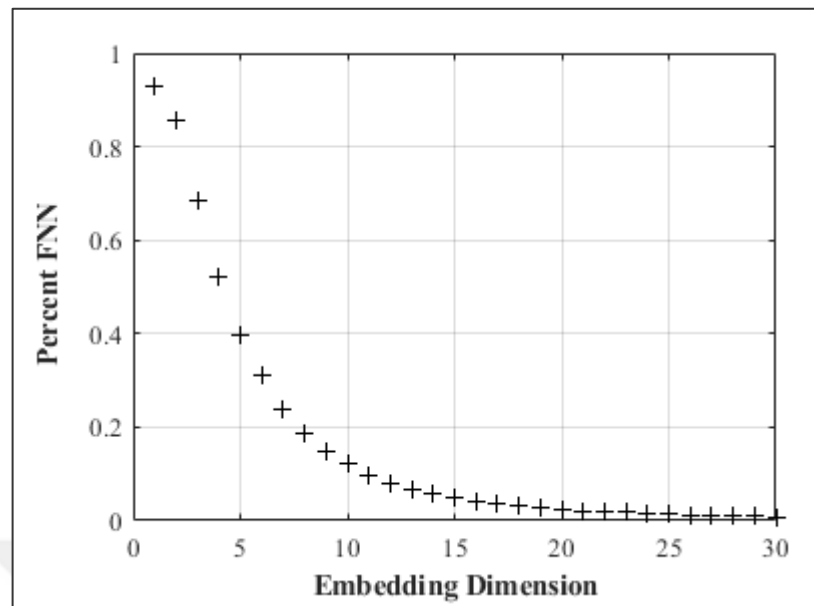
Figure 2.10. Percentage of false nearest neighbors vs. embedding dimension for data set under 0.1 V at room temperature.
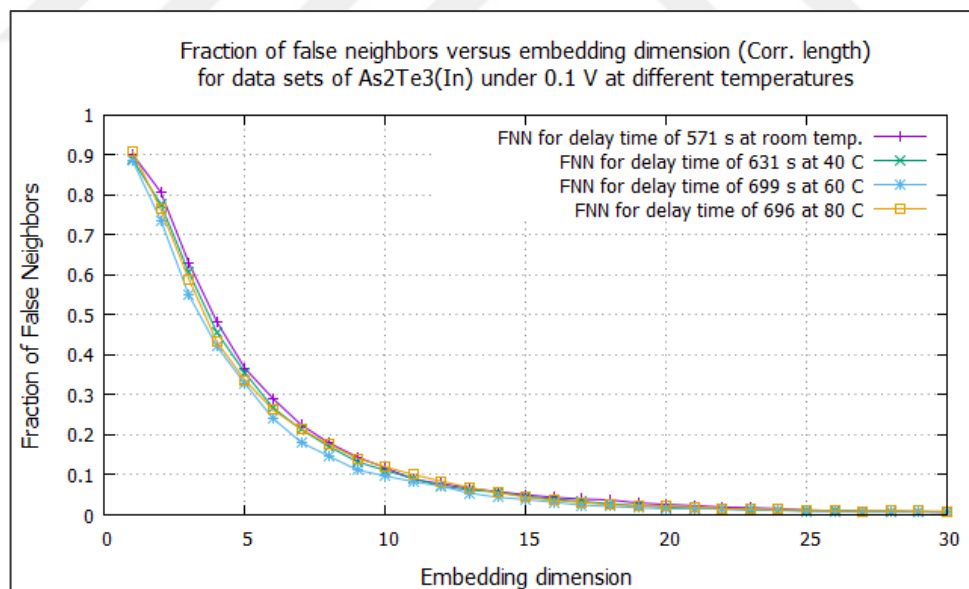
Figure 2.11. Fraction of false neighbors vs. embedding dimension for data sets under 0.1 V at different temperatures of 296 K (23 °C), 313 K (40 °C), 333 K (60 °C) and 353 K (80 °C) for different delay times with respect to correlation lengths of autocorrelation function.
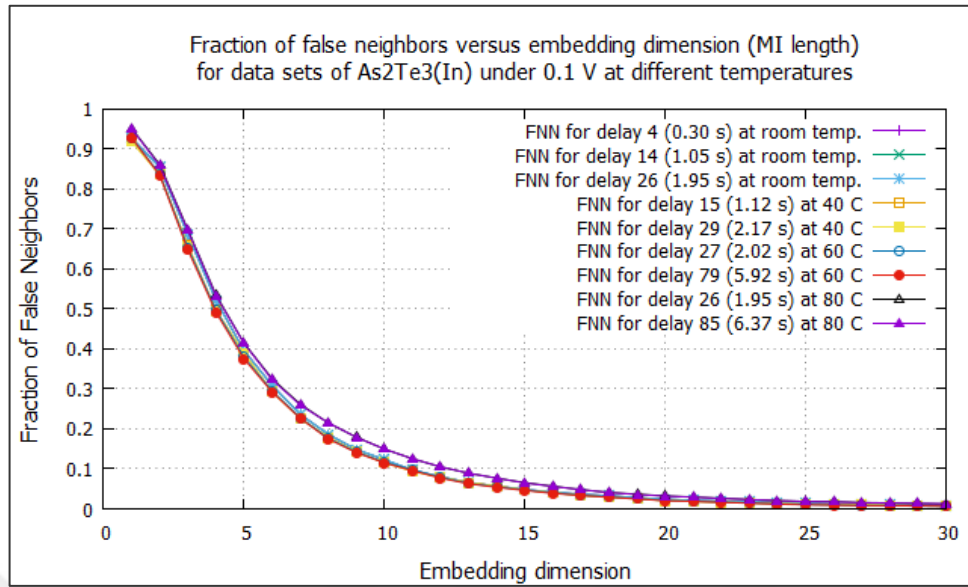
Figure 2.12. Fraction of false neighbors vs. embedding dimension for data sets under 0.1 V at different temperatures of 296 K (23 °C), 313 K (40 °C), 333 K (60 °C) and 353 K (80 °C) for different delay times with respect to mutual information lengths for average mutual information.

The ratios of false neighbors for data sets under 0.1 V at different temperatures approach to a stable point (approximately zero) after embedding dimension of thirteen (as a satisfactory value); hence an embedding dimension of thirteen is a good estimate for the minimal embedding dimension in most cases. According to the method of *False Nearest Neighbors (FNN)*, estimated values of embedding dimension are represented by scaling considerations in the Lyapunov exponent calculation. To add more, all of these methods mentioned in this section are correlatively applied to the data sets which have particular cases under conditions of changing voltages and temperatures.

2.2.   ESTIMATING LYAPUNOV EXPONENTS

The maximal Lyapunov exponents are calculated as the indicator of chaotic behavior in the data sets (Table 2.13). Many references including those which define possible ways of calculating the maximal Lyapunov exponents are given in [50–52]. In this work, the stretching factor approach was used because of its ability to minimize the effect of Gaussian noise with a reasonable computational power [53]. Stretching factor $(S(\Delta n))$ is defined as shown by Kantz [54]

$$S(\Delta n) = \frac{1}{N} \sum_{n_0}^{N} \ln \left(\frac{1}{|u_n(\vec{s_0})|} \sum_{\vec{s_n} \in u(\vec{s_{n_0}})} |\overrightarrow{s_{n_0+\Delta n}} - \overrightarrow{s_{n+\Delta n}}| \right) \tag{2.4}$$

where $\vec{s}_{n_0}$ is the constructed phase space vector in embedding space of dimension m which stands for a reference point. Then, all the neighbors within an ε neighborhood $(u_n(\overrightarrow{s_0}))$ of the reference point are found and their distances to the reference point at time Δn are calculated and averaged. The process is repeated with different embedding dimensions. If $S(\Delta n)$ shows a linear increase of identical slopes for any embedding dimension m, then the slope is accepted as an estimate of maximal Lyapunov exponent (Figure 2.13). For details see Kantz [54].
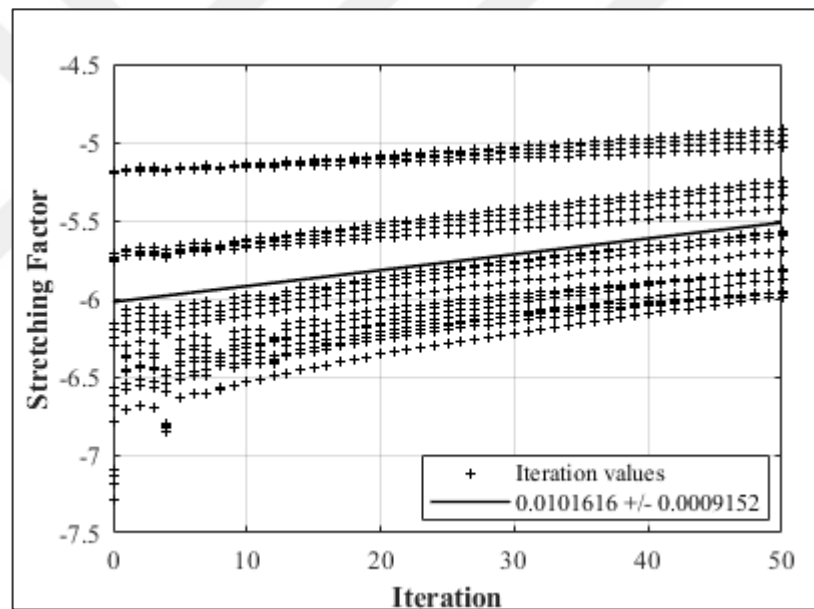
Figure 2.13. Logarithm of the stretching factor vs. iteration for data set under 0.1 V at room temperature. (The slope of line that was sketched to the curve using least squares fit corresponds to the maximum Lyapunov exponent.)

Table 2.13. Maximum Lyapunov exponent values relatively under different dc voltages (V) at 296 K (23 °C).

Voltage (V)	Temperature (°C)	Maximum Lyapunov Exponent
0.001	23.0 ± 0.5	0.00874356
0.002	23.0 ± 0.5	0.0150629
0.005	23.0 ± 0.5	0.0144451
0.01	23.0 ± 0.5	0.0137073
0.1	23.0 ± 0.5	0.0101616
0.5	23.0 ± 0.5	0.0193461
1	23.0 ± 0.5	0.0154997

Figure 2.14, 2.16, 2.18, 2.20 and 2.22 shows the Lyapunov exponents versus temperature for all embedding dimensions and delay time values relatively data sets under 0.001 V, 0.002 V, 0.005 V, 0.01 V and 0.1 V at different temperatures. All Lyapunov exponent values are shown in Table 2.14 – 2.18. Figure 2.15, 2.17, 2.19, 2.21 and 2.23 also shows how Lyapunov exponents change when temperature increases. The graphs indicate maximum Lyapunov exponents versus temperature for data sets under 0.001 V, 0,002 V, 0.005 V, 0.01 V and 0.1 V at different temperatures for mutual information delay times and correlation delay times.
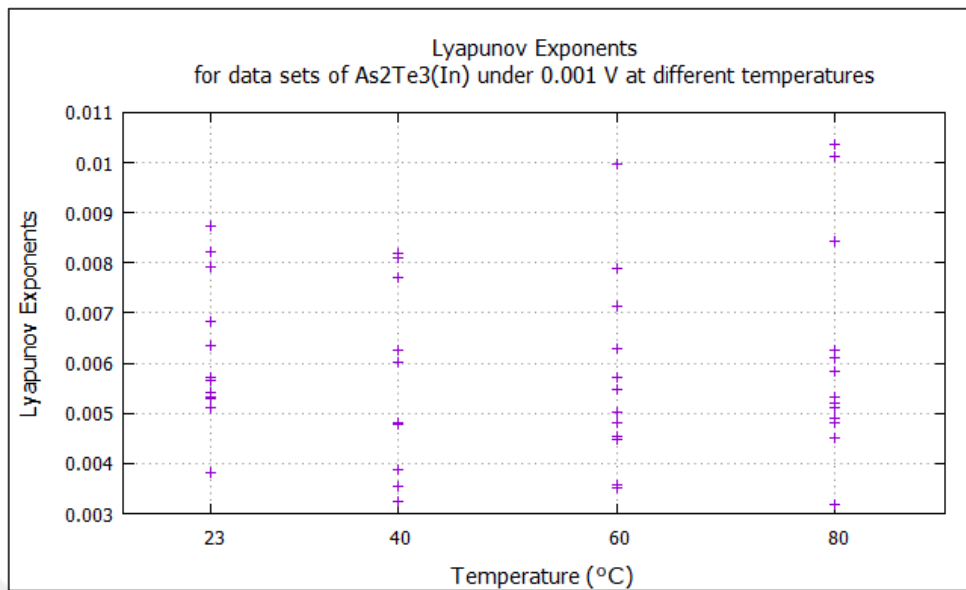
Figure 2.14. Lyapunov exponents vs. temperature for data sets under 0.001 V at different temperatures for all embedding dimensions and delay time values.

Table 2.14. Lyapunov exponents for data sets under 0.001 V.

Voltage (V)	Temperature (°C)	Maximum Lyapunov Exponent
0.001	23.0 ± 0.5	Max.(all) → 0.00874356 Max. (mut. delay) → 0.00874356 Max. (corr. delay) → 0.00633555
0.001	40.0 ± 0.3	Max. (all) → 0.00818405 Max. (mut. delay) → 0.00818405 Max. (corr. delay) → 0.00478044
0.001	60.0 ± 0.3	Max. (all) → 0.00996882 Max. (mut. delay) → 0.00996882 Max. (corr. delay) → 0.00548019
0.001	80.0 ± 0.7	Max. (all) → 0.0103663 Max. (mut. delay) → 0.0103663 Max. (corr. delay) → 0.00488809
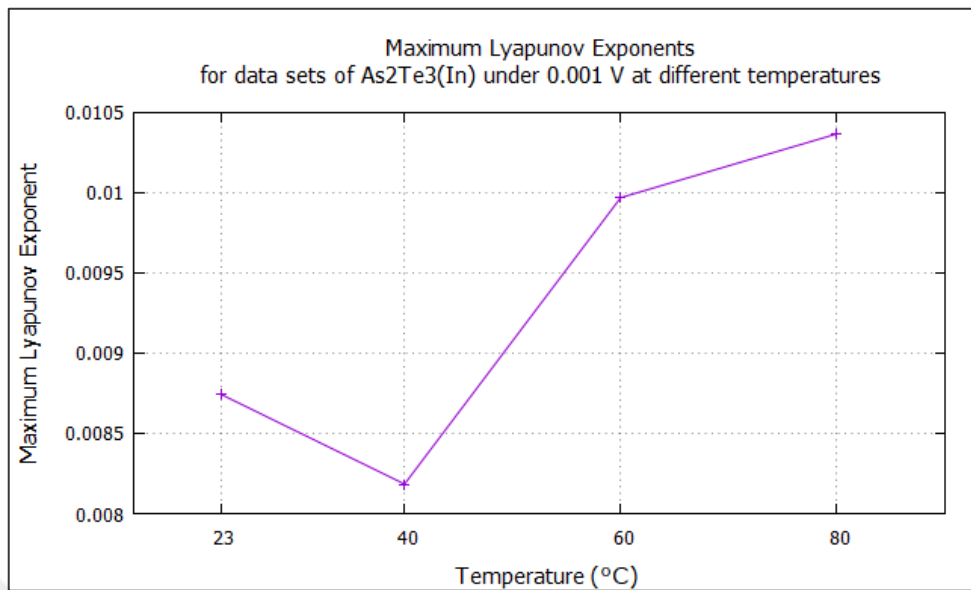
Figure 2.15. Maximum Lyapunov exponent vs. temperature for data sets under 0.001 V at different temperatures for mutual information delay times and correlation delay times.
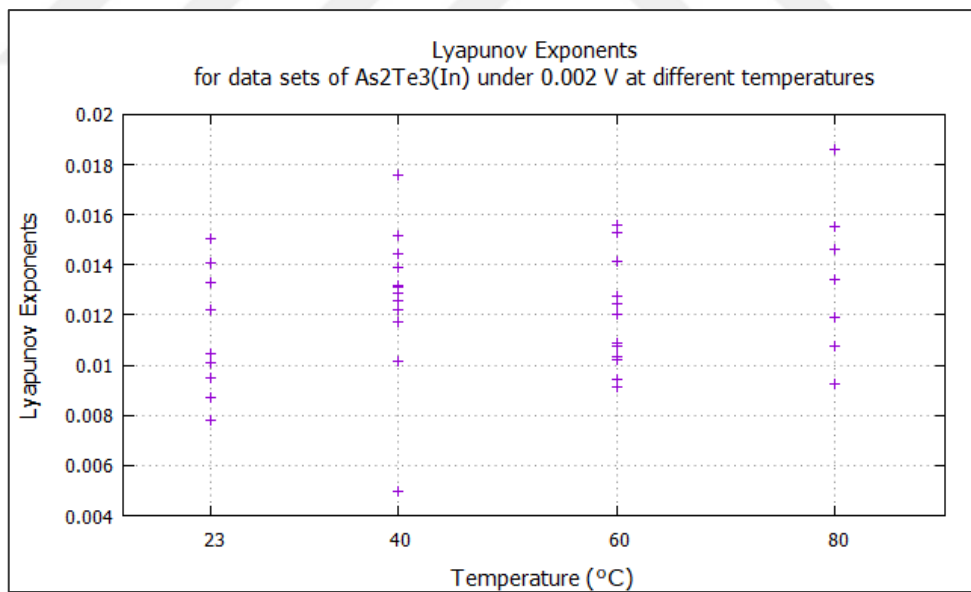
Figure 2.16. Lyapunov exponents vs. temperature for data sets under 0.002 V at different temperatures for all embedding dimensions and delay time values.

Table 2.15. Lyapunov exponents for data sets under 0.002 V.

Voltage (V)	Temperature (°C)	Maximum Lyapunov Exponent
0.002	23.0 ± 0.5	Max.(all) → 0.0150629 Max. (mut. delay) → 0.0150629 Max. (corr. delay) → 0.0122346
0.002	40.0 ± 0.3	Max. (all) → 0.0175814 Max. (mut. delay) → 0.0175814 Max. (corr. delay) → 0.0101656
0.002	60.0 ± 0.3	Max. (all) → 0.0156131 Max. (mut. delay) → 0.0156131 Max. (corr. delay) → 0.00915119
0.002	80.0 ± 0.7	Max. (all) → 0.0185919 Max. (mut. delay) → 0.0185919 Max. (corr. delay) → 0.0118765
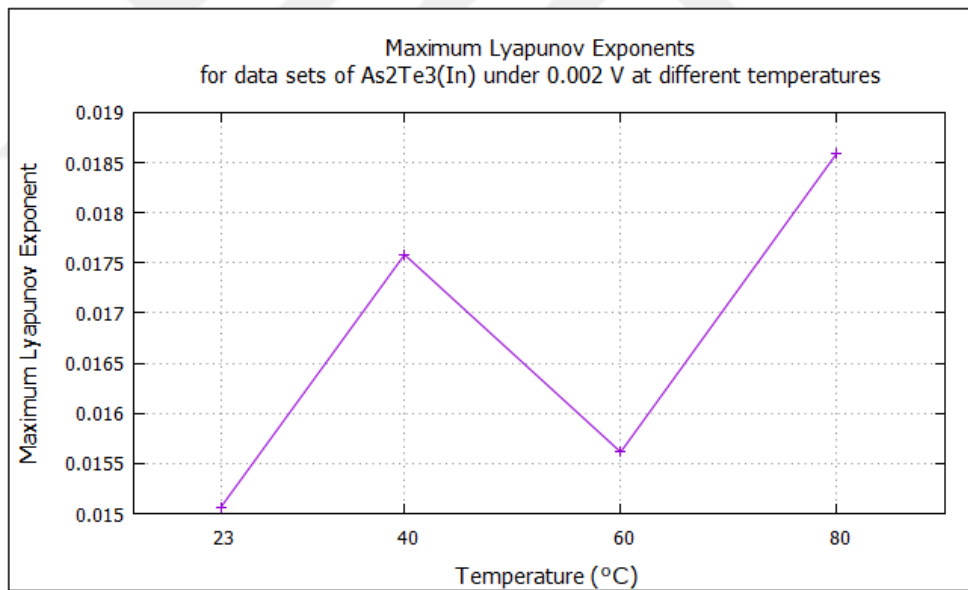
Figure 2.17. Maximum Lyapunov exponent vs. temperature for data sets under 0.002 V at different temperatures for mutual information delay times and correlation delay times.
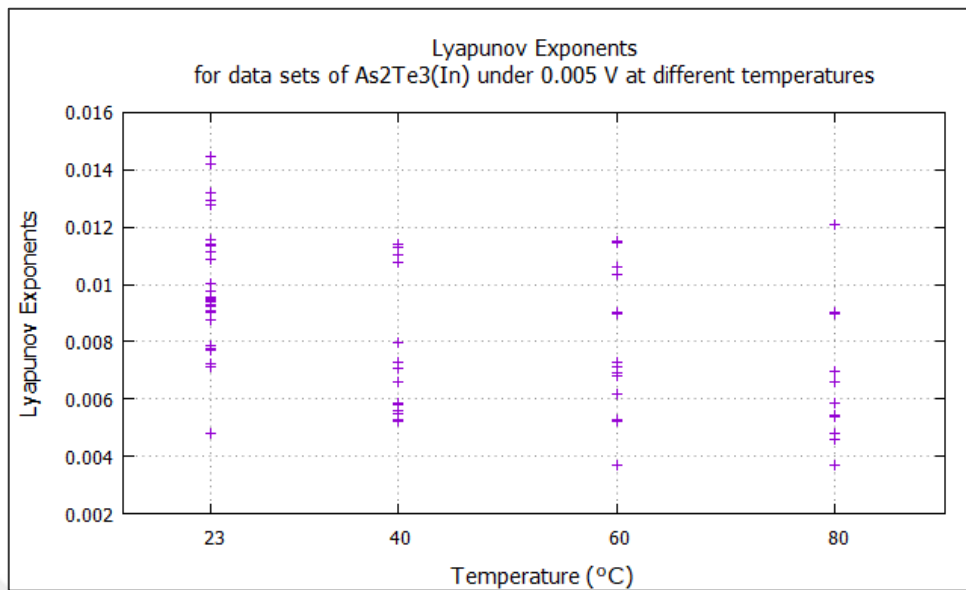
Figure 2.18. Lyapunov exponents vs. temperature for data sets under 0.005 V at different temperatures for all embedding dimensions and delay time values.

Table 2.16. Lyapunov exponents for data sets under 0.005 V.

Voltage (V)	Temperature (°C)	Maximum Lyapunov Exponent
0.005	23.0 ± 0.5	Max.(all) → 0.0144451 Max. (mut. delay) → 0.0144451 Max. (corr. delay) → 0.00776497
0.005	40.0 ± 0.3	Max. (all) → 0.0114146 Max. (mut. delay) → 0.0114146 Max. (corr. delay) → 0.00796501
0.005	60.0 ± 0.3	Max. (all) → 0.0115009 Max. (mut. delay) → 0.0115009 Max. (corr. delay) → 0.0072728
0.005	80.0 ± 0.7	Max. (all) → 0.0120878 Max. (mut. delay) → 0.0120878 Max. (corr. delay) → 0.00536763
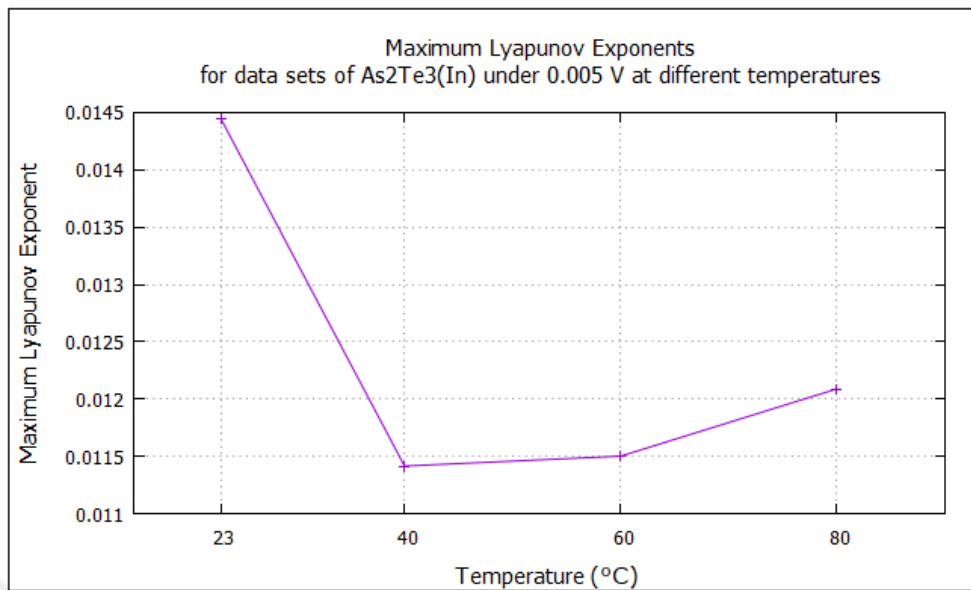
Figure 2.19. Maximum Lyapunov exponent vs. temperature for data sets under 0.005 V at different temperatures for mutual information delay times and correlation delay times.
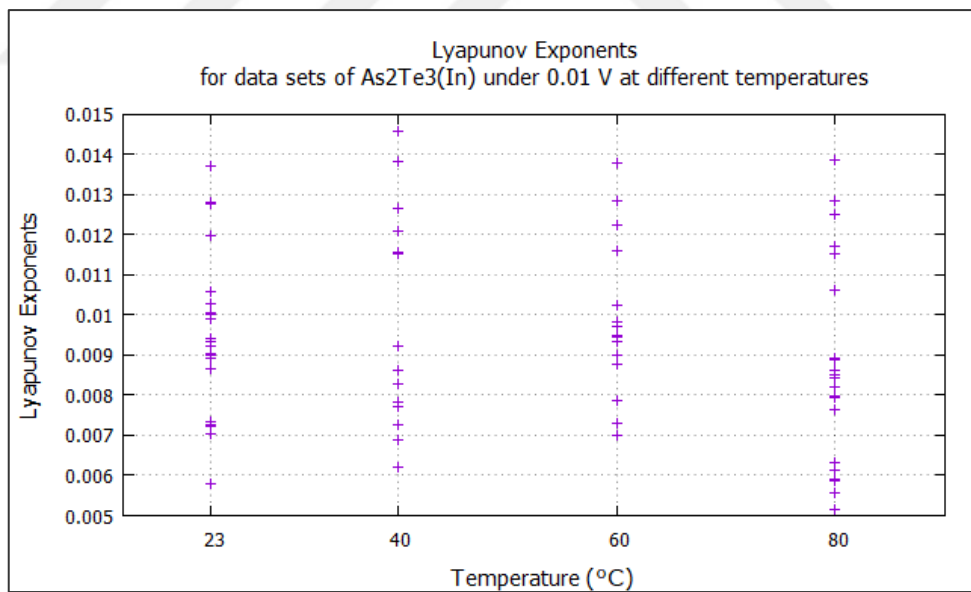
Figure 2.20. Lyapunov exponents vs. temperature for data sets under 0.01 V at different temperatures for all embedding dimensions and delay time values.

Table 2.17. Lyapunov exponents for data sets under 0.01 V.

Voltage (V)	Temperature (°C)	Maximum Lyapunov Exponent
0.01	23.0 ± 0.5	Max.(all) → 0.0137073 Max. (mut. delay) → 0.0137073 Max. (corr. delay) → 0.00991306
0.01	40.0 ± 0.3	Max. (all) → 0.0145948 Max. (mut. delay) → 0.0145948 Max. (corr. delay) → 0.00770646
0.01	60.0 ± 0.3	Max. (all) → 0.0137982 Max. (mut. delay) → 0.0137982 Max. (corr. delay) → 0.0102329
0.01	80.0 ± 0.7	Max. (all) → 0.01385 Max. (mut. delay) → 0.01385 Max. (corr. delay) → 0.00862996
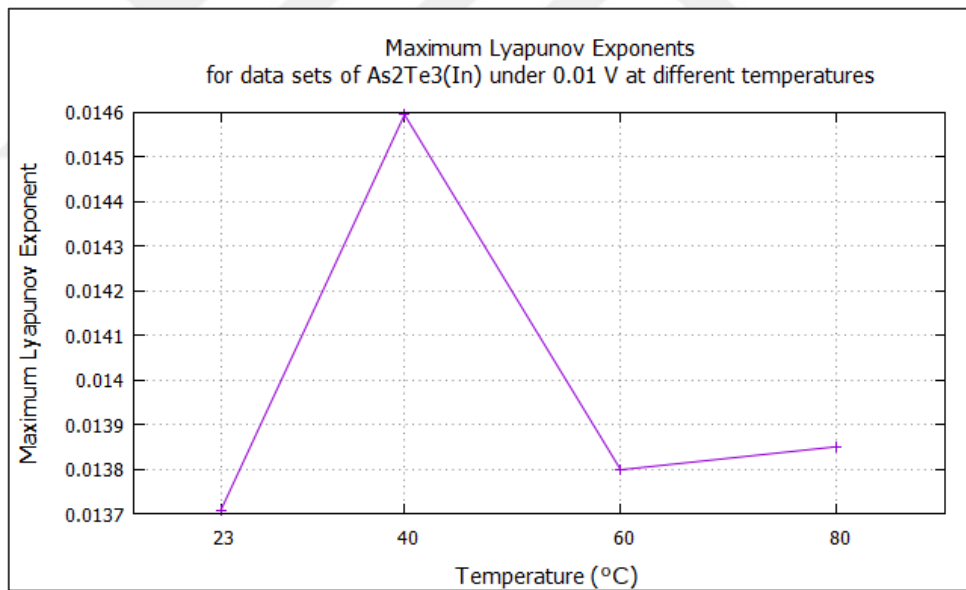
Figure 2.21. Maximum Lyapunov exponent vs. temperature for data sets under 0.01 V at different temperatures for mutual information delay times and correlation delay times.
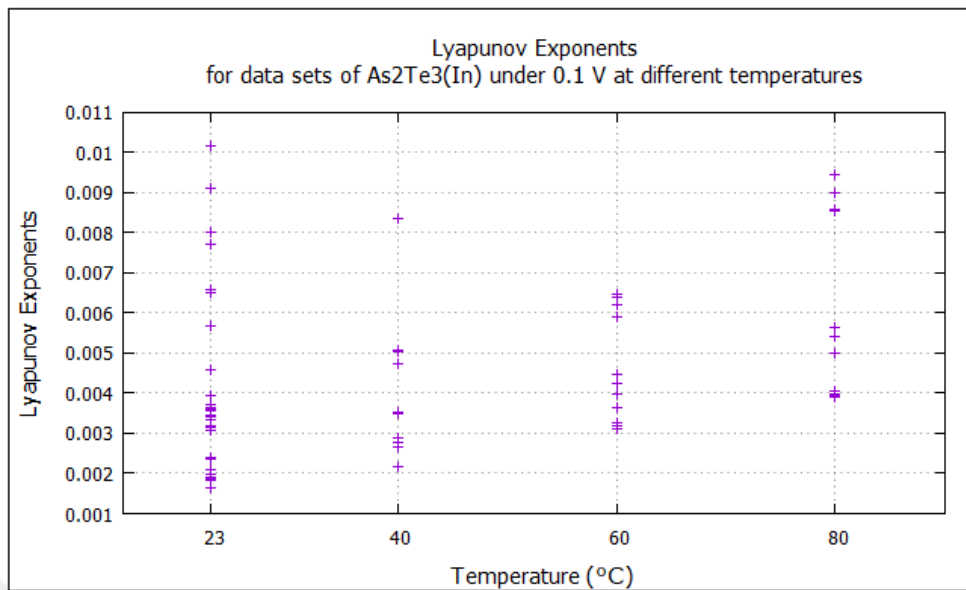
Figure 2.22. Lyapunov exponents vs. temperature for data sets under 0.1 V at different temperatures for all embedding dimensions and delay time values.

Table 2.18. Lyapunov exponents for data sets under 0.1 V.

Voltage (V)	Temperature (°C)	Maximum Lyapunov Exponent
0.1	23.0 ± 0.5	Max.(all) → 0.0101616 Max. (mut. delay) → 0.0101616 Max. (corr. delay) → 0.0036981
0.1	40.0 ± 0.3	Max. (all) → 0.00836942 Max. (mut. delay) → 0.00836942 Max. (corr. delay) → 0.00507845
0.1	60.0 ± 0.3	Max. (all) → 0.00648787 Max. (mut. delay) → 0.00622102 Max. (corr. delay) → 0.00648787
0.1	80.0 ± 0.7	Max. (all) → 0.00945466 Max. (mut. delay) → 0.00945466 Max. (corr. delay) → 0.00857255
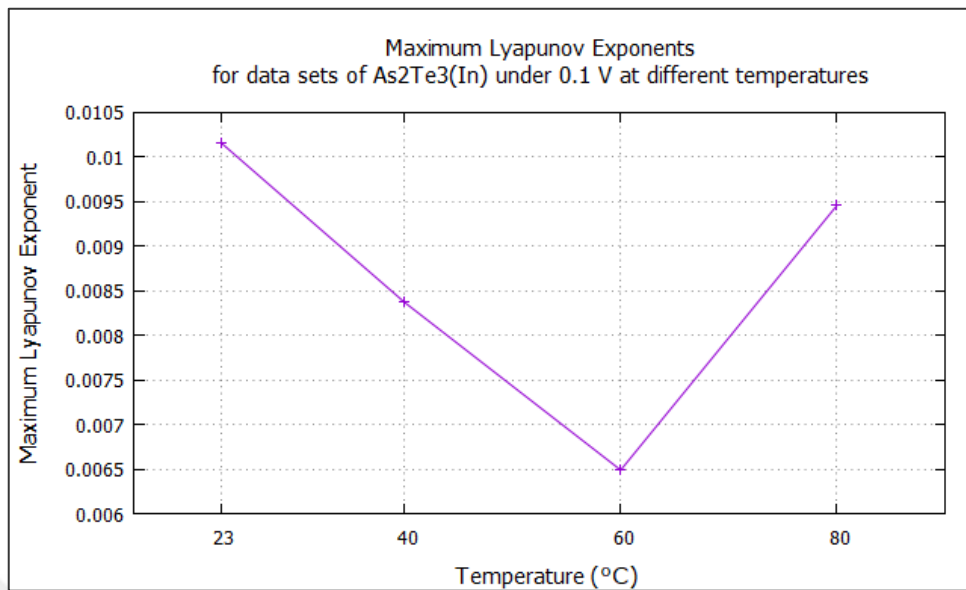
Figure 2.23. Maximum Lyapunov exponent vs. temperature for data sets under 0.1 V at different temperatures for mutual information delay times and correlation delay times.

In the literature, there is a wide amount of research on the relation between phase transitions and corresponding changes observed in the maximal Lyapunov exponent. Such a significant change in the maximal Lyapunov exponent has been observed for the phase transitions. Phase transitions in simulated atomic systems interacting with the Lenard Jones potential [55] and of couple an-harmonic oscillator systems [56] can give a point of view about this subject. For other instance of detecting the electric field and thermal dependencies of conductivity via the change in the maximal Lyapunov exponents can be seen in [15] which specifies the α and β phase transitions. Using Lyapunov exponents as an indicator of choice for a model in the conduction mechanism in polymers can be considered as another example [21].

Despite of multitude of scientific activity (theoretical, experimental studies and computer simulations) on the properties of amorphous materials, no consensus exists on a universally agreed model or a coherent view of the problem [3,34]. In most experimental studies, the nonlinear properties of the materials, such as amorphous phase change materials, amorphous thin films, polymers etc., are seen as obstacles to be avoided most of the time. These studies and investigations are usually confined to ohmic region for inspecting the underlying mechanism of current transport. In this thesis, dc current in *As₂Te₃(In)* thin

films in the non-ohmic regime are investigated to find a measurable repeatable observable. The existence of intrinsic randomness in the amorphous materials cause the irregularity of current transport. This irregular behavior prevents applying and using the statistical observations which identify customary characteristics of seemingly different resultants under same conditions. Therefore, detrended fluctuation analysis [57] is used to overcome this problem.

2.3. DETRENDED FLUCTUATION ANALYSIS

Non-equilibrium processes that are generated by weak chaos are non-stationary and become more complex in case above mentioned systems are driven by external fields (of which amorphous systems are an example with their memory like history dependence/aging with relaxation towards equilibrium and long-range correlations with more than one-time scale) [7,10]. This work utilized *Detrended Fluctuation Analysis (DFA)* as a measure since it is one of the mostly accepted methods in analyzing non-stationary time series and long-range correlations.

DFA is a method for estimating long-range power-law correlation exponents in non-stationary time series [57–59]. The algorithm is as follows: first, the time series of length N is integrated; then, the outcome is partitioned by boxes of size n. The data in each box is fitted by a least squares line. The y coordinate of the fitted straight-line in each box is denoted as $y_n(k)$. The integrated time series (denoted by $y(k)$) is detrended by subtracting $y_n(k)$. The root-mean-square fluctuation of the detrended time series [60,61] is calculated by

$$F(n) = \sqrt{\frac{1}{N}\sum_{k=1}^{N}[y(k) - y_n(k)]^2} \tag{2.5}$$

This calculation is repeated over a range of varying box sizes which relates $F(n)$ (the average fluctuation) to box size, n. A linear relation on a *log-log* plot (see Figure 2.24 for different dc voltages at 296 K (23 °C) and Figure 2.25 – 2.29 for different temperatures respectively at constant dc voltages of 0.001 V, 0.002 V, 0.005 V, 0.01 V and 0.1 V) demonstrates the closeness of power-law scaling. Under such conditions, the fluctuations can be identified by a scaling exponent, α, where $F(n) \propto n^{\alpha}$.
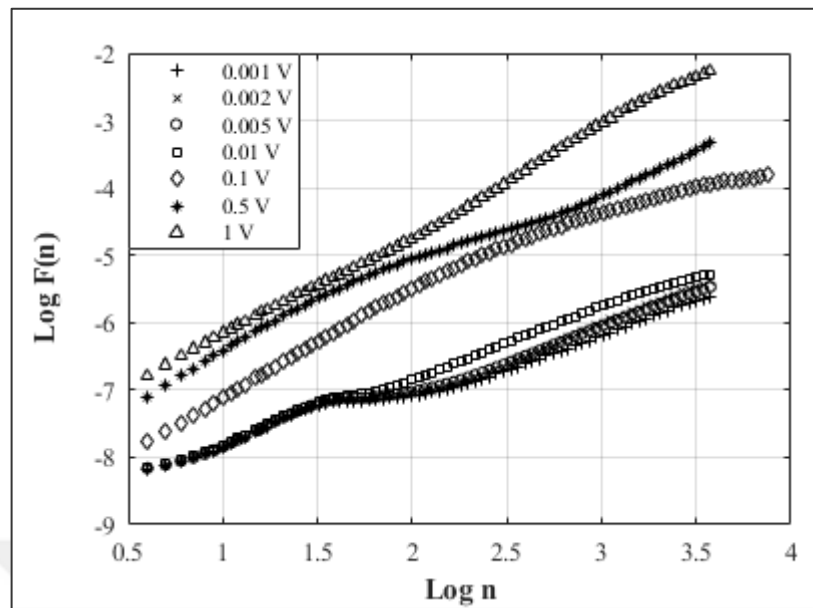
Figure 2.24. Average fluctuation vs. box size for the sample of $As_2Te_3(In)$ at different dc voltages (V) (the graph was sketched in descending order of the voltages that are respectively 1 V (at the top), 0.5 V, 0.1 V, 0.01 V, 0.005 V, 0.002 V, 0.001 V (at the bottom)) at 296 K (23 °C).
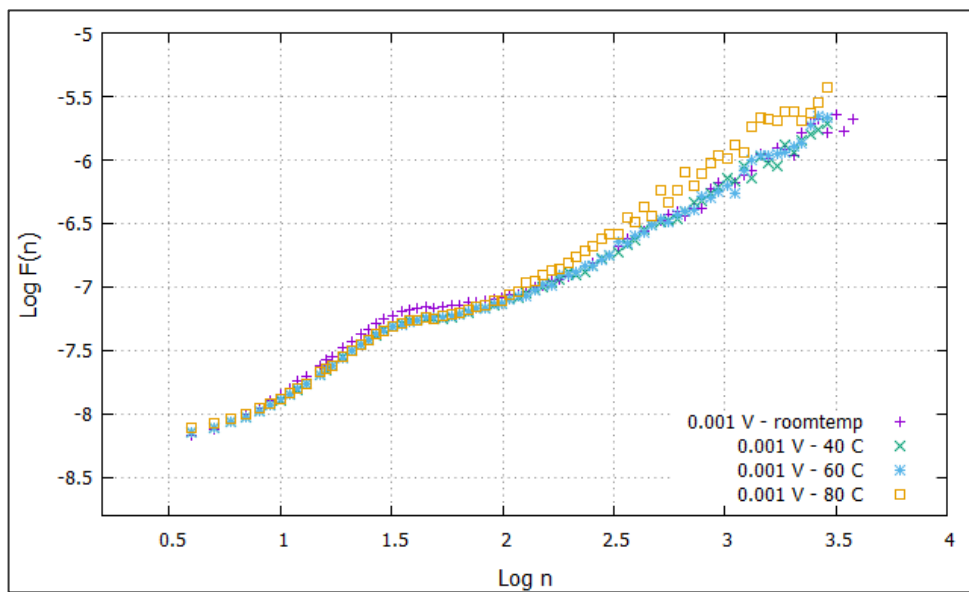
Figure 2.25. Average fluctuation vs. box size for the sample of $As_2Te_3(In)$ under dc voltage of 0.001 V at different temperatures (°C).
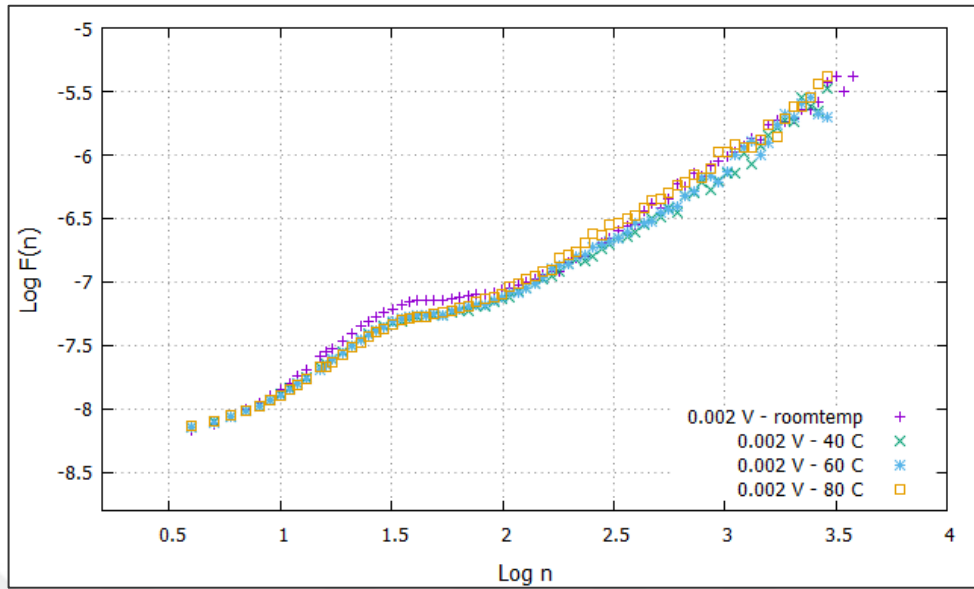
Figure 2.26. Average fluctuation vs. box size for the sample of $As_2Te_3(In)$ under dc voltage of 0.002 V at different temperatures (°C).
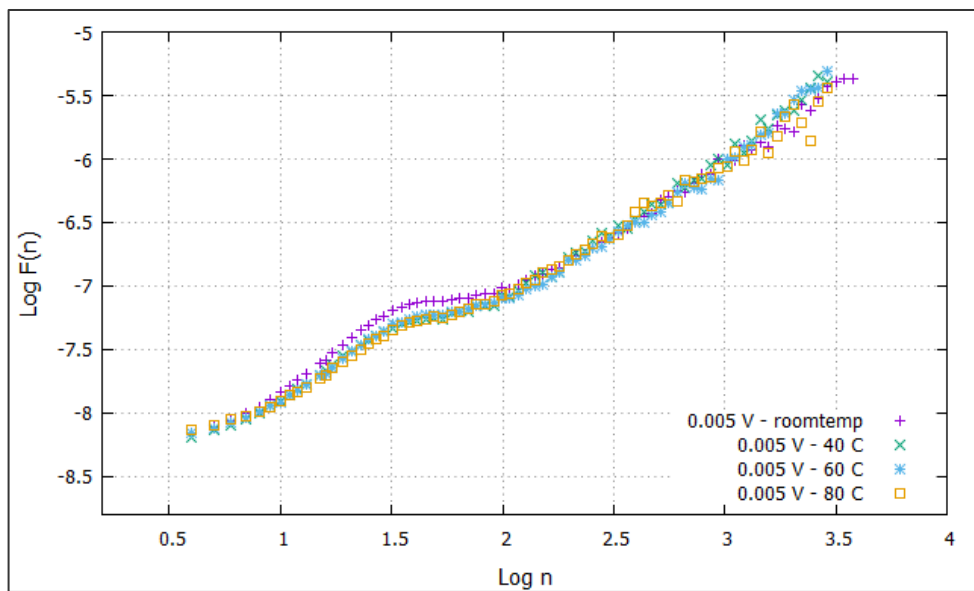
Figure 2.27. Average fluctuation vs. box size for the sample of $As_2Te_3(In)$ under dc voltage of 0.005 V at different temperatures (°C).
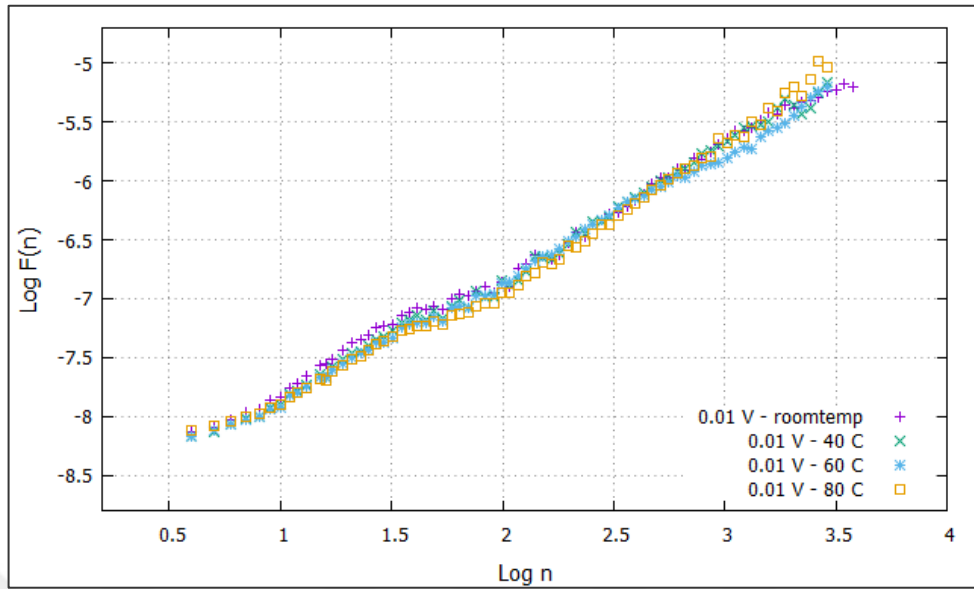
Figure 2.28. Average fluctuation vs. box size for the sample of $As_2Te_3(In)$ under dc voltage of 0.01 V at different temperatures (°C).
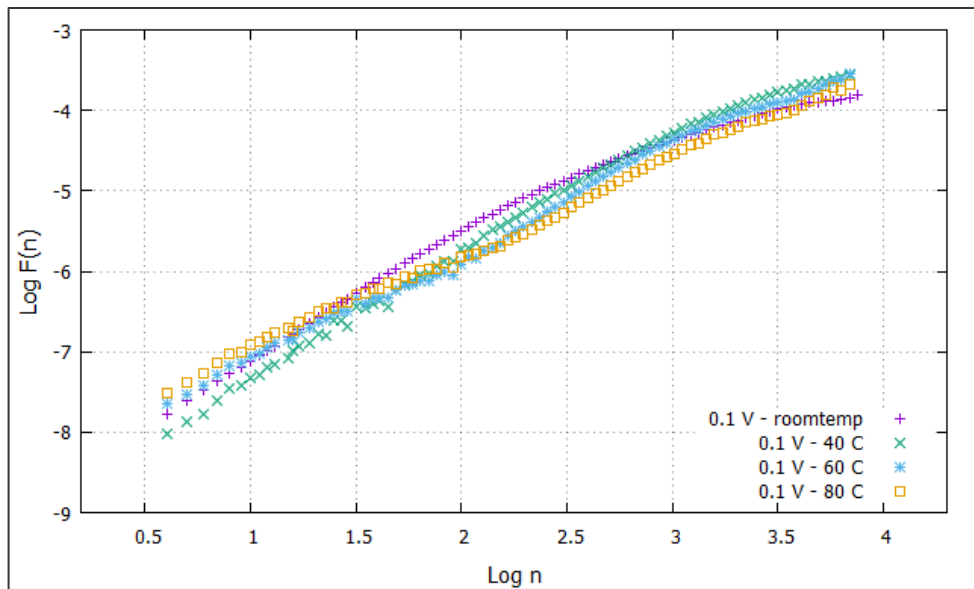
Figure 2.29. Average fluctuation vs. box size for the sample of $As_2Te_3(In)$ under dc voltage of 0.1 V at different temperatures (°C).

3. ELECTRIC FIELD DEPENDENCE OF DC CONDUCTIVITY

Even though there are generally no expected charge transport mechanisms in amorphous chalcogenides, the mostly accepted mechanisms are the Poole-Frenkel effect, Schottky emission, field induced delocalization of tail states, space charge limited current, hopping conduction, and optimum channel hopping percolation conduction [35,62]. The existence of current $(1/f)$ noise in chalcogenides as well as approximate proportionality in the dc current at low voltages and super-linearity at high voltages contrary to the equilibrium Nyquist noise [35,62–64] was reported.

Another aspect of most of the reports in the literature is that the analysis is limited to the linear regime which is not clearly defined (for the *As₂Te₃*; in [62], in the case that the voltage starts from 10 V and in [35], at 4 V).

Despite the lack of consensus on transport mechanisms of amorphous chalcogenide materials and their I-V characteristics, the conduction is divided to three major field-dependent regions (based on experimental results: i) a low field region, ii) an exponentially field-dependent region and iii) a stronger non-linear field-dependent region [35]).

Detrended Fluctuation Analysis (DFA) is chosen as the tool of investigation (combined with the existence of weak chaos represented as Lyapunov exponents near to zero) based on its ability to analyze time series related to the memory processes and $(1/f)$ noise. Otherwise, *DFA* detects transitions among different type of underlying correlations.

In Figure 2.24, root mean squared fluctuation versus calling box size is presented for dc voltages of 0.001 V, 0.002 V, 0.005 V, 0.01 V, 0.1 V, 0.5 V and 1 V on *log-log* scale. The effect of increasing voltage on the scaling properties can be summarized as follows: The scaling behavior (hence the long-range temporal correlations) of the current is separated in three regimes:

    i.   Below 0.01 V (shown in Figure E.1, E.5, E.9, E.13) where three scaling crossovers with smaller scaling exponents (α) can be observed. Three different scaling exponents indicate an interplay between three competing mechanisms. The voltage value of 0.1 V is in accordance with the low field region mentioned in [35]. The scaling exponents for each voltage value below 0.01 V is presented in Table 3.1.

ii. Between 0.1 V and up to 1 V (shown in Figure E.17, E.21) where two scaling regimes exist (in accordance with the intermediate field region mentioned in [35]). Relevant scaling exponents are listed in Table 3.2.

iii. For 1 V (shown in Figure E.22 and listed in Table 3.2) where all the crossovers are smoothened and only one scaling factor is present (in accordance with the high field region mentioned in [35]).

Table 3.1. The scaling exponents for applied voltages between 0.001 V and 0.01 V.

Voltage (V)	Temperature (°C)	α_1	α_2	α_3
0.001	23.0 ± 0.5	1.14121	0.259518	1.01244
0.002	23.0 ± 0.5	1.16478	0.280271	1.15126
0.005	23.0 ± 0.5	1.16281	0.321382	1.05897
0.01	23.0 ± 0.5	1.15915	0.524115	1.03695

Table 3.2. The scaling exponents for the applied voltages between 0.1 V and 1 V.

Voltage (V)	Temperature (°C)	α_1	α_2	α_3
0.1	23.0 ± 0.5	1.63128	0.842932	-
0.5	23.0 ± 0.5	1.49447	1.07034	-
1	23.0 ± 0.5	1.55397	-	-

In Figure 3.1, the variance of Lyapunov exponent values varying with the applied electric fields is explicitly shown. Maximum Lyapunov exponent values are presented against voltages in logaritmic scale (semi-log) in order to show briefly how the values change. On the other hand, Lyapunov exponent values indicate that the system based on the transient

current behavior of *As₂Te₃(In)* thin films is weakly chaotic. One can see that both of the transitions from low field region to intermediate field region and from intermediate field region to high field region are distinguishable in the graph. The trend of maximum Lyapunov exponent values indicates the weakly chaotic current behavior of *As₂Te₃(In)* thin films and supports the threshold switching of three distinct regimes based on the conduction mechanisms. The rising trend of the maximum Lyapunov exponents on the low field regime might be a result of the variance inflicted by strong polaron effects (polaron clouds) on the atomic level of sample. In the transition from low field region to intermediate field region (starting from 0.1 V for our sample of *As₂Te₃(In)*), the exponentially field dependence affect the chaoticity of the current behavior. Second rising trend on the intermediate field region may indicate the everchanging conduction mechanisms depending on the IV characteristics of the current transport. Moreover, in the transition from the intermediate field region to high field region (starting from 1 V for our sample of *As₂Te₃(In)*), the chaoticity of the current behavior is influenced by the stronger non-linear field dependence. Relaxation processes and phase changes on the material may also cause to alter the chaoticity of system based on the threshold switching mechanism of current behavior [28,65].
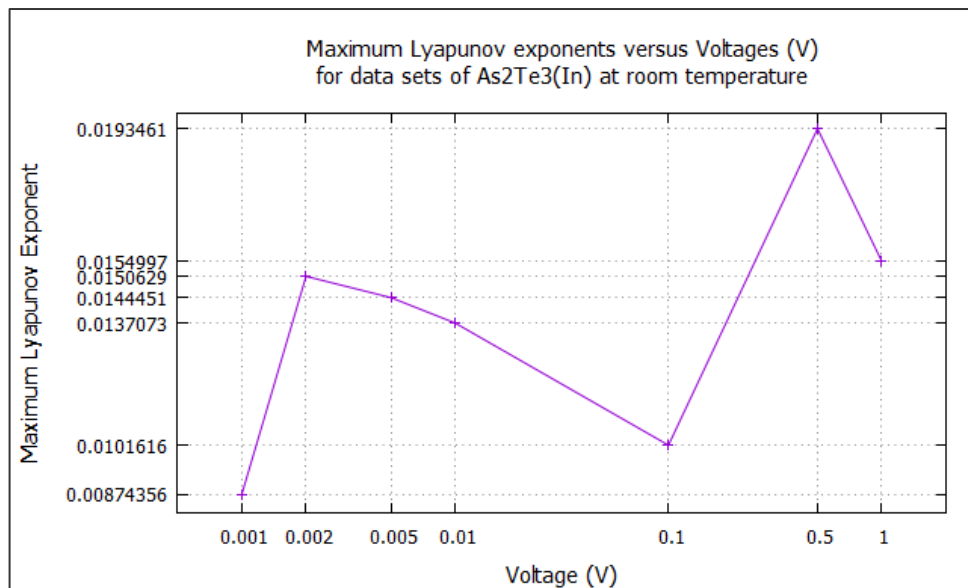
Figure 3.1. Maximum Lyapunov exponent vs. voltage for data sets under different voltages at room temperature.

4. TEMPERATURE DEPENDENCE OF DC CONDUCTIVITY

Temperature dependence has an important role in the conduction mechanisms of amorphous thin films. In [66–68], the subthreshold dc conduction in some PCM devices is researched through a temperature range of 298 K (25 °C) to 358 K (85 °C). The IV data at the applied voltages lower than 0.3 V shows an apparent exponential dependence of $lnI \propto V$ [35]. On the other hand, the relation of $lnI \propto V$ has an inverse proportion with temperature at higher voltages from 0.8 V to 1 V. The IV characteristics and temperature dependencies are also studied for amorphous films and other compositions in [69]. With inspiration of these studies, we want to reveal the underlying mechanisms of $As_2Te_3(In)$ thin films according to temperature change in low field regime and the beginning of intermediate field regime. In the direction of this aim, the transitions among different type of underlying correlations are detected by using DFA method again.

In Figure 2.25 – 2.29, root mean squared fluctuation versus calling box size is presented separately for dc voltages of 0.001 V, 0.002 V, 0.005 V, 0.01 V and 0.1 V at different temperatures of 296 K (23 °C), 313 K (40 °C), 333 K (60 °C) and 353 K (80 °C) on *log-log* scale. The effect of increasing temperatures respectively varying voltages (considered as a constant parameter) on the scaling properties can be summarized as follows: The scaling behavior (correspondingly the long-range temporal correlations) of the current at different temperatures is separated in two regimes:

i. Between 0.001 V and up to 0.01 V (shown in Figure E.1 – E.16) where three scaling crossovers with smaller scaling exponents (α) can be observed just as the scaling crossovers of inceasing voltages. Three different scaling exponents indicate an interplay between three competing mechanisms. The scaling exponents for each voltage value between 0.001 V and 0.01 V (included) is presented in Table 4.1 – 4.4 according to increasing temperatures.

ii. For 0.1 V (shown in Figure E.17 – E.20) where two scaling regimes exist. In this case, the voltage value of 0.1 V can be approximately considered as the transition from the low field region to the intermediate field region mentioned in [35]. This regime can be also referred to as the sub-threshold regime. Relevant scaling exponents are listed in Table 4.5.

Table 4.1. The scaling exponents under 0.001 V at different temperatures of 296 K (23 °C), 313 K (40 °C), 333 K (60 °C) and 353 K (80 °C).

Voltage (V)	Temperature (°C)	α_1	α_2	α_3
0.001	23.0 ± 0.5	1.14121	0.259518	1.01244
0.001	40.0 ± 0.3	1.00995	0.362418	0.997254
0.001	60.0 ± 0.3	1.01497	0.350428	1.00552
0.001	80.0 ± 0.7	0.976758	0.403503	1.14395

Table 4.2. The scaling exponents under 0.002 V at different temperatures of 296 K (23 °C), 313 K (40 °C), 333 K (60 °C) and 353 K (80 °C).

Voltage (V)	Temperature (°C)	α_1	α_2	α_3
0.002	23.0 ± 0.5	1.16478	0.280271	1.15126
0.002	40.0 ± 0.3	0.999923	0.346189	1.11798
0.002	60.0 ± 0.3	1.00411	0.346026	1.08678
0.002	80.0 ± 0.7	0.972234	0.458124	1.10784

Table 4.3. The scaling exponents under 0.005 V at different temperatures of 296 K (23 °C), 313 K (40 °C), 333 K (60 °C) and 353 K (80 °C).

Voltage (V)	Temperature (°C)	α_1	α_2	α_3
0.005	23.0 ± 0.5	1.16281	0.321382	1.05897
0.005	40.0 ± 0.3	1.03651	0.435322	1.18778
0.005	60.0 ± 0.3	1.0207	0.382609	1.22588
0.005	80.0 ± 0.7	0.939227	0.486673	1.0573

Table 4.4. The scaling exponents under 0.01 V at different temperatures of 296 K (23 °C), 313 K (40 °C), 333 K (60 °C) and 353 K (80 °C).

Voltage (V)	Temperature (°C)	α_1	α_2	α_3
0.01	23.0 ± 0.5	1.15915	0.524115	1.03695
0.01	40.0 ± 0.3	1.09065	0.682048	1.16762
0.01	60.0 ± 0.3	1.01036	0.810874	1.07399
0.01	80.0 ± 0.7	0.949668	0.60901	1.31795

Table 4.5. The scaling exponents under 0.1 V at different temperatures of 296 K (23 °C), 313 K (40 °C), 333 K (60 °C) and 353 K (80 °C).

Voltage (V)	Temperature (°C)	α_1	α_2	α_3
0.1	23.0 ± 0.5	1.63128	0.842932	-
0.1	40.0 ± 0.3	1.56633	0.865561	-
0.1	60.0 ± 0.3	1.33514	0.931157	-
0.1	80.0 ± 0.7	1.1779	0.964567	-

When the temperature dependencies of scaling behaviors are investigated, one can see that the second crossovers of scaling behaviors (represented by α_2 in Table 4.1 – 4.4) begin to get higher scaling exponents while temperature increases under applying voltages from 0.001 V to 0.01 V. Mid-crossovers begin to get lost and to be almost undistinguishable as from 0.01 V (see Figure 2.28). Between the voltage range of 0.01 V and up to 0.1 V, the scaling behaviors indicate that the transient current mechanism of *As₂Te₃(In)* thin films prominently perform and accomplish the transition that has two scaling regimes. This manner can be an indicator that of how the current mechanism change naturally from the low field region to the intermediate field region on the system.

On the other hand, only if the changing mechanism under 0.1 V (the beginning of the intermediate field region named as sub-threshold regime) is debated, one can see that the underlying mechanism has non-stationary state while temperature increases hence the persistent long-range power-law correlations are mostly gained and the current behavior almost has three regimes as like as in the low field region (see Figure 2.29).

Consequently, increasing temperature may seem to effect the current behavior at very low fields based on the ranging voltages from 0.001 V up to 0.01 V. Hence it definitely effects the transitions of conduction mechanims on the system as is known to all. The process of multi-trapping and annihilating the existing traps increases depending upon not only the applied electric field change based on the changing voltages but also the temperature change. Thermally induced and activated charges are considered to be trapped in some of the pinning states arising from the defects in the structure of the material like as impurities, dopants and dangling bonds. Some impurities may be partially diminished by increasing temperature but this creates some circumstances which cause to change the nature of conduction mechanisms. Mean free paths which charge carriers move on may be localized or delocalized at the structure based on the amorphous phase and the numbers of the free paths increase or decrease due to the changing of voltages and temperatures. Also, the local structural network defects increase or decrease with the fact of the heterogeneities and the trapping of charge carriers.

However, the Lyapunov exponent values under applied constant electric fields (are particularly represented in Figure 4.1) have temperature dependence. Lyapunov exponent values indicate that the system based on the transient current behavior of $As_2Te_3(In)$ thin films with varying temperatures is weakly chaotic. Moreover, the tendency of maximum Lyapunov exponents with varying temperature can be considered as an indicator of these structural variations and trapping behavior of charge carriers. Fluctuations of transient current may also increase depending upon the temperature change as it is well known. Hence the chaoticity of the conduction transport may increase. Because of this fact, on the basis of the maximum Lyapunov exponent values, it can be considered that the current behavior in the beginning of intermediate field region (determined as 0.1 V for our sample of $As_2Te_3(In)$) begin to get a similar conduction pattern as like as in the low field regime while temperature increases (especially at 353 K (80 °C) – see Figure 2.29).
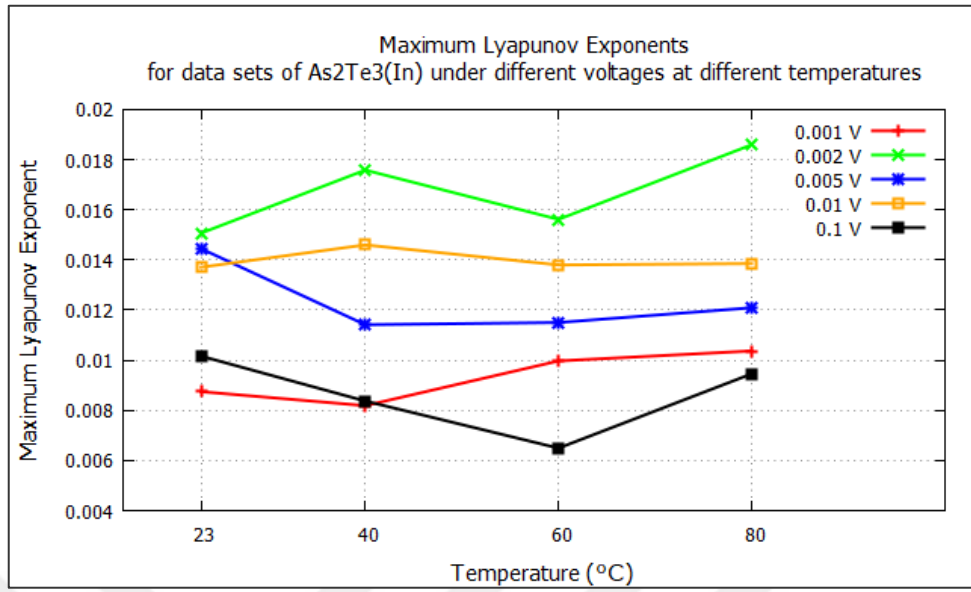
Figure 4.1. Maximum Lyapunov exponent vs. temperature for data sets under different voltages at different temperatures of 296 K (23 °C), 313 K (40 °C), 333 K (60 °C) and 353 K (80 °C) related to mutual information delay times and correlation delay times.

5. CONDUCTION MECHANISMS IN $As_2Te_3(In)$ THIN FILMS

In this section, the physical bases for different nonohmic conduction mechanisms are provided. For prominent mechanisms, analytical expressions are considered and limiting assumptions are made based upon [35].

5.1. POOLE-FRENKEL EFFECT

Originally suggested mechanism for the PF effect is decrease in the ionization energy of a single coulombic potential well in the direction of applied electric field (explaining $\ln I \propto \sqrt{V}$) or that of a pair of coulombic centers (explaining $\ln I \propto V$). As originally proposed [70], this mechanism was proposed to explain the data over non-crystalline materials [35]. The relevance of PF type dependencies to non-crystalline materials may indicate that their nature is related to disorder effects rather than individual coulomb centers [35].

For the case of two centers separated by distance $2a$ in the electric field of strength F, the electron energy along the axis is given by

$$U(x) = -\frac{q^2}{\varepsilon(a-x)} - \frac{q^2}{\varepsilon(a+x)} - Fqx \tag{5.1}$$

where q is the electron charge, ε is the dielectric permitivity, and x is distance from the midpoint between two centers. The position of the lowest barrier maximum, $dU/dx = 0$ is determined from the equation given below [35],

$$\tilde{x} = \tilde{F}(\tilde{x}^2 - 1)^2 \text{ where } \tilde{x} = \frac{x}{a}, \tilde{F} = \frac{F}{4q/a^2\varepsilon} \tag{5.2}$$

The original PF result $x = 1 + \sqrt{q/\varepsilon F}$, $\delta = \sqrt{4q^3F/\varepsilon}$ follows from Equations (5.1) and (5.2) when $\tilde{F} \gg 1$ (i.e., $F \gg q/4\varepsilon a^2$); however, it remains approximately valid numerically even at $\tilde{F} = 1$. The characteristic field is $4q/a^2\varepsilon \sim 10^5$ V/cm fort the typically assumed [66–68,71] center concentration of $\sim 10^{18}$ cm^{-3} [35].

In the opposite limiting case of *weak* fields, $F \ll 4q/\varepsilon a^2$, Equations (5.1) and (5.2) yield $x = a$ and $\delta = qFa$, corresponding to the so-called modified PF effect with [35]

$$\ln(I/I_0) = qVa/L \tag{5.3}$$

where L is the glass thickness given in [66–68].

Quantum tunneling puts limitations on the activation PF effect. The corresponding analysis by Hill [72] neglects the role of atomic vibrations on tunneling. Electron tunneling becomes most likely when electron energy is significantly above its average position, and the principal exponential term in the non-ohmic current is given by [35]

$$\ln(I/I_0) = \frac{F^2 q^2 h}{6\pi(kT^*)^2 m} \quad \text{with} \quad \frac{1}{kT^*} = \frac{1}{kT} + \frac{1}{kT_{ph}} \tag{5.4}$$

where m is the effective mass of localized charge carrier, which is taken to be close to the true electron mass [73,74], and kT_{ph} is on the order of the characteristic phonon energy ($\sim 0.01 - 0.03 \ eV$).

It was shown [75] that PF results become invalid and the effect is better described by Equation (5.4) when

$$F > F_t \equiv \sqrt{\frac{8\pi^2 mE}{h^2}} \frac{kT^*}{q} \left(\frac{kT^*}{E}\right)^{1/3} \tag{5.5}$$

where E is the ionization energy (≈ 0.4 eV in $Ge_2Sb_2Te_5$). Using the above numerical parameters, one can estimate $F_t \sim 10^5$ V/cm [35]. It is important to note that the dependence in Equation (5.4), rather than the standard PF law, experimentally confirmed for many crystalline semiconductors even for fields below 10^5 V/cm [75].

5.2. SCHOTTKY EMISSION

The Schottky effect [76] originates from the image force induced lowering of the interfacial energy for charge carrier emission when an electric field is applied. This leads to

$$\ln(I/I_0) = \frac{1}{kT}\sqrt{\frac{q^3 F}{\varepsilon}} \quad \text{with} \quad I_0 \propto exp(-\Phi/kT) \tag{5.6}$$

where Φ is the interfacial barrier height between the semiconductor and the contact metal [35]. The dependence in Equation (5.6) was experimentally verified in the range $\sim 10^4 - 10^5$ V/cm for various junctions of crystalline semiconductors with metals [35]. However, on empirical grounds, it is hard to believe that it can apply to the case under consideration because of the established $\ln I_0 \propto (-E_a/kT)$, where E_a is half of the mobility gap in the chalcogenide material and is independent of contact properties [35]. Some studies reveal that the current is independent of polarity and electrode material, which is additional evidence against Schottky mechanism [77].

5.3.   FIELD-INDUCED DELOCALIZATION OF TAIL STATES

Similar to PF mechanism of decreasing the ionization energies of the coulombic centers, the electric field can decrease energies of localized tail states in the mobility gap and even destroy them if they are shallow enough.

It was assumed that each fluctuation potential well has the same radius r_0 regardless of the energy of its localized state, thus governed only by the well depth. Correspondingly, the condition of electric field induced delocalization was given in the form $E < E_D \equiv Fqr_0$. Assuming also a simple representation of the density of tail states, $g(E) = g_0 exp(-E/E_0)$, the fiel-induced increase in concentration of charge carriers becomes $n(F) \propto g(E_D)exp(E_D/kT)$, where the first multiplier describes the decrease in the activation energy by E_D. As such, the conductivity increases with field by [35]

$$\sigma(F) = \sigma_0 exp\left[Fqr_0\left(\frac{1}{kT} - \frac{1}{E_0}\right)\right] \tag{5.7}$$

where it is assumed that $E_0 > kT$. The model could be refined by taking into account that the characteristic size of the localized state of energy E is $h/2\pi\sqrt{mE}$ and so is that of its corresponding potential well [78]. As a result, the condition of delocalization, approximately $Fq\, h/2\pi\sqrt{mE} = E$, gives the characteristic delocalization energy $E_D = \left(hqF/2\pi\sqrt{m}\right)^{2/3}$ and, similar to Equation (5.7) [35].

$$\sigma(F) = \sigma_0 exp\left[\left(\frac{hqF}{2\pi\sqrt{m}}\right)^{2/3}\left(\frac{1}{kT} - \frac{1}{E_0}\right)\right] \tag{5.8}$$

This prediction is in numerically relevant range yielding $E_D \sim 0.1\text{eV}$ when $F \sim 10^5 \text{V/cm}$. Further implementations of the theory of disordered systems [78] calls upon using the density of tail states in the form,

$$g(E) = g_0 exp\left[-\left(\frac{E}{E_0}\right)^\alpha\right] \tag{5.9}$$

where $\alpha = 1/2$ and $\alpha = 2$ for the case of uncorrelated and strongly correlated disorder corresponding, respectively to the energies $E \ll h^2/4\pi^2 mr_c^2$ and $E \gg h^2/4\pi^2 mr_c^2$. Using Equation (5.9) will modify the results in Equations (5.7) and (5.8) without changing them qualitatively [35].

Overall, it is hard to discriminate the shapes predicted by Equations (5.7) and (5.8), but it is important to note that these predictions pertain to relevant range of $E_D \sim 0.1$ eV when $F \sim 10^5$ V/cm, ensuring strong enough non-ohmicity to explain the observed effects. It is also remarkable that in contrast to PF model, this model gives an explanation of why PF type non-ohmicity is observed in glass rather than crystalline materials [35].

5.4. SPACE CHARGE LIMITED CURRENT

The exponential current-voltage characteristic can be explained by the space charge limited current in a system with almost energy independent density of states [79]. In energy space, charge carriers occupy a layer of certain width δE near the Fermi energy (E_F). Therefore, their charge density is estimated by $\rho = g(E_F)q\delta E$. The corresponding electrostatic potential is $V \approx 2\pi\rho L^2/\varepsilon$ where L is the sample thickness. Expressing from here δE through V and taking into account that the activation energy of the conduction is by δE lower than in the ohmic regime [35], one gets

$$\sigma = \sigma_0 exp\left(\frac{F}{F_0}\right) \text{ with } F_0 = \frac{2\pi gqLkT}{\varepsilon} \tag{5.10}$$

Assuming realistic $g = 10^{17} \text{cm}^{-3} \text{ eV}^{-1}$ and L = 100 nm yields a relevant field scale of the non-ohmicity $F_0 \sim 10^4$ V/cm; however that scale strongly depends on the system thickness and density of state, which can make F_0 too large and irrelevant to the observed non-ohmicity in some chalcogenide glasses [35]. The explanation of space charge limited current was put forward in [80] where F_0 linear in L was observed below room

temperature, F_0 was found to be independent of thickness [80–82], this data may suggest that space charge limited transport mechanisms play important role in thicker samples ($L > 1\mu m$) below room temperature [35].

5.5. HOPPING CONDUCTION

High density of localized states $[g_F]$ at the Fermi level (E_F) in non-crystalline semiconductors can give rise to hopping transport. The mechanism is based on electronic tunneling (*"hops"*) between localized states that are randomly distributed in real space and energy space [71,83]. In materials where hopping does occur, it dominates at low temperatures (T) and is described by the Mott law [71].

$$\sigma = \sigma_0 exp\big[-(T_0/T)^{1/4}\big], \qquad T_0 = \beta/kg_F\alpha^3 \qquad (5.11)$$

where α is the localization radius of the electron wave function, and $\beta \sim 1$ is a numerical factor. However, at room or higher T, the primary transport mechanism in bulk materials is typically band conduction [35].

Polaron effect on hopping conduction was explicitly taken into account in [84]. It was shown that in high temperature regime the exponent of conductivity contains both the well-known Mott term $(T_0/T)^{1/4}$ and polaron related term $W/2kT$ with the polaron shift W close to $G/4$. The latter combination cannot be reduced to the observed activation conductivity exponent $\approx G/2$ [35].

On the ther hand, hopping cannot provide the high current densities $j \sim 10^4$ A/cm^2 observed in the glassy state of modern PCM,

$$j \sim \frac{qv}{R^2} exp\left(-\frac{E_a}{kT}\right) \sim 5 \ \ \text{A/cm}^2 \qquad (5.12)$$

where typical frequency of attempts $v \sim 10^{13}$ s^{-1}, inter-center distance $R \sim 10$ nm, and $E_a = 0.4$ eV. For comparison, the devices of area 10^{-10} cm^2 with average current of $1 \ \mu A$ used in [66–68] corresponding to a current density of 10^4 A/cm^2, decades higher than expected for hopping from Equation (5.12) [35].

The same hopping – without – tunneling mechanism was originally proposed for ionic conduction, i.e., for heavy (atomic) classical particles that possess continuous energy

spectrum above the barrier [85,86]. For the case of light quantum particles such as electrons or holes, the spectrum is discrete and may have no quantum states between the barrier and the mobility edge [35].

5.6. OPTIMUM CHANNEL HOPPING

Similar to classical hopping conduction, optimum channel hopping involves tunneling between localized states but it differs from the classical mechanism in the following ways: (i) optimum channel hopping does not occur on the macroscopically isotropic percolation cluster but, rather, through untypical and nearly rectilinear hopping chains of spatially close localized states; (ii) it is characterized by laterally nonuniform (or pinhole) current flow; and (iii) it can dominate over typical band transport in systems that are thin enough or subject to sufficiently strong electric fields [35]. For the case of thin amorphous films, it was shown [87,88] that optimum channel hopping leads to a transverse conductivity given by

$$\sigma = \sigma_0 exp\left(-\sqrt{\frac{8L\lambda}{\alpha}}\right) \tag{5.13}$$

where L is the thickness, α is the localization radius, $\lambda \approx -\ln(g_0 kT\alpha L^2) \gg 1$, and g_0 is the density of localized states [35].

5.6.1. Optimum Channel in Thin Films

For the case of thin amorphous films subject to moderate fields $(F < E_F/qL)$, it was shown [87,88] that optimum channel hopping leads to transverse conductivity given by

$$\sigma = \sigma_0 exp\left(-\sqrt{\frac{8L\lambda}{\alpha}} + 1.6\sqrt{\frac{qFL}{kT}}\right) \tag{5.14}$$

where the parameters are the same as in Equation (5.13) [35]. Polaron effects are neglected in Equation (5.14) and, therefore, in chalcogenide glasses this form of hopping conduction can not rely on the typical electronic states near the Fermi level. However, these channels through extremely thin films or in the presence of strong fields can be formed by untypical

spatially close states, for which the effects of polaron cloud are less significant, or they can be formed by states far from the Fermi level having much smaller polaron shifts [35].

5.6.2. Optimum Channel Field Emission

The standard interpretation of field emission is based on the model of electron tunneling through a triangular potential barrier with a slope F due to an electric field. The model here proceeds from the premise of a continuous energy spectrum of localized states in the mobility gap, typical of amorphous materials and capable of giving rise to hopping conduction [35].

For the case [88] of strong fields, $(F \gg E_F/qL)$, Equation (5.13) remains valid with the substitution $L \to l = E_F/qF$. As a result, one obtains

$$\sigma = \sigma_0 exp\left(-\sqrt{\frac{8E_F\lambda}{\alpha qF}}\right) \tag{5.15}$$

which is different from the standard field emission conduction with $\ln(\sigma/\sigma_0) \propto -1/F$. The corresponding field emission is significantly nonuniform and occurs through rare optimum channels, this may lead to local heating, facilitating structural transformations in chalcogenide glasses [35]. Another feature related to such lateral nonuniformity is that very small area devices, $A \lesssim \alpha L exp\left(\sqrt{E_F\lambda/\alpha qF}\right)$, may not have an optimum channel with certainty, in which case their resistances will be determined by the most efficient of available random channels; hence, there will be strong variations between the conductance of nominally identical cells [35].

5.7. PERCOLATION CONDUCTION

In general, conductivity of randomly nonuniform materials is described in terms of percolation [89], this concept includes both the hopping conduction and band conduction in a medium where charge carrier concentration exponentially varies between different locations due to spatial variations in the electron potential energy [35].

Following a theory of high-field percolation conduction [90], each cell of the percolation cluster accommodates voltage $V_c = VL_c/L$. The field affected maximum resistor in the

filament decreases its resistance down to the second maximum, after which the voltage distributes evenly between the two resistors (1-max and 2-max), modifying both of them, and then extending to the third maximum resistor, etc [35]. Such equalization will sequentially take place in a number of resistors having ξ_i from the maximum one (ξ_c) down to $\xi_0(V)$ defined by the condition,

$$\sum_{\xi_0}^{\xi_c} \xi_i = \frac{qV_c}{kT} \tag{5.16}$$

Approximating the sum by the integral gives $(\xi_c - \xi_0)^2/2\xi_{max} = qV_c/kT$, where it is assumed that the random parameter ξ is uniformly distributed in the interval from 0 to $\xi_{max} \sim \xi_c$ [35]. As a result, the effective conduction is described by

$$\sigma \propto \exp(-\xi_0) = exp\left(-\xi_c + \sqrt{\frac{2\xi_{max}qV_c}{kT}}\right) \tag{5.17}$$

Substituting here the definition $V_c = VL_c/L$ and $F = V/L$. One finally obtains

$$\sigma(F) = \sigma_0 exp\left(\eta\sqrt{\frac{qFL_c}{kT}}\right) \tag{5.18}$$

where η is numerical coefficient. It is noted that in the case of very thin films, $L < L_c$, assuming that the resistors with $R = R_0 exp(\xi)$ and $\xi < \xi_L$ are involved, one can also impose the condition $\sigma = \sigma_\infty \equiv \sigma_0 \exp(-E_a/kT)$ when $L = L_c$, where σ_∞ is the meaning of the bulk conductivity [35]. As a result, the effective conductivity of thin ($L < L_c$) structures can be written in the form,

$$\sigma = \sigma(F)\exp\left\{\frac{L_c-L}{2r_c}\left[\ln\left(\frac{V_{max}2r_c}{kTL}\right) + 1\right]\right\} \tag{5.19}$$

where $\sigma(F)$ is given by Equation (5.18). Here we have neglected the difference between logarithmic terms evaluated at L_c and L and have taken into account that $\xi_{max} = V_{max}/kT$, where V_{max} is the maximum transport barrier [35]. For such devices, conductance will be determined by the most efficient of the available channels, which will differ between samples; hence, there will be strong fluctuations in conductance between nominally identical devices; according to rough estimates, that might occur well below the 10 nm scale [35].

5.8. DISCUSSION

Chalcogenide materials have an ability that of transformation between disordered (amorphous – glassy, reset process) and ordered (crystalline, set process) structures. Digital data stores as 1s and 0s. They are recorded by the transition of the amorphous (glassy – high resistive and low reflective states) and crystalline (low resistive an high reflective states). As an example, recently known optical memory disks use laser light for converting the varying parts of a thin film between the high reflective and low reflective states. Also, phase change memory devices (PCM) uses the voltage bias for converting this type of material between these states. PCM has an advantage of storing the data as optical memory disks. They use smaller area and they have higher speeds to read and write processes [35]. PCM in the amorphous phase has a strongly dependencies of electric field and temperature. The transition from the low field regime to intermediate field regime has very important role for the reading process. On the other hand, the high field regime has an essential feature for the writing process [65].

The procedure of PCM devices depends upon the charge transport based on their inclusive content concentration and type of chalcogenide glasses. If the devices are in the reset state (amorphous phase), the electrical conduction may be non-ohmic under varying voltages and temperatures. Hence this non-ohmic behavior gives an advantage of acquiring more energy faster than ohmic behavior. At that point, new aspects of conduction mechanisms are needed to develop modern devices and to be discovered for underlying mechanisms of the materials [35].

Conduction mechanisms of chalcogenides which are depend on electric field have been extensively studied since the 1970s [91–94]. The basic conduction mechanisms that are detailly mentioned above in this section can be summarized as follows with their electric field range [35]:

1. The Pool-Frenkel mechanism

   - Poole-Frenkel 1-center activation (Field range of $F \sim 10^4 - 10^5 \, V/cm$)

   - Poole-Frenkel 2-center activation (Field range of $F < 10^4 \, V/cm$)

   - Poole-Frenkel 1-center tunneling (Field range of $F > 10^5 \, V/cm$)

2. Schottky emission (uncertain range)

3. Field induced delocalization of tail states (Field range of $F \sim 10^5 \ V/cm$)

4. Space charge limited currents (Field range of $F \sim 10^4 \ V/cm$)

5. Field effects in hopping conduction

   - Optimum channel hopping in thin films (Field range of $F < \frac{E_F}{qL}$)

   - Optimum channel field emission (Field range of $F \gg \frac{E_F}{qL}$)

6. Percolation conduction

   - Percolation band conduction (Field range of $F > 10^4 \ V/cm$)

   - Percolation band conduction in thin films (Field range of $F > 10^4 \ V/cm$)

7. Conduction through crystalline inclusions in amorphous matrix

   - Crystalline inclusions 1 (Field range of $F \sim 10^5 - 10^6 \ V/cm$)

   - Crystalline inclusions 2 (Field range of $F < 10^5 \ V/cm$)

Our samples of *As₂Te₃(In)* thin films are in the nanometer scale. The thickness range of the samples are briefly shown in [95]. Moreover, the experimental data are taken in the three major field-dependent regimes such as [35]:

- A low field region at low electric field ranging from $F \sim 10 - 10^3 \ V/cm$ that refers to the range between 0.001 V and 0.1 V (can be considered as the threshold of non-ohmic dependence of the samples)

- An exponentially field dependent regime at electric field ranging from $F \sim 10^3 - 10^5 \ V/cm$ that refers to the range between 0.1 V (can be considered as the subthreshold from low to intermediate field range) and 1 V – (dedicated as intermediate field regime that has a relation of $lnI \propto V$ and $lnI \propto \sqrt{V}$)

- A stronger field dependence regime at electric field as $F \gtrsim 10^5 \ V/cm$ that refers to the beginning from 1 V (can be considered as the threshold from intermediate to

high field range) – (dedicated as the high field regime that has a relation of $lnI \propto V^2$)

In the electric field range of $F \sim 10 - 10^3 \, V/cm$ (low field region for the sample of $As_2Te_3(In)$ thin films) which include the voltage range between 0.001 V and 0.1 V, the conduction mechanisms may be degraded to the hopping conduction. High density of localized states which occurs in noncrystalline semiconducting thin films can give a rise to hopping transport mechanism. It can be determined that band conduction has a prevailing role on the conduction of chalcogenide glasses at room temperature. However, at higher temperatures than room tempereture, band conduction is the primary transport mechanism in this type of materials. All chalcogenide glasses have the conduction activation energy which is around to the half of the mobility gap. Whereas, the strong polaron effect (polaron clouds) for localized charge carriers dilutes the hopping mechanism. This strong polaron effect requires the electron transitions with respect to the inter-center transfer of atomic deformations. Charge carriers have thermal emission that is enhanced by the electric field. Hence they are trapped at the defects in the amorphous material and excited above the mobility edge. After that, they are suddenly re-trapped at a magnitude of a distance s which is known as the inter-trap distance [65]. Because of these manners, chalcogenide glasses differs from other amorphous semiconductors.

According to increasing temperatures, first crossovers have apparently smaller scaling exponents (represented by α_1 in Table 4.1 – 4.2 – 4.3) and approach 1/f noise (pink noise). In spite of the fact that the electric fields are not shown in the notable interval for the conduction mechanism of the space charge limited currents, this mechanism can be considered to verify the conduction transport in the $As_2Te_3(In)$ thin films at this voltage range. The transient current mechanism can be measured and simulated by using the artificial data which has 1/f noise [35]. This indicates that the system may behave like space charge limited transport mechanism. For short time scales, crossovers appear for the scaling behavior of the transient current mechanism on data sets at this regime which has voltages of 0.001 V, 0.002 V and 0.005 V.

Second crossovers of Detrended Fluctuation Analysis (DFA) on low field regime which has voltages of 0.001 V, 0.002 V and 0.005 V have the scaling exponents (α) (represented by α_2 in Table 4.1 – 4.2 – 4.3) that are in the range of 0.25 and 0.48. These values indicate that the current values in varying time have anti correlation ($0 < \alpha < 0.5$). Anti-

correlation is a different type of power-law correlations. In this state, large and small values of the correlations in the given time series are more likely to alternate on the system. The scaling exponents become to reach around 0.5 related to increasing temperature. This type of uncorrelated data corresponds to white noise which is known as random walk. The random fluctuations have local site energies. They create the localized states in material [96]. This may imply that the strong polaron effects increase while the steady electric field is applied for a length of time. On the other hand, trapping process of the charge carriers may increase. Due to these facts, hopping mechanism may not occur.

Moreover, third crossovers begin to get greater scaling exponents (represented by α_3 in Table 4.1 – 4.2 – 4.3) than first crossover ones, which are in the range of non-stationary state ($\alpha > 1$) that indicates non-persistent correlation. At 0.001 V, the current fluctuations get scaling exponents around 1 and begin to behave like 1/f noise. But they are in the range of non-stationary state at 353 K (80 °C). When the box size is increased, all data sets at the voltages of 0.002 V and 0.005 V have non-stationary state and get non-persistent correlations according to the increasing temperature. This manner may indicate that the conduction mechanism turns into the polaron hopping mechanism [97].

At 0.01 V, first crossovers apparently have smaller scaling exponents (represented by α_1 in Table 4.4) and approach 1/f noise (pink noise) while temperature increases like as the scaling exponents of first crossovers at the voltages of 0.001 V, 0.002 V and 0.005 V. The mechanism of space charge limited currents also may comprise at 0.01 V. But there are different scaling properties for the second crossovers at this voltage. These scaling exponents (represented by α_2 in Table 4.4) in the range of 0.52 and 0.81 correspond to persistent long-range power-law correlations. Furthermore, one can see that the scaling exponent values of the mid-crossovers reach to get closer values to the scaling exponent values of the first crossovers, especially at 333 K (60 °C) and 353 K (80 °C). This implies that the current behaviors begin to get two competing current mechanisms. 0.01 V can be considered as the beginning of the transition from three competing mechanisms to two competing mechanisms on the system. According to [98], the resistivity of the binary chalcogen of amorphous As_2S_3 decreases related to increasing temperature. Our samples of $As_2Te_3(In)$ have some similar properties with other binary chalcogenides. The competing mechanisms of space charge limited currents and optimum channel hopping may occur correlatively with changing crossovers. In the cases of chemically imperfects, structural

defects and impurities, hopping in optimum channels could be determined. However, the conduction of excited charge carriers into the band states near the mobility edges could be determined by the dc conductivity. A phonon asisted hopping of polarons could occur as a conduction mechanism on the system. At 353 K (80 °C), the scaling exponent of the third crossover that has a value of 1.31 can indicate the transition of the Poole conduction regime ($lnI \propto V$) that is considered as a regime for intermediate field region [28].

Secondly, at 0.1 V, there are two separative conduction mechanisms. 0.1 V can be attributed to subthreshold regime which is the transition between low field region and intermediate field region. The intermediate field regime has significant technological relevance. This regime has an importance for storing informations in memory and has sufficient applications of currently active researches [28]. Temperature dependence of electrical transport in disordered materials such as *As₂Te₃(In)* thin films is demonstrated because of these facts mentioned here. The scaling exponents of the first crossovers are varying from 1.63 to 1.17 (represented by α_1 in Table 4.5) through changing temperatures from 296 K (23 °C) to 353 K (80 °C). The scaling exponents except the one at 353 K (80 °C) have the values around 1.5 which correspond Brownian motion (Brown noise). To add more, the scaling exponent of DFA which is named as α is an indicator that describes the "roughness" of the time series. If α gets the larger values, the time series become smoother [61]. Due to this fact, the scaling exponents of first crossovers can indicate that the current behavior can has the conduction mechanism of Poole-Frenkel 2 center activation. The two center model predicts $lnI \propto V$ relation. This relation also corresponds to the Poole regime [99]. According to increasing temperature, the scaling exponent α takes smaller values. At 353 K (80 °C), it gets the value of 1.17. This scaling exponent value corresponds that the current behavior on the system have long-range power-law correlations. This manner can imply that there may be a temperature threshold toward the transition of the current mechanisms which are in the low field region. At higher temperatures, the current mechanisms under the intermediate field regime can behave like the current mechanisms under the low field regime. Because of the effects of fluctuations depending on temperature increase, the two center model of the Poole-Frenkel mechanism (Poole regime) is influenced critically [35].

On the other hand, the second crossovers apparently begin to get greater scaling exponent values with increasing temperature at this intermediate field regime threshold. They get the

values varying between 0.84 and 0.96 (represented by α_2 in Table 4.5). These scaling exponents that reach the value of 1 indicate that the current behavior approaches 1/f noise (pink noise) again. At that point, space charge limited current mechanism under 0.1 V at room temperature can be modeled with using the artificial data on 1/f noise measurements. Otherwise, at higher temperatures than room temperature, random fluctuations in the concentration of the *As₂Te₃(In)* thin films generate random variations of activation energies as exponentially. For this reason, the local carrier concentrations will vary exponentially between different locations [35]. At that point, second crossovers may introduce the percolation band conduction mechanism to analyze these types of systems. After room temperature, the patterns of conduction mechanisms under 0.1 V begin to show similar characteristics like in the low field region. According to increasing temperatures, particularly at 353 K (80 °C), one can see that polaron hopping conduction and optimum channel hopping conduction mechanisms can take into account again depending upon the scaling exponents of second crossovers.

As a continuation of these arguments, one can notice that apparent two competing conduction mechanisms remain under 0.5 V (intermediate field regime) at room temperature. First crossover has the scaling exponent value of 1.49 (represented by α_1 in Table 3.2). This value exactly corresponds to the Brownian motion (Brownian noise). This manner may clarify that the two center model of the Poole-Frenkel mechanism (Poole regime) is resumed as an essential conduction mechanism by the system. When second crossover is observed, it can be seen that the scaling exponent (α) (represented by α_2 in Table 3.2) takes a value around 1 once again. The scaling behavior may sign that there is the space charge limited current mechanism under this condition. On the other hand, it can be assumed that the transition of the conduction mechanisms begins to arise from the Poole-Frenkel 2 center activation model (Poole regime – the relation of $lnI \propto V$) to the Poole-Frenkel 1 center activation model (Poole-Frenkel regime – the relation of $lnI \propto \sqrt{V}$) according to increasing electric field [100,101]. Due to this fact, temperature dependence on the conduction mechanisms of *As₂Te₃(In)* thin films has not been examined beginning from 0.5 V. Because the $\sqrt{V}$ dependence of current increases slightly with temperature [35,66–68].

Thirdly, at 1 V (start of the high field regime), a distinctive scaling behavior (represented by α_1 in Table 3.2) which has the value of 1.55 as the scaling exponent (α) remains. It

shows us that there can be a one conduction mechanism of current behavior in this regime. The Poole-Frenkel 1 center activation model (Poole-Frenkel regime – the relation of $lnI \propto \sqrt{V}$) can be considered as that single conduction mechanism. The Poole-Frenkel model is based on thermal emission from ioanizable defect centers and it can be assumed that these defect centers create a Coulomb potential [28]. The Poole-Frenkel model of current transport was generally observed at high field regime [92,102]. To add more, beginning from 1 V, a strong non-linear field dependent region starts. At higher fields, there may be a transition from Poole-Frenkel 1 center activation model (the relation of $lnI \propto \sqrt{V}$) to Poole-Frenkel 1 center tunneling model (the relation of $lnI \propto V^2$) for our samples of *As$_2$Te$_3$(In)* thin films [35]. Furthermore, all of these transitions between the conduction mechanisms may depend upon the relaxation process on the structure [103].

Finally, from another point of view, it can be said that the conduction mechanism of Schottky emission effect may be examined in some cases because of the junctions of *As$_2$Te$_3$* thin films. Metalic indium contacts may cause to reduce the interfacial emission energy of force induced charge carriers based on the applied electric fields [76]. The glass transition temperature of *As$_2$Te$_3$* thin films is around 379 K (106 °C) [97]. But, the Schottky mechanism can be modelled and simulated below 320 K (47 °C). Hence, the Schottky emission effect can not be assigned as a conduction mechanism of *As$_2$Te$_3$(In)* thin films between these temperatures.

6. ALTERNATIVE MODELLING AND FITTING METHODS FOR CURRENT BEHAVIOR OF $As_2Te_3(In)$ THIN FILMS

In this section, *Mackey-Glass equation* is performed to a part of an empirical dataset. The *Mackey-Glass equation* is simulated as an artificial data which is generated by using a tool of MATLAB named as NAR (nonlinear autoregressive) Neural Network Analysis. On the other hand, this section involves the observations and results of the *Stretched exponential parametrization*. This method is fitted to a part (first 4000 data points) of our empirical data set to describe the relaxation mechanism of glassy systems when a constant electric field is applied and to see how transient current behavior changes with different temperatures.

6.1. SIMULATION OF MACKEY-GLASS EQUATION

The data sets which have hysteresis shown in Figure 6.1 are obtained as the current values versus the changing voltage (0 V – 4 V) values in constant interval of ΔV at varying time steps of Δt. Respectively, the program is arranged as forward bias from 0 V to 4 V and backward bias from 4 V and 0 V. So, the hysteresis and memory effect on semiconductor glass substrates (chalcogenides) of $As_2Te_3(In)$ are broadly examined. The Mackey-Glass equation is applied to our empirical data set of $As_2Te_3(In)$ glass substrate. The artificial data set is simulated to determine the chaotic mechanism of the empirical data set with using a tool of MATLAB named as NAR (nonlinear autoregressive) Neural Network Analysis applied by P. Potocnik [104]. The Mackey-Glass equation is the nonlinear time delay differential equation

$$\frac{dx}{dt} = \beta \, \frac{x_\tau}{1+x_\tau{}^n} - \gamma x \quad \text{where} \quad \gamma, \beta, n > 0. \tag{6.1}$$

where β, γ, τ, n are real numbers and x_τ represents the value of the variable x at time $(t - \tau)$ [105]. Depending on the values of the parameters, this equation displays a range of periodic and chaotic dynamics. Figure 6.2 shows how the tool of NAR Neural Network Analysis figures the prediction step with regard to the validation process which uses the training data of selected current values. In addition to this, Figure 6.3 shows us the

dynamics in the *Mackey-Glass equation* which base on the parameters of γ = 0.53, β = 1.02, τ = 30, n = 7.
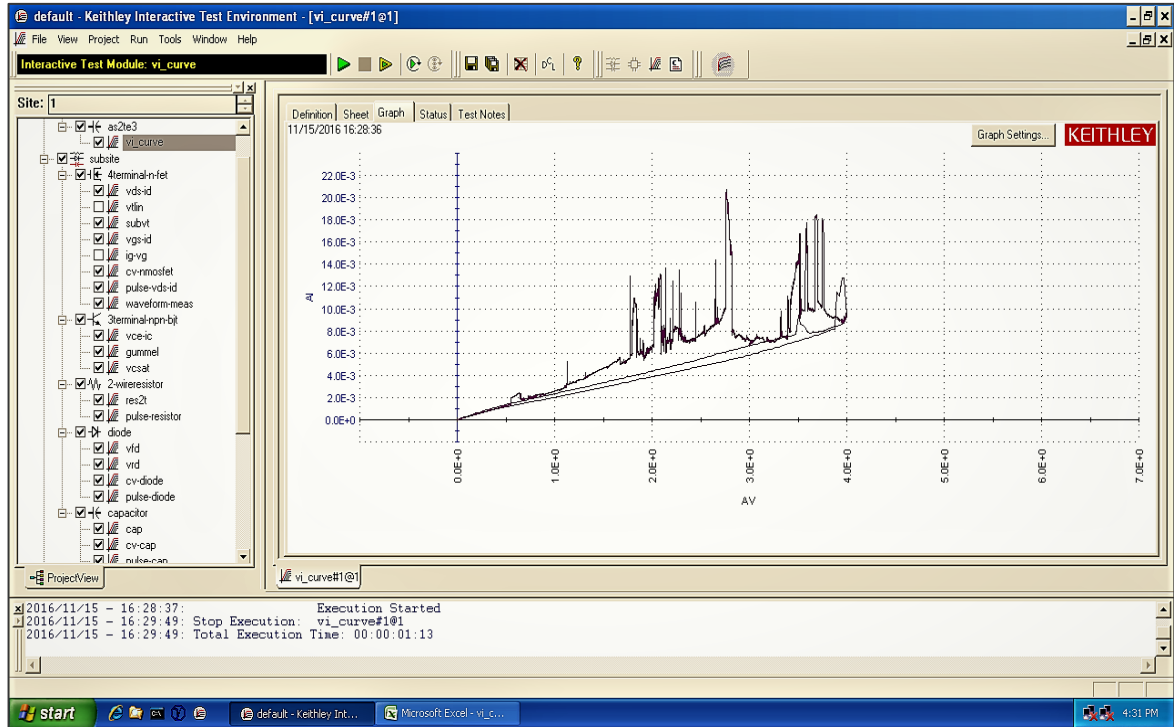
Figure 6.1. Data set which has hysteresis (I versus V at varying time).
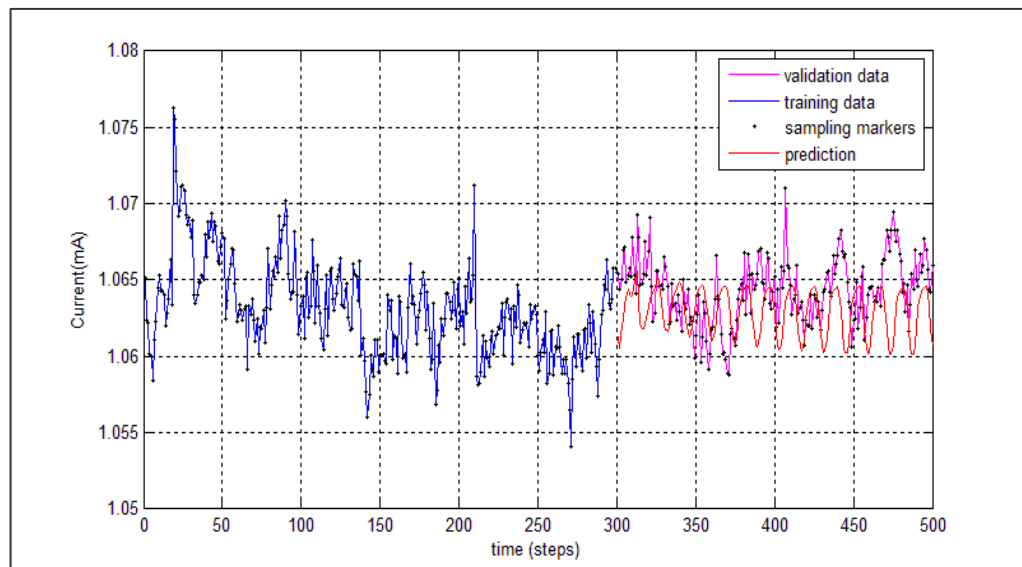
Figure 6.2. Dynamics in a piece of empirical data set of $As_2Te_3(In)$. (500 samples were arbitrarily chosen from entire data set.)
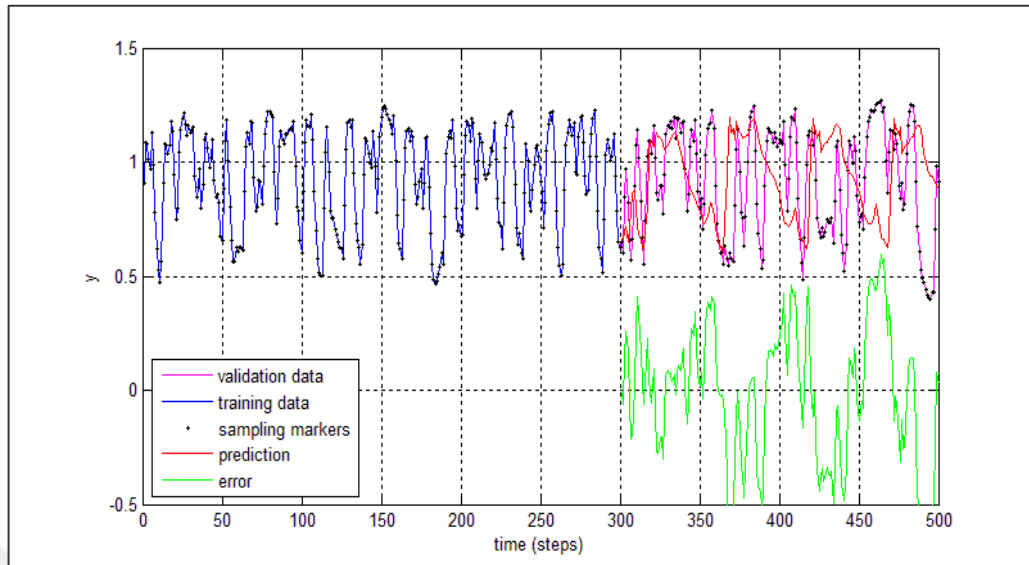
Figure 6.3. Dynamics in simulation of *Mackey-Glass equation*, for $\gamma = 0.53$, $\beta = 1.02$, $\tau = 30$, $n = 7$.

The relation between the validation data and training data sets which has nearly close prediction depends on the error. Firstly, the simulation is taken from the first 300 numbers of samples from a piece of the empirical data set to recognize the initial dynamics of the transient current mechanism. After this process, the simulation is iterated to the last 200 numbers of samples to validate artificial data. When the numerical difference between sampling data and predicted data has been calculated, the error has been determined. Figure 6.4 shows how dynamics of dataset have changed [106]. In Figure 6.4, simulated data has best validation performance when the number of iterations increases. Meaningfully, more accurate results are obtained when simulation codes are mostly iterated. In Table 6.1 and 6.2, the maximal Lyapunov exponents for validation and prediction values of the simulation are represented. So, they can be compared for the simulated dataset and empirical dataset.
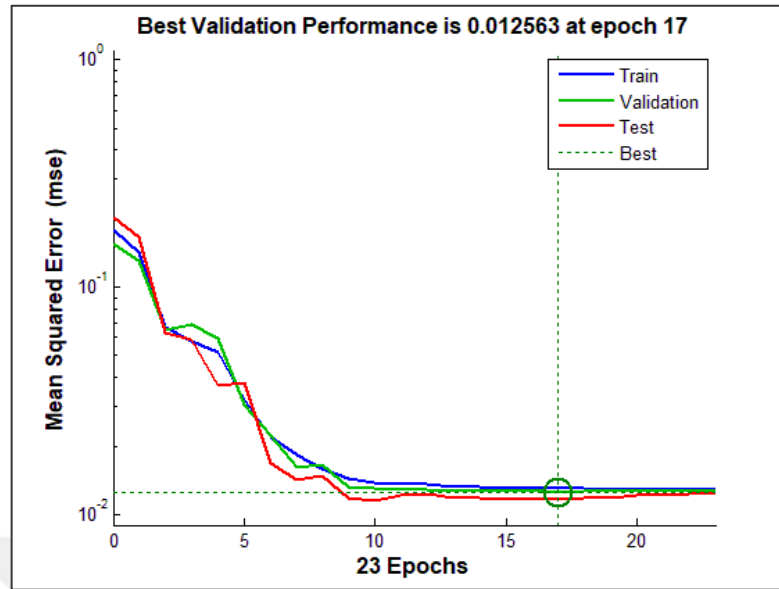
Figure 6.4. Dynamical graph of the simulation.

Table 6.1. Lyapunov exponent values for different embedding dimensions of data set for validation.

Embedding Dimensions	m=2	m=3	m=4	m=5
Lyapunov Exponents	0.0133	0.0159	0.0160	0.0178

Table 6.2. Lyapunov exponent values for different embedding dimensions of data set for prediction.

Embedding Dimensions	m=2	m=3	m=4	m=5
Lyapunov Exponents	0.0117	0.0181	0.0194	0.0191

6.2. STRETCHED EXPONENTIAL PARAMETRIZATION AND FITTING

Distribution and relaxation process of stretched exponential form are extensively used for complex physical systems which involve many types of semiconductors [14,107–109], multi-trapping models based on temporal behaviors [110], charge density waves [111,112], coupled nonlinear systems, transient current through various thin films and polymers [14,109,113], spin glasses [114], turbulance and dynamics of alloys [115]. The functional form $\exp(-(t/t_0)^\alpha)$ of simple exponential relaxation or stretched exponential relaxation models is generally studied and applied for the relaxation processes in disordered materials. The method of stretched exponential model is commonly used to define the relaxation process for the temporal behaviors of the physical systems. The exponent α is a universal parameter. By the way of this parameter, we can realize the stabilization of non-equilibrium charateristics in the physical environment of glassy systems. Moreover, the relaxation process in consideration of the external effects is determined with the aid of this parameter [14]. In order to fit and interpret the transient current behavior of *As₂Te₃(In)* with varying time, we have used a modified stretched exponential function which is given by

$$I(t) = A_1 - A_2 \, exp \left(\frac{t}{t_0}\right)^\alpha \tag{6.2}$$

where A_1, A_2 and α are constant parameters. Possible chaotic behavior in the transient current of *As₂Te₃(In)* thin films could come from either the impacts of different temperatures or from the physical properties.

In Figure 6.5 – 6.8, the fitting curves are representing these impacts by examining the transient current behaviors with varying times under 0.1 V at temperatures of 296 K (23 °C), 313 K (40 °C), 333 K (60 °C) and 353 K (80 °C) for the first 4000 data points of empirical data sets. In addition, the graph which has the name of relaxation rate / stretched exponent vs. temperature is presented in Figure 6.9. The results of stretched exponents and relaxation times are listed in Table 6.3.

On the basis of stretched exponential parametrization, we have aimed to determine whether these parameters depend on temperature and applied electric field. At first glance, it can be seen that the relaxation times and streched exponent values increase while temperature increases. The method of modified stretched exponential function in Equation 6.2 reveals

sufficient responses for the transient current behavior of $As_2Te_3(In)$. But, one can see that the fitting curves can not give exact solutions for the current behaviors of sample at higher temperatures which are particularly corresponding to 333 K (60 °C) and 353 K (80 °C) due to increasing fluctuations. Because of this manner, it can be considered that this method may provide de facto patterns for the current behaviors of sample, but it cannot suggest more detailed solutions under definite conditions.
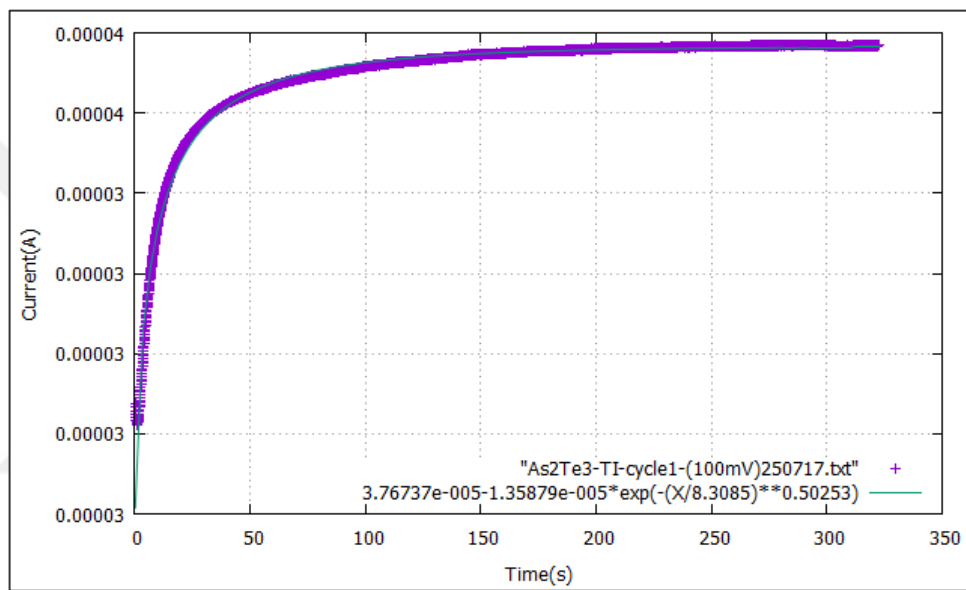
Figure 6.5. Fitting graph for evaluating the stretched exponent and relaxation time values for the first 4000 data points of emprical data sets under 0.1 V at room temperature (296 K (23 °C)). $A_1 = 3.76737 \ e^{-5}$ and $A_2 = 1.35879 \ e^{-5}$. The sum of least squares is $7.02513 \ e^{-11}$.
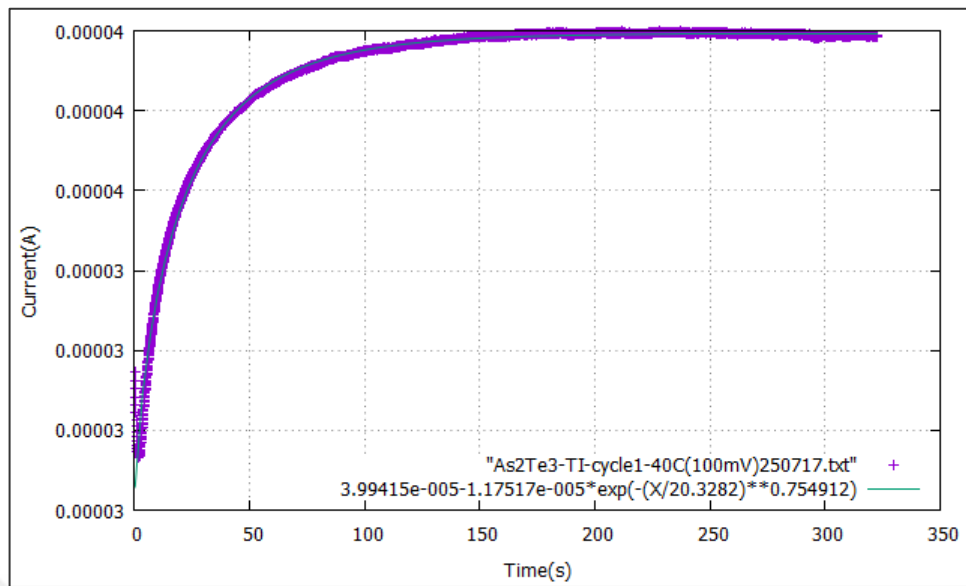
Figure 6.6. Fitting graph for evaluating the stretched exponent and relaxation time values for the first 4000 data points of emprical data sets under 0.1 V at 313 K (40 °C). $A_1 =$ 3.99415 e^{-5} and $A_2 = 1.17517$ e^{-5}. The sum of least squares is 6.55594 e^{-11}.
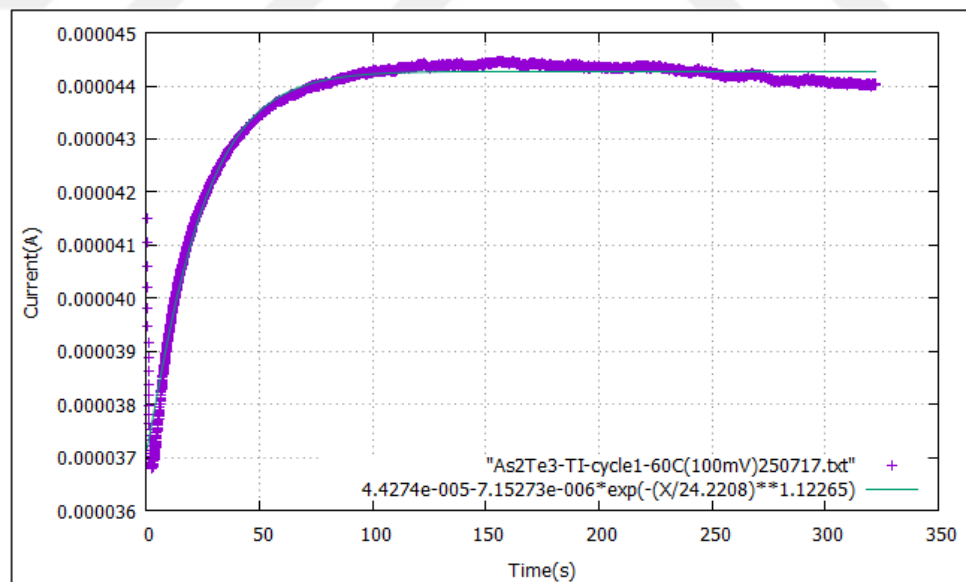
Figure 6.7. Fitting graph for evaluating the stretched exponent and relaxation time values for the first 4000 data points of emprical data sets under 0.1 V at 333 K (60 °C). $A_1 =$ 4.4274 e^{-5} and $A_2 = 7.15273$ e^{-6}. The sum of least squares is 1.66336 e^{-10}.
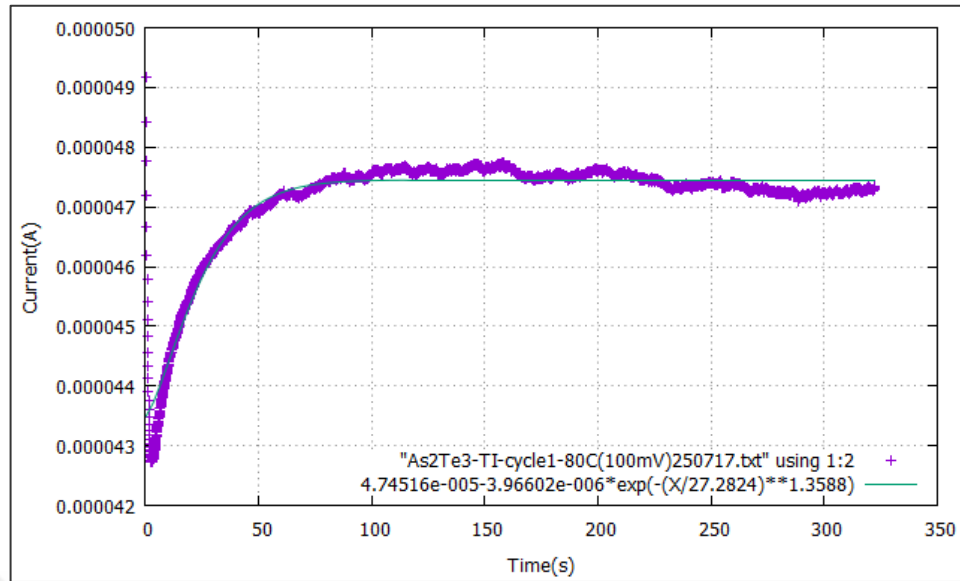
Figure 6.8. Fitting graph for evaluating the stretched exponent and relaxation time values for the first 4000 data points of emprical data sets under 0.1 V at 353 K (80 °C). $A_1 =$ 4.74516 e^{-5} and $A_2 = 3.96602$ e^{-6}. The sum of least squares is 2.30823 e^{-10}.
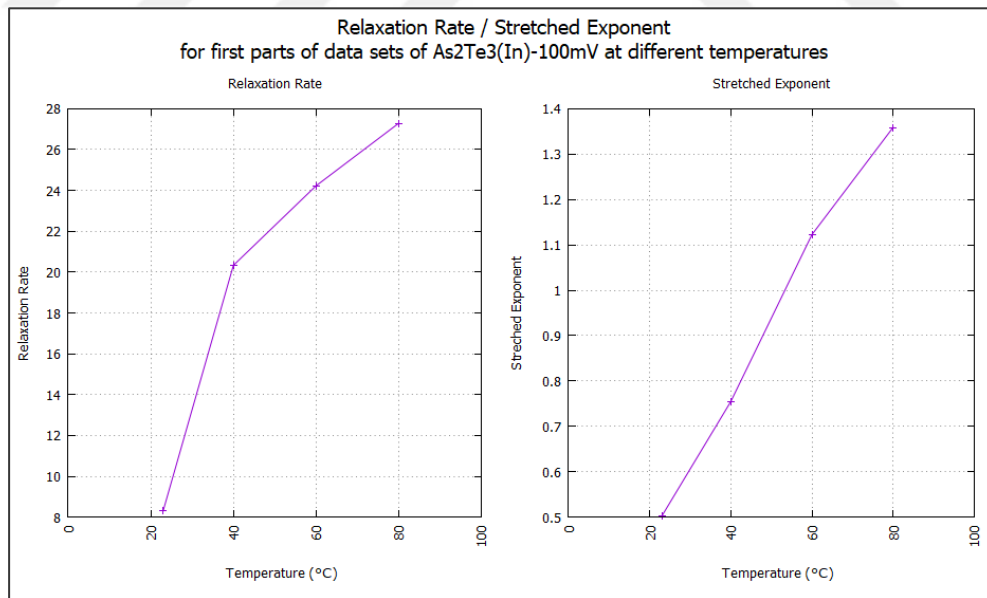
Figure 6.9. Relaxation rate / Stretched exponent vs. temperature for the first 4000 data points of emprical data sets under 0.1 V at different temperatures of 296 K (23 °C), 313 K (40 °C), 333 K (60 °C) and 353 K (80 °C).

Table 6.3. Relaxation rates and stretched exponent values for the first 4000 data points of emprical data sets under 0.1 V at different temperatures.

Voltage (V)	Temperature (°C)	Relaxation Rate / Relaxation Time (s)	Stretched Exponents
0.1	23.0 ± 0.5	8.3085	0.50253
0.1	40.0 ± 0.3	20.3282	0.754912
0.1	60.0 ± 0.3	24.2208	1.12265
0.1	80.0 ± 0.7	27.2824	1.3588

7. CONCLUSION

The Lyapunov exponent values for different embedding dimensions are very close to each other, so it can be said that the data which have noise and are purified from noise point to analogous transient current mechanism at this environmental condition. Both the false nearest neighbors method and application of maximal exponent were used as different approaches to gain reliable value of the embedding dimension. The ratios of false neighbors for data sets approach to a stable point after embedding dimension thirteen; hence an embedding dimension of thirteen is a good estimate for the minimal embedding dimension of data sets in most cases. The complex identity of glass substrates implies many degrees of freedom and a multifractal structure. So, obtaining identical results under same conditions will not be so easy. Based on this difficulty, conductivity of the thin films needs to be analyzed with nonlinear methods such as the maximal Lyapunov exponent and the DFA scaling exponent. Many additional important studies about using of nonlinear methods analyze the conduction mechanism in different amorphous structures which have irregular behavior [15,21,116].

Both of the first zero of the linear autocorrelation function and the first minimum of the mutual information function give different time scales at different temperatures. There are local minima values in the mutual information function, but these values have same order of magnitude under the first zero of the autocorrelation function. Consequently, this manner indicates that there are two different time scales in the conduction mechanism of glass substrates. When the electric field is applied, the system is forced because of created new traps (multi-trapping process). Also, it behaves a dissipative agent by annihilating them. These conflicting manners exhibit two significances, so these significances may cause a bifurcation effect and may be have two different time scales. If both occur in a complex structure of a glass substrate, the chaotic time evolution of the current appears. It can be considered that there is a transition which the fluctuations of the current through glass substrate saturate. After that, the conduction mechanism of the sample recognizes the condition and it properly behaves in regard to its memory.

Positive maximal Lyapunov exponents of dc current time series are found to be close to zero which indicates weak or low-dimensional chaos. Sensitive dependence on initial conditions (represented by positive Lyapunov exponents) combined with the continuous

temporal evolution of the transport properties explain the non-repeatability of the time series under the same voltage values.

Detrended Fluctuation Analysis is invariant to initial conditions, and a useful tool to analyze nonstationary time series. The results of analysis revealed three distinct conduction regimes as suggested by "the experimental data" reported in the literature [35].

These regimes are found to be :

i.   Low field regime: represented by three scaling exponents indicating to three different conduction mechanisms. For our sample of *As₂Te₃(In)*, this regime is below 0.01 V (down to 0.01 V in this case).

ii.   Intermediate field regime: represented by two scaling exponents indicating to two different conduction mechanisms. For our sample of *As₂Te₃(In)*, this regime is between 0.01 V and 1 V.

iii. High field regime: represented by one scaling exponent. For our sample of *As₂Te₃(In)*, this regime starts at 1 V.

On the other hand, the scaling behavior of the current at different temperatures is separated in two distinct conduction regimes. These regimes are also found to be:

i.   Low field regime: represented by three scaling exponents indicating to three different conduction mechanisms. For our sample of *As₂Te₃(In)*, three scaling crossovers with smaller scaling exponents (α) between 0.001 V and up to 0.01 V (included) can be observed just as the scaling crossovers of inceasing voltages.

ii.   Intermediate field regime: represented by two scaling exponents indicating to two different conduction mechanisms. For our sample of *As₂Te₃(In)*, two scaling regimes exist for 0.1 V which is referred to the sub-threshold regime. In this case, the voltage value of 0.1 V can be considered as the transition from the low field region to the intermediate field region mentioned in [35].

It is also reported that "it is difficult to identify a particular mechanism through the analysis of I-V data alone and further studies are required to discriminate between the different mechanisms. The possibility of interplay between them makes the problem even more challenging" [28,35].

Even though we can not also identify the particular mechanism(s), DFA reveals the long range correlation properties and the existence of interplay between them. A crossover in the DFA graph indicates different mechanisms with different time scales [117].

The different scaling exponents that are reported in this analysis correspond to the crossovers that are found in the DFA graphs. Therefore; in the low field region, DFA suggests an interplay among three different conduction mechanisms based on applied electric fields. The first scaling exponents (represented by α_1 in Table 3.1) for all the voltages below (including) 0.01 V are between 1.14 and 1.16. When $1 < \alpha < 1.5$, the underlaying process is nonstationary (indicating a dispersive transport mechanism possibly). The second scaling exponents (represented by α_2 in Table 3.1) are in the range 0.26 and 0.52. For $0 < \alpha < 0.5$, anti correlation exists in the fluctuation of time series. The third scaling exponents (represented by α_3 in Table 3.1) are around 1 for all the voltages in the low field regime. $\alpha = 1$ corresponds to pink noise. Pink noise is generated when a current flows through a non-homogeneous media. Moreover, first crossovers have apparently smaller scaling exponents (represented by α_1 in Table 4.1 – 4.2 – 4.3) and approach 1/f noise (pink noise) according to increasing temperatures at this regime which has voltages of 0.001 V, 0.002 V and 0.005 V. These scaling exponents are taking values respectively from 1.14 to 0.97 under 0.001 V, from 1.16 to 0.97 under 0.002 V and from 1.16 to 0.93 under 0.005 V at different temperatures. Second crossovers on low field regime which has voltages of 0.001 V, 0.002 V and 0.005 V have the scaling exponents (α) (represented by α_2 in Table 4.1 – 4.2 – 4.3) that are respectively in the ranges of 0.25 and 0.40 for 0.001 V, 0.28 and 0.45 for 0.002 V, 0.32 and 0.48 for 0.005 V. These values indicate that the current values in varying time have anti correlation ($0 < \alpha < 0.5$). Anti-correlation is a different type of power-law correlations. Also, the scaling exponents become to reach around 0.5 related to increasing temperature. This type of uncorrelated data corresponds to white noise which is known as random walk. Third crossovers begin to get greater scaling exponents (represented by α_3 in Table 4.1 – 4.2 – 4.3) than first crossover ones, which are in the range of non-stationary state ($1 < \alpha < 1.5$) that indicates non-persistent correlation. These scaling exponents are taking values respectively in the ranges of 0.99 and 1.14 under 0.001 V, 1.08 and 1.15 under 0.002 V, 1.05 and 1.22 under 0.005 V at different temperatures. At 0.01 V, first crossovers apparently have smaller scaling exponents (represented by α_1 in Table 4.4) and approach 1/f noise (pink noise) while temperature increases. The scaling exponents of second crossovers under 0.01 V at

different temperatures (represented by α$_2$ in Table 4.4), which are in the range of 0.52 and 0.81, correspond to persistent long-range power-law correlations. However, the third scaling exponents under 0.01 V (represented by α$_3$ in Table 4.4) are taking values in the range of 1.03 and 1.31 in accordance with temperatures. This manner indicates that the underlaying process is nonstationary ($1 < \alpha < 1.5$) and there are non-persistent correlations again.

In the intermediate field regime, DFA reveals mainly two different scaling exponents where α$_1$ (represented in Table 3.2) is approximate to 1.5. A scaling exponent that is equal to 1.5 ($\alpha = 1.5$) indicates a process creating Brown noise. The second scaling exponents (represented by α$_2$ in Table 3.2) is around 1. In this regime, DFA points to two different competing mechanisms based on the applied electric field. According to increasing temperature, the scaling exponents of the first crossovers are varying from 1.63 to 1.17 (represented by α$_1$ in Table 4.5) at 0.1 V. The scaling exponents except the one under 0.1 V at 353 K (80 °C) have the values around 1.5 which correspond Brownian motion. But at 353 K (80 °C), the scaling exponent gets the value of 1.17. This scaling exponent value corresponds that the current behavior on the system has long range power law correlations. On the other hand, the second scaling exponents begin to get greater values with increasing temperature at this intermediate field regime threshold. They get the values in the range of 0.84 and 0.96 (represented by α$_2$ in Table 4.5). These scaling exponents around 1 indicate that the current behavior approaches 1/f noise again.

In the start of high field regime, we see only one dominant scaling exponent (represented by α$_1$ in Table 3.2) with a value of 1.55 (around Brown noise).

By applying the simulation of the *Mackey-Glass equation* (delay-differantial equation) with using computational environment, we have targeted to fit artificial data blocks to our empirical data sets. As final concept, the physical behavior of the samples has been definitely explained to a general phenomenon. The range of maximal Lyapunov exponents for prediction dataset ($0.0171 \pm 0.0007 \ s^{-1}$) is greater than the range of maximal Lyapunov exponents for validation dataset ($0.0157 \pm 0.0007 \ s^{-1}$). The maximal Lyapunov exponents of validation and prediction dataset have similar values with the maximal Lyapunov exponents of empirical dataset. This implies that the Mackey-Glass equation is a suitable simulation method to analyze and predict transient current mechanism of *As$_2$Te$_3$(In)* glass substrates as of micro-state concept.

On the other side, we have aimed to fit the function of stretched exponential relaxation to first 4000 data points of our empirical data sets as of macro-state concept by applying of the *Stretched exponential parametrization* with using computational environment. The relaxation time and stretched exponent values increase with temperature.

The dependencies of scaling factors on the applied electric field and temperature indicate that i) electric field and temperature dependencies of the conductivity are based on multi competing conduction mechanisms each of which exhibit different correlation properties ii) the variation of these correlation values is probably caused by the structural changes induced by the electric field and temperature. Universally excepted conduction mechanisms should take the nonlinearities into account in order the discriminate among the proposed conduction mechanisms and the correlation properties of resultant current stand as a good candidate to discriminate among them. Therefore, we have attempted to determine extensively the possible types of conduction mechanims for transient current behavior of $As_2Te_3(In)$ thin fims in the discussion sub-section of section 5.

For future studies, DFA might be used in discriminating among the possible conduction models by creating the time series of the simulated current and comparing the fluctuation relations of the simulated current with the fluctuation relations of the experimental data [117].

REFERENCES

1. Sprott JC. *Chaos and time-series analysis*. Oxford: Oxford University Press; 2003.

2. Lorenz EN. Deterministic nonperiodic flow. *Journal of the Atmospheric Sciences.* 1963;20(2):130–41.

3. Singh J, Shimakawa K. *Advances in amorphous semiconductors.* London: CRC Press; 2003.

4. Singh AK. Crystallization kinetics of chalcogenide glasses. *Crystallization - Science and Technology.* 2012;1(2):29–64.

5. Fritzsche H. Optical and electrical energy gaps in amorphous semiconductors. *Journal of Non-Crystalline Solids.* 1971;6(1):49–71.

6. Klages R. *Microscopic chaos, fractals and transport in nonequilibrium statistical mechanics.* Singapore: World Scientific; 2007.

7. Klages R, Radons G, Sokolov IM. *Anomalous transport : foundations and applications.* Darmstadt: John Wiley and Sons; 2008.

8. Rebenshtok A, Barkai E. Weakly non-ergodic statistical physics. *Journal of Statistical Physics.* 2008;133(3):565–86.

9. Stefani FD, Hoogenboom JP, Barkai E. Beyond quantum jumps: blinking nanoscale light emitters. *Physics Today.* 2009;62(2):34–9.

10. Klages R. Weak chaos, infinite ergodic theory, and anomalous dynamics. *From Hamiltonian Chaos to Complex Systems.* 2013;1:3–42.

11. Metzler R, Klafter J. The random walk's guide to anomalous diffusion: a fractional dynamics aproach. *Physics Reports.* 2000;339(1):1–77.

12. Metzler R, Klafter J. The restaurant at the end of the random walk: recent developments in the description of anomalous transport by fractional dynamics. *Journal of Physics A: Mathematical and General.* 2004;37(31):161–208.

13. Bunde A, Havlin S. *Fractals and disordered systems.* New York: Springer Science

and Business Media; 1996.

14. Hacınlıyan A, Skarlatos Y, Sahin G, Atak K, Aybar OO. Possible stretched exponential parametrization for humidity absorption in polymers. *The European Physical Journal E*. 2009;28(4):369–76.

15. Hacinliyan A, Skarlatos Y, Yildirim HA, Sahin G. Characterization of chaoticity in the transient current through PMMA thin films. *Fractals*. 2006;14(02):125-131.

16. Shpotyuk O, Balitska V, Kozdras A, Hacinliyan AS, Skarlatos Y, Kusbeyzi Aybar I, Aybar OO. Chaotic behavior of light-assisted physical aging in arsenoselenide glasses. *Chaos: An Interdisciplinary Journal of Nonlinear Science*. 2014;24(4):043138.

17. Mazur K. More data about dielectric and electret properties of poly (methyl methacrylate). *Journal of Physics D: Applied Physics*. 1997;30(9):1383–98.

18. Adamec V, Calderwood JH. Electrical conduction and polarisation phenomena in polymeric dielectrics at low fields. *Journal of Physics D: Applied Physics*. 1978;11(6):781–800.

19. Boettcher S, Paczuski M. Aging in a model of self-organized criticality. *Physical Review Letters*. 1997;79(5):889–92.

20. Bellon L, Ciliberto S, Laroche C. Memory in the aging of a polymer glass. *EPL (Europhysics Letters)*. 2000;51(5):551–6.

21. Hacinliyan A, Skarlatos Y, Yildirim HA, Sahin G. Simulation of transient current through PMMA thin films based on a random walk model. *Physical Review B*. 2006;73(13):134302.

22. Morin C, Corallini S, Carreaud J, Vaney JB, Delaizir G, Crivello JC, Lopes EB, Piarristeguy A, Monnier J, Candolf C, Nassif V, Cuello GJ, Pradel A, Goncalves AP, Lenoir B, Alleno E. Polymorphism in thermoelectric As2Te3. *Inorganic Chemistry*. 2015;54(20):9936–47.

23. Platakis NS. Phase transitions and electrical properties of As2Te3. *Journal of Non-Crystalline Solids*. 1977;24(3):365-376.

24. Ho CH. Electronic structure and optical property of As2(Te1−xSx)3 and As2(Te1−xSex)3 crystals. *Journal of Alloys and Compounds*. 2011;509(26):7198–204.

25. Pal K, Waghmare UV. Strain induced Z2 topological insulating state of β-As2Te3. *Applied Physics Letters*. 2014;105(6):062105.

26. Marshall JM, Owen AE. Field-effect measurements in disordered As30Te48Si12Ge10 and As2Te3. *Philosophical Magazine*. 1976;33(3):457–74.

27. Croitoru N, Vescan L, Popescu C, Lăzărescu M. Non-ohmic properties of some amorphous semiconductors. *Journal of Non-Crystalline Solids*. 1970;4:493–503.

28. Gallo ML, Kaes M, Sebastian A, Krebs D. Subthreshold electrical transport in amorphous phase-change materials. *New Journal of Physics*. 2015;17(9):093035.

29. Hassanien AS, Akl AA. Influence of thermal and compositional variations on conduction mechanisms and localized state density of amorphous Cd50S50−xSex thin films. *Journal of Non-Crystalline Solids*. 2018;487:28–36.

30. Hassanien AS, Akl AA. Effect of Se addition on optical and electrical properties of chalcogenide CdSSe thin films. *Superlattices and Microstructures*. 2016;89:153–69.

31. Hassanien AS. Studies on dielectric properties, opto-electrical parameters and electronic polarizability of thermally evaporated amorphous Cd50S50−xSex thin films. *Journal of Alloys and Compounds*. 2016;671:566–78.

32. Hassanien AS, Akl AA. Crystal imperfections and Mott parameters of sprayed nanostructure IrO2 thin films.. *Physica B: Condensed Matter.* 2015;473:11–9.

33. Nardone M, Kozub VI, Karpov IV., Karpov VG. Possible mechanisms for 1/f noise in chalcogenide glasses: A theoretical description. *Physical Review B*. 2009;79(16):165206.

34. Binder K, Kob W. *Glassy materials and disordered solids: An introduction to their statistical mechanics*. Singapore: World Scientific; 2011.

35. Nardone M, Simon M, Karpov IV, Karpov VG. Electrical conduction in chalcogenide glasses of phase change memory. *Journal of Applied Physics*.

2012;112(7):071101.

36. Brazhkin VV, Bychkov E, Tsiok OB. As2Te3 glass under high hydrostatic pressure: Polyamorphism, relaxation, and metallization. *Physical Review B*. 2017;95(5):054205.

37. González-Salas JS, Shbat MS, Ordaz-Salazar FC, Simón J. Analyzing chaos systems and fine spectrum sensing using detrended fluctuation analysis algorithm. *Mathematical Problems in Engineering*. 2016;2016:1–18.

38. Mackey MC, Glass L. Oscillation and chaos in physiological control systems. *Science*. 1977;197(4300):287–9.

39. Hegger R, Kantz H, Schreiber T. Practical implementation of nonlinear time series methods: The TISEAN package. *Chaos: An Interdisciplinary Journal of Nonlinear Science*. 1999;9(2):413–35.

40. Kantz H, Schreiber T. *Nonlinear time series analysis*. New York: Cambridge University Press; 1997.

41. Schreiber T. Interdisciplinary application of nonlinear time series methods. *Physics Reports*. 1999;308(1):1–64.

42. Abarbanel HDI, Brown R, Sidorowich JJ, Tsimring LS. The analysis of observed chaotic data in physical systems. *Reviews of Modern Physics*. 1993;65(4):1331–92.

43. Takens F. Detecting strange attractors in turbulence. *Dynamical systems and turbulence*. 1981;898:366–81.

44. Sauer T, Yorke JA, Casdagli M. Embedology. *Journal of Statistical Physics*. 1991;65(3–4):579–616.

45. Abarbanel HDI. Choosing time delays. *Analysis of observed chaotic data*. 1996:25–37.

46. Kennel MB, Brown R, Abarbanel HDI. Determining embedding dimension for phase-space reconstruction using a geometrical construction. *Physical Review A*. 1992;45(6):3403–11.

47. Fraser AM, Swinney HL. Independent coordinates for strange attractors from

mutual information. *Physical Review A*. 1986;33(2):1134–40.

48. Abarbanel HDI. *Analysis of observed chaotic data*. New York, NY: Springer-Verlag; 1996.

49. Martinerie JM, Albano AM, Mees AI, Rapp PE. Mutual information, strange attractors, and the optimal estimation of dimension. *Physical Review A*. 1992;45(10):7058–64.

50. Wolf A, Swift JB, Swinney HL, Vastano JA. Determining Lyapunov exponents from a time series. *Physica D: Nonlinear Phenomena*. 1985;16(3):285–317.

51. Abarbanel HDI, Brown R, Kennel MB. Variation of Lyapunov exponents on a strange attractor. *Journal of Nonlinear Science*. 1991;1(2):175–99.

52. Sano M, Sawada Y. Measurement of the Lyapunov spectrum from a chaotic time series. *Physical Review Letters*. 1985;55(10):1082–5.

53. Eckmann JP, Kamphorst SO, Ruelle D, Ciliberto S. Liapunov exponents from time series. *Physical Review A*. 1986;34(6):4971–9.

54. Kantz H. A robust method to estimate the maximal Lyapunov exponent of a time series. *Physics Letters A*. 1994;185(1):77–87.

55. Nayak SK, Ramaswamy R, Chakravarty C. Maximal Lyapunov exponent in small atomic clusters. *Physical Review E*. 1995;51(4):3376–80.

56. Barré J, Dauxois T. Lyapunov exponents as a dynamical indicator of a phase transition. *EPL (Europhysics Letters)*. 2001;55(2):164–70.

57. Hu K, Ivanov PC, Chen Z, Carpena P, Eugene Stanley H. Effect of trends on detrended fluctuation analysis. *Physical Review E*. 2001;64(1):011114.

58. Chen Z, Ivanov PC, Hu K, Stanley HE. Effect of nonstationarities on detrended fluctuation analysis. *Physical Review E: Statistical Nonlinear Soft Matter Physics*. 2002;65(4):041107.

59. Goldberger AL, Amaral LAN, Glass L, Hausdorff JM, Ivanov PC, Mark RG, Mietus JE, Moody GB, Peng CK, Stanley E. PhysioBank, PhysioToolkit, and PhysioNet: components of a new research resource for complex physiologic signals.

Circulation. 2000;101(23):E215–20.

60. Peng CK, Buldyrev SV, Havlin S, Simons M, Stanley HE, Goldberger AL. Mosaic organization of DNA nucleotides. *Physical Review E*. 1994;49(2):1685–9.

61. Peng CK, Havlin S, Stanley HE, Goldberger AL. Quantification of scaling exponents and crossover phenomena in nonstationary heartbeat time series. *Chaos: An Interdisciplinary Journal of Nonlinear Science*. 1995;5(1):82–7.

62. Main C, Owen AE. Current noise in vitreous semiconductors. *Physica Status Solidi (A)*. 1970;1(2):297–306.

63. Smith W, Shaw RF, Henisch HK. Aspects of threshold switching. *Active and Passive Electronic Components*. 1974;1(2):137–9.

64. Scharnhorst KP. The specific current noise power of amorphous GeTe. *Journal of Non-Crystalline Solids*. 1977;23(3):435–9.

65. Kaes M, Le Gallo M, Sebastian A, Salinga M, Krebs D. High-field electrical transport in amorphous phase-change materials. *Journal of Applied Physics*. 2015;118(13):135707.

66. Ielmini D, Zhang Y. Analytical model for subthreshold conduction and threshold switching in chalcogenide-based memory devices. *Journal of Applied Physics*. 2007;102(5):054517.

67. Ielmini D, Zhang Y. Evidence for trap-limited transport in the subthreshold conduction regime of chalcogenide glasses. *Applied Physics Letters*. 2007;90(19):192102.

68. Ielmini D. Threshold switching mechanism by high-field energy gain in the hopping transport of chalcogenide glasses. *Physical Review B*. 2008;78(3):035308.

69. Voronkov EN, Kozyukhin SA. Electrical conductivity of amorphous films of chalcogenide compounds in high electric fields. *Semiconductors*. 2009;43(7):921–4.

70. Frenkel J. On pre-breakdown phenomena in insulators and electronic semi-conductors. *Physical Review*. 1938;54(8):647–8.

71. Mott NF, Davis EA. *Electronic processes in non-crystalline materials*. Oxford:

Clarendon Press; 1979.

72. Hill RM. Poole-Frenkel conduction in amorphous solids. *Philosophical Magazine*. 1971;23(181):59–86.

73. Lee BS, Abelson JR, Bishop SG, Kang DH, Cheong B, Kim KB. Investigation of the optical and electronic properties of Ge2Sb2Te5 phase change material in its amorphous, cubic, and hexagonal phases. *Journal of Applied Physics*. 2005;97(9):093509.

74. Frumar M, Wagner T, Hrdlicka M, Frumarova B, Nemec P. Non-volatile phase change memory materials and their induced changes. *EPCOS*. 2005;5:25.

75. Abakumov VN, Perel VI, Yassievich IN. *Nonradiative recombination in semiconductors*. North-Holland: Elsevier; 1991.

76. Sze SM, Ng KK. *Physics of semiconductor devices*. New York: Wiley-Interscience; 2007.

77. El-Samanoudy MM. Modified Poole–Frenkel mechanisms in Ge25BixSb15−xS60 thin films. *Applied Surface Science*. 2003;207(1–4):219–26.

78. Lifshits IM, Gredeskul SA, Pastur LA. *Introduction to the theory of disordered systems*. New York: Wiley; 1988.

79. Lampert MA, Mark P. *Current injection in solids*. New York: Academic Press; 1970.

80. Kodgespirova IF, Shkut VA, Kostylev SA, editors. *Proceedings of the International Conference on Amorphous Semiconductors, Bucharest, 1982*; 1982: Springer.

81. De Wit HJ, Crevecoeur C. The electrical conduction of glassy As2Se3 at high fields. *Journal of Non-Crystalline Solids*. 1972;8–10:787–92.

82. Robertson JM. *Ph.D. Dissertation*. An investigation of switching phenomena in amorphous semiconductors. University of Edinburgh; 1971.

83. Lebedev EA, Rogachev NA. Mobility distribution in the drift of carriers in glassy materials. *Soviet Physics Semiconductors-USSR*. 1981;15:86.

84. Baranovskii SD, Karpov VG. Multiphonon hopping conduction. *Soviet Physics Semiconductors-USSR*. 1986;20(10):1137-40.

85. Owen AE, Robertson JM. Electronic conduction and switching in chalcogenide glasses. *IEEE Transactions on Electron Devices*. 1973;20(2):105–22.

86. Bagley BG. The field dependent mobility of localized electronic carriers. *Solid State Communications*. 1970;8(5):345–8.

87. Raikh ME, Ruzin IM. Altshuller BL, Lee PA, Webb WR, editors. *Mesoscopic phenomena in solids*. New York: Elsevier; 1991.

88. Baranovskii SD, Fritzsche H, Levin EI, Ruzin IM, Shklovskii BI. Theory of low-temperature photoconductivity and photoluminescence in amorphous semiconductors. *Soviet Physics JETP*. 1989;69(4):773-82.

89. Shklovskii BI, Efros AL. *Electronic properties of doped semiconductors*. Berlin Heidelberg: Springer-Verlag Berlin Heidelberg; 1984.

90. Shklovskii BI. Percolation mechanism of electrical-conduction in strong electric-fields. *Soviet Physics Semiconductors-USSR*. 1979;13(1):53-6.

91. Walsh PJ, Vogel R, Evans EJ. Conduction and electrical switching in amorphous chalcogenide semiconductor films. *Physical Review*. 1969;178(3):1274–8.

92. Stubb T, Suntola T, Tiainen OJA. High field effects in chalcogenide thin films. *Solid State Electronics*. 1972;15(6):611–6.

93. Marshall JM, Miller GR. Field-dependent carrier transport in non-crystalline semiconductors. *Philosophical Magazine*. 1973;27(5):1151–68.

94. Suntola T. On the mechanism of switching effects in chalcogenide thin films. *Solid-State Electronics*. 1971;14(10):933–8.

95. Bilen B, Skarlatos Y, Aktas G. Frequency-dependent conductivity in As2Se3 and As2Te3 thin films. *Journal of Non-Crystalline Solids*. 2005;351(27–29):2153–8.

96. Anderson PW. Absence of diffusion in certain random lattices. *Physical Review*. 1958;109(5):1492–505.

97. Seager CH, Quinn RK. DC electronic transport in binary arsenic chalcogenide glasses. *Journal of Non-Crystalline Solids*. 1975;17(3):386–400.

98. Nkum RK, Ampong FK, Boakye F. Conduction mechanism in amorphous As2S3. *Journal of Science and Technology (Ghana)*. 2012;32(3):11–7.

99. Pillonnet A, Ongaro R. Synthetic representations of the Poole Frenkel (PF) and Poole regimes. *Revue de Physique Appliquée*. 1990;25(2):229–42.

100. Calderoni A, Ferro M, Ielmini D, Fantini P. A unified hopping model for subthreshold current of phase-change memories in amorphous state. *IEEE Electron Device Letters*. 2010;31(9):1023–5.

101. Betti Beneventi G, Guarino L, Ferro M, Fantini P. Three-dimensional Poole-Frenkel analytical model for carrier transport in amorphous chalcogenides. *Journal of Applied Physics*. 2013;113(4):044506.

102. Bahl SK, Chopra KL. Amorphous versus crystalline GeTe films. III. Electrical properties and band structure. *Journal of Applied Physics*. 1970;41(5):2196–212.

103. Ielmini D, Sharma D, Lavizzari S, Lacaita AL. Reliability impact of chalcogenide-structure relaxation in phase-change memory (PCM) cells—Part I: Experimental study. *IEEE Transactions on Electron Devices*. 2009;56(5):1070–7.

104. Potocnik P. Neural Networks: MATLAB examples. Neural Networks course (practical examples),2012:36-9; [cited 2017 14 July]. Available from: https://www.academia.edu/22782673/Neural_Networks_MATLAB_examples_Neural_Networks_course_practical_examples_2012_Primoz_Potocnik.

105. Glass L, Mackey MC. Pathological conditions resulting from instabilities in physiological control systems. *Annals of the New York Academy of Sciences*. 1979;316(1):214–35.

106. Keles AC, Hacinliyan AS, Skarlatos Y, editors. Chaos in the transient current through As2Te3(In) and Mackey-Glass simulation of hysteresis effect on glass substrates. *Chaotic Modeling and Simulation (CMSIM), 2017 CHAOS 10th International Conference in Casa Convalescència, Barcelona, Spain*; 2018: CMSIM.

107. Ookubo N, Ono H, Ochiai Y, Mochizuki Y, Matsui S. Effects of thermal annealing on porous silicon photoluminescence dynamics. *Applied Physics Letters*. 1992;61(8):940–2.

108. Böhmer R, Ngai KL, Angell CA, Plazek DJ. Nonexponential relaxations in strong and fragile glass formers. *The Journal of Chemical Physics*. 1993;99(5):4201–9.

109. Erdamar O, Skarlatos Y, Aktas G, Inci MN. Experimental investigation of the conduction mechanism of hydrogenated PEG thin films at high relative humidities. *Solid State Ionics*. 2006;177(37–38):3217–21.

110. Nelson J, Haque SA, Klug DR, Durrant JR. Trap-limited recombination in dye-sensitized nanocrystalline metal oxide electrodes. *Physical Review B*. 2001;63(20):205321.

111. Kriza G, Mihaly G. Stretched-exponential dielectric relaxation in a charge-density-wave system. *Physical Review Letters*. 1986;56(23):2529–32.

112. Biljakovic K, Lasjaunias JC, Monceau P, Levy F. Aging effects and nonexponential energy relaxations in charge-density-wave systems. *Physical Review Letters*. 1989;62(13):1512–5.

113. Petry W, Bartsch E, Fujara F, Kiebel M, Sillescu H, Farago B. Dynamic anomaly in the glass transition region of orthoterphenyl. *Zeitschrift für Physik B Condensed Matter*. 1991;83(2):175–84.

114. Fischer KH, Hertz JA. *Spin glasses*. Cambridge: Cambridge University Press; 1993.

115. Tatsumisago M, Halfpap BL, Green JL, Lindsay SM, Angell CA. Fragility of Ge-As-Se glass-forming liquids in relation to rigidity percolation, and the Kauzmann paradox. *Physical Review Letters*. 1990;64(13):1549–52.

116. Hacınlıyan A, Skarlatos Y, Sahin G, Akin G. Signals of chaotic behavior in PMMA. *Chaos, Solitons and Fractals*. 2003;17(2–3):575–83.

117. Şahin G, Keleş AC. Electric field dependence of dc conductivity in As2Te3 (in) thin films. *Journal of Non-Crystalline Solids*. 2019;503–504:13–9.

APPENDIX A: MUTUAL INFORMATION SOURCE CODE

In Mutual Information part delay time is calculated by the use of TISEAN software package. It estimates the time delayed mutual information of the data. It is the simplest possible realization. It uses a fixed mesh of boxes. No finite sample corrections are implemented so far. This package is called by typing mutual.exe in command prompt then type data which is time series then output file name is created. Result calculations are collected in given name output file in computer documentary.

Using C-source code below, one can enter following;

Enter the command line.

" mutual.exe filename.dat -D (maximal time delay example 30) -o filename_mut.dat"

The first line contains the number of occupied boxes, the second one the shannon entropy (normalized to the number of occupied boxes), the last D lines the mutual information (first column: delay, second column: mutual information).

Here is the C-source code below:

```
/*Author: Rainer Hegger. Last modified, Sep 20, 2000 */
#include <stdio.h>
#include <stdlib.h>
#include <math.h>
#include <limits.h>
#include <string.h>
#include "routines/tsa.h"

#define WID_STR "Estimates the time delayed mutual information\n\t\
of the data set"


char *file_out=NULL,stout=1;
char *infile=NULL;
unsigned long length=ULONG_MAX,exclude=0;
unsigned int column=1;
unsigned int verbosity=0xff;
long partitions=16,corrlength=20;
long *array,*h1,*h11,**h2;

void show_options(char *progname)
{
```

```c
    what_i_do(progname,WID_STR);
    fprintf(stderr," Usage: %s [Options]\n\n",progname);
    fprintf(stderr," Options:\n");
    fprintf(stderr,"Everything not being a valid option will be interpreted"
          " as a possible"
          " datafile.\nIf no datafile is given stdin is read. Just - also"
          " means stdin\n");
    fprintf(stderr,"\t-l # of points to be used [Default is all]\n");
    fprintf(stderr,"\t-x # of lines to be ignored [Default is 0]\n");
    fprintf(stderr,"\t-c column to read  [Default is 1]\n");
    fprintf(stderr,"\t-b # of boxes [Default is 16]\n");
    fprintf(stderr,"\t-D max. time delay [Default is 20]\n");
    fprintf(stderr,"\t-o output file [-o without name means 'datafile'.mut;"
            "\n\t\tNo -o means write to stdout]\n");
    fprintf(stderr,"\t-V verbosity level [Default is 1]\n\t\t"
          "0='only panic messages'\n\t\t"
          "1='+ input/output messages'\n");
    fprintf(stderr,"\t-h  show these options\n");
    fprintf(stderr,"\n");
    exit(0);
}

void scan_options(int n,char** in)
{
  char *out;

  if ((out=check_option(in,n,'l','u')) != NULL)
    sscanf(out,"%lu",&length);
  if ((out=check_option(in,n,'x','u')) != NULL)
    sscanf(out,"%lu",&exclude);
  if ((out=check_option(in,n,'c','u')) != NULL)
    sscanf(out,"%u",&column);
  if ((out=check_option(in,n,'b','u')) != NULL)
    sscanf(out,"%lu",&partitions);
  if ((out=check_option(in,n,'D','u')) != NULL)
    sscanf(out,"%lu",&corrlength);
  if ((out=check_option(in,n,'V','u')) != NULL)
    sscanf(out,"%u",&verbosity);
  if ((out=check_option(in,n,'o','o')) != NULL) {
    stout=0;
    if (strlen(out) > 0)
      file_out=out;
  }
}

double make_cond_entropy(long t)
{
  long i,j,hi,hii,count=0;
  double hpi,hpj,pij,cond_ent=0.0,norm;
```

```
  for (i=0;i<partitions;i++) {
   h1[i]=h11[i]=0;
   for (j=0;j<partitions;j++)
    h2[i][j]=0;
  }
  for (i=0;i<length;i++)
   if (i >= t) {
    hii=array[i];
    hi=array[i-t];
    h1[hi]++;
    h11[hii]++;
    h2[hi][hii]++;
    count++;
   }

  norm=1.0/(double)count;
  cond_ent=0.0;

  for (i=0;i<partitions;i++) {
   hpi=(double)(h1[i])*norm;
   if (hpi > 0.0) {
    for (j=0;j<partitions;j++) {
        hpj=(double)(h11[j])*norm;
        if (hpj > 0.0) {
         pij=(double)h2[i][j]*norm;
         if (pij > 0.0)
           cond_ent += pij*log(pij/hpj/hpi);
        }
    }
   }
  }

  return cond_ent;
}

int main(int argc,char** argv)
{
 char stdi=0;
 long tau,i;
 double *series,min,interval,shannon;
 FILE *file;

 if (scan_help(argc,argv))
  show_options(argv[0]);

 scan_options(argc,argv);
#ifndef OMIT_WHAT_I_DO
 if (verbosity&VER_INPUT)
  what_i_do(argv[0],WID_STR);
#endif
```

```
infile=search_datafile(argc,argv,&column,verbosity);
if (infile == NULL)
  stdi=1;

if (file_out == NULL) {
  if (!stdi) {
    check_alloc(file_out=(char*)calloc(strlen(infile)+5,(size_t)1));
    strcpy(file_out,infile);
    strcat(file_out,".mut");
  }
  else {
    check_alloc(file_out=(char*)calloc((size_t)10,(size_t)1));
    strcpy(file_out,"stdin.mut");
  }
}
if (!stout)
  test_outfile(file_out);

series=(double*)get_series(infile,&length,exclude,column,verbosity);
rescale_data(series,length,&min,&interval);

check_alloc(h1=(long *)malloc(sizeof(long)*partitions));
check_alloc(h11=(long *)malloc(sizeof(long)*partitions));
check_alloc(h2=(long **)malloc(sizeof(long *)*partitions));
for (i=0;i<partitions;i++)
  check_alloc(h2[i]=(long *)malloc(sizeof(long)*partitions));
check_alloc(array=(long *)malloc(sizeof(long)*length));
for (i=0;i<length;i++)
  if (series[i] < 1.0)
    array[i]=(long)(series[i]*(double)partitions);
  else
    array[i]=partitions-1;
free(series);

shannon=make_cond_entropy(0);
if (corrlength >= length)
  corrlength=length-1;

if (!stout) {
  file=fopen(file_out,"w");
  if (verbosity&VER_INPUT)
    fprintf(stderr,"Opened %s for writing\n",file_out);
  fprintf(file,"#shannon= %e\n",shannon);
  fprintf(file,"%d %e\n",0,shannon);
  for (tau=1;tau<=corrlength;tau++) {
    fprintf(file,"%ld %e\n",tau,make_cond_entropy(tau));
    fflush(file);
  }
  fclose(file);
}
```

```
  else {
    if (verbosity&VER_INPUT)
      fprintf(stderr,"Writing to stdout\n");
    fprintf(stdout,"#shannon= %e\n",shannon);
    fprintf(stdout,"%d %e\n",0,shannon);
    for (tau=1;tau<=corrlength;tau++) {
      fprintf(stdout,"%ld %e\n",tau,make_cond_entropy(tau));
      fflush(stdout);
    }
  }

  return 0;
}
```

APPENDIX B: FALSE NEAREST SOURCE CODE

This program looks for the nearest neighbors of all data points in m dimensions and iterates these neighbors one step into the future. If the ratio of the distance of the iteration and that of the nearest neighbor exceeds a given threshold the point is marked as a wrong neighbor. The output is the fraction of false neighbors for the specified embedding dimensions. Program implemented a new second criterion. If the distance to the nearest neighbor becomes smaller than the standard deviation of the data divided by the threshold, the point is omitted as mentioned before in embedding dimension part. This turns out to be a stricter criterion, but can show the effect that for increasing embedding dimensions, the number of points which enter the statistics is so small, that the whole statistics is meanlingless.

In command prompt, one can call by typing false_ nearest.exe then one must call original time series data by typing data file name then create a new file name; therefore, calculated false nearest dimensions are collected in this new file name data in the directory.

Embedding dimensions of applied data of the transient currents in $As_2Te_3(In)$ thin films are found by using TISEAN false_nearest C-source code. Code is given below and code can be used by typing;

false_nearest.exe filename.dat -o filename_fnn.dat

```
/*Author: Rainer Hegger. Last modified: Sep 3, 1999 */
#include <stdio.h>
#include <stdlib.h>
#include <string.h>
#include <limits.h>
#include <math.h>
#include "routines/tsa.h"

#define WID_STR "Determines the fraction of false nearest neighbors."

char *outfile=NULL;
char *infile=NULL;
char stdo=1;
unsigned long length=ULONG_MAX,exclude=0,theiler=0;
unsigned int column=1,delay=1,maxdim=5,mindim=1;
unsigned int verbosity=0xff;
double rt=10.0;
```

```c
double eps0=1.0e-5;
double *series;
double aveps,vareps;
double varianz;

#define BOX 1024
int ibox=BOX-1;
long **box,*list;
unsigned long toolarge;

void show_options(char *progname)
{
  what_i_do(progname,WID_STR);
  fprintf(stderr," Usage: %s [options]\n",progname);
  fprintf(stderr," Options:\n");
  fprintf(stderr,"Everything not being a valid option will be interpreted"
      " as a possible"
      " datafile.\nIf no datafile is given stdin is read. Just - also"
      " means stdin\n");
  fprintf(stderr,"\t-l # of data [default: whole file]\n");
  fprintf(stderr,"\t-x # of lines to ignore [default: 0]\n");
  fprintf(stderr,"\t-c column to read [default: 1]\n");
  fprintf(stderr,"\t-m minimal embedding dimension [default: 1]\n");
  fprintf(stderr,"\t-M maximal embedding dimension [default: 5]\n");
  fprintf(stderr,"\t-d delay [default: 1]\n");
  fprintf(stderr,"\t-f escape factor [default: 10.0]\n");
  fprintf(stderr,"\t-t theiler window [default: 0]\n");
  fprintf(stderr,"\t-o output file [default: 'datafile'.fnn; without -o"
          " stdout]\n");
  fprintf(stderr,"\t-V verbosity level [default: 3]\n\t\t"
      "0='only panic messages'\n\t\t"
      "1='+ input/output messages'\n\t\t"
      "2='+ information about the current state\n");
  fprintf(stderr,"\t-h show these options\n");
  exit(0);
}

void scan_options(int n,char **in)
{
 char *out;

 if ((out=check_option(in,n,'l','u')) != NULL)
   sscanf(out,"%lu",&length);
 if ((out=check_option(in,n,'x','u')) != NULL)
   sscanf(out,"%lu",&exclude);
 if ((out=check_option(in,n,'c','u')) != NULL)
   sscanf(out,"%u",&column);
 if ((out=check_option(in,n,'m','u')) != NULL)
   sscanf(out,"%u",&mindim);
 if ((out=check_option(in,n,'M','u')) != NULL)
```

```
   sscanf(out,"%u",&maxdim);
 if ((out=check_option(in,n,'d','u')) != NULL)
   sscanf(out,"%u",&delay);
 if ((out=check_option(in,n,'f','f')) != NULL)
   sscanf(out,"%lf",&rt);
 if ((out=check_option(in,n,'t','u')) != NULL)
   sscanf(out,"%lu",&theiler);
 if ((out=check_option(in,n,'V','u')) != NULL)
   sscanf(out,"%u",&verbosity);
 if ((out=check_option(in,n,'o','o')) != NULL) {
   stdo=0;
   if (strlen(out) > 0)
     outfile=out;
 }
}

char find_nearest(long n,unsigned int dim,double eps)
{
 int x,y,x1,x2,y1,i,i1;
 long element,which= -1;
 double dx,maxdx,mindx=1.1,factor;

 x=(int)(series[n-(dim-1)*delay]/eps)&ibox;
 y=(int)(series[n]/eps)&ibox;

 for (x1=x-1;x1<=x+1;x1++) {
   x2=x1&ibox;
   for (y1=y-1;y1<=y+1;y1++) {
     element=box[x2][y1&ibox];
     while (element != -1) {
         if (labs(element-n) > theiler) {
           maxdx=fabs(series[n]-series[element]);
           for (i=1;i<dim;i++) {
             i1=i*delay;
             dx=fabs(series[n-i1]-series[element-i1]);
             if (dx > maxdx)
               maxdx=dx;
           }
           if ((maxdx < mindx) && (maxdx > 0.0)) {
             which=element;
             mindx=maxdx;
           }
         }
         element=list[element];
     }
   }
 }

 if ((which != -1) && (mindx <= eps) && (mindx <= varianz/rt)) {
   aveps += mindx;
```

```
    vareps += mindx*mindx;
    factor=fabs(series[n+1]-series[which+1])/mindx;
    if (factor > rt)
      toolarge++;
    return 1;
   }
  return 0;
}

int main(int argc,char **argv)
{
 char stdi=0;
 FILE *file=NULL;
 double min,inter,epsilon,av;
 char *nearest,alldone;
 long i;
 unsigned int dim;
 unsigned long donesofar;

 if (scan_help(argc,argv))
   show_options(argv[0]);

 scan_options(argc,argv);
#ifndef OMIT_WHAT_I_DO
 if (verbosity&VER_INPUT)
   what_i_do(argv[0],WID_STR);
#endif

 infile=search_datafile(argc,argv,&column,verbosity);
 if (infile == NULL)
   stdi=1;

 if (outfile == NULL) {
  if (!stdi) {
    check_alloc(outfile=(char*)calloc(strlen(infile)+5,(size_t)1));
    strcpy(outfile,infile);
    strcat(outfile,".fnn");
   }
   else {
    check_alloc(outfile=(char*)calloc((size_t)10,(size_t)1));
    strcpy(outfile,"stdin.fnn");
   }
 }
 if (!stdo)
  test_outfile(outfile);

 series=(double*)get_series(infile,&length,exclude,column,verbosity);
 rescale_data(series,length,&min,&inter);
 variance(series,length,&av,&varianz);
```

```
check_alloc(list=(long*)malloc(sizeof(long)*length));
check_alloc(nearest=(char*)malloc(length));
check_alloc(box=(long**)malloc(sizeof(long*)*BOX));
for (i=0;i<BOX;i++)
  check_alloc(box[i]=(long*)malloc(sizeof(long)*BOX));

if (!stdo) {
  file=fopen(outfile,"w");
  if (verbosity&VER_INPUT)
    fprintf(stderr,"Opened %s for writing\n",outfile);
}
else {
  if (verbosity&VER_INPUT)
    fprintf(stderr,"Writing to stdout\n");
}

for (dim=mindim;dim<=maxdim;dim++) {
  epsilon=eps0;
  toolarge=0;
  alldone=0;
  donesofar=0;
  aveps=0.0;
  vareps=0.0;
  for (i=0;i<length;i++)
    nearest[i]=0;
  if (verbosity&VER_USR1)
    fprintf(stderr,"Start for dimension=%u\n",dim);
  while (!alldone && (epsilon < 2.*varianz/rt)) {
    alldone=1;
    make_box(series,box,list,length-1,BOX,dim,delay,epsilon);
    for (i=(dim-1)*delay;i<length-1;i++)
        if (!nearest[i]) {
          nearest[i]=find_nearest(i,dim,epsilon);
          alldone &= nearest[i];
          donesofar += (unsigned long)nearest[i];
        }
    if (verbosity&VER_USR1)
        fprintf(stderr,"Found %lu up to epsilon=%e\n",donesofar,epsilon*inter);
    epsilon*=sqrt(2.0);
    if (!donesofar)
        eps0=epsilon;
  }
  if (donesofar == 0) {
    fprintf(stderr,"Not enough points found!\n");
    exit(FALSE_NEAREST_NOT_ENOUGH_POINTS);
  }
  aveps *= (1./(double)donesofar);
  vareps *= (1./(double)donesofar);
  if (stdo) {
    fprintf(stdout,"%u %e %e %e\n",dim,(double)toolarge/(double)donesofar,
```

```
              aveps,vareps);
      fflush(stdout);
     }
    else {
     fprintf(file,"%u %e %e %e\n",dim,(double)toolarge/(double)donesofar,
              aveps,vareps);
     fflush(file);
    }
  }
  if (!stdo)
   fclose(file);

  if (infile != NULL)
   free(infile);
  if (outfile != NULL)
   free(outfile);
  free(series);
  free(list);
  free(nearest);
  for (i=0;i<BOX;i++)
   free(box[i]);
  free(box);
  return 0; }
```

APPENDIX C: LYAPUNOV EXPONENT SOURCE CODE

Lyapunov exponents are calculated in two different algorithms. One is with Kantz algorithm that is called Lyap_k. In this study, this algorithm is used.

A n-dimensional system will have n Lyapunov exponents. The Lyapunov exponents are used to study the stability of a system, e. g., a fixed point has only negative Lyapunov exponents, periodic systems have one zero and else negative Lyapunov exponents, and chaotic systems have at least one positive Lyapunov exponent.

To estimate the Lyapunov exponent of time series, several approaches were suggested, like the methods of Wolf, Kantz or Rosenstein. Here we used the method of Kantz provided by the TISEAN toolbox.

Here is the TISEAN software C-source code below:

Lyap_k code:

```
/*Author: Rainer Hegger. Last modified: Sep 3, 1999*/
#include <math.h>
#include <limits.h>
#include <stdio.h>
#include <stdlib.h>
#include <string.h>
#include "routines/tsa.h"

#define WID_STR "Estimates the maximal Lyapunov exponent using the Kantz\n\t\
algorithm"

#define BOX 128
const unsigned int ibox=BOX-1;

unsigned long length=ULONG_MAX;
unsigned long exclude=0;
unsigned long reference=ULONG_MAX;
unsigned int maxdim=2;
unsigned int mindim=2;
unsigned int delay=1;
unsigned int column=1;
unsigned int epscount=5;
unsigned int maxiter=50;
unsigned int window=0;
unsigned int verbosity=0xff;
```

```
double epsmin=1.e-3,epsmax=1.e-2;
char eps0set=0,eps1set=0;
char *outfile=NULL;
char *infile=NULL;

double *series,**lyap;
long box[BOX][BOX],*liste,**lfound,*found,**count;
double max,min;

void show_options(char *progname)
{
  what_i_do(progname,WID_STR);

  fprintf(stderr," Usage: %s [options]\n",progname);
  fprintf(stderr," Options:\n");
  fprintf(stderr,"Everything not being a valid option will be "
          "interpreted as a possible datafile.\nIf no datafile "
          "is given stdin is read. Just - also means stdin\n");
  fprintf(stderr,"\t-l # of data [default: whole file]\n");
  fprintf(stderr,"\t-x # of lines to be ignored [default: 0]\n");
  fprintf(stderr,"\t-c column to read [default: 1]\n");
  fprintf(stderr,"\t-M maxdim [default: 2]\n");
  fprintf(stderr,"\t-m mindim [default: 2]\n");
  fprintf(stderr,"\t-d delay [default: 1]\n");
  fprintf(stderr,"\t-r mineps [default: (data interval)/1000]\n");
  fprintf(stderr,"\t-R maxeps [default: (data interval)/100]\n");
  fprintf(stderr,"\t-# # of eps [default: 5]\n");
  fprintf(stderr,"\t-n # of reference points [default: # of data]\n");
  fprintf(stderr,"\t-s # of iterations [default: 50]\n");
  fprintf(stderr,"\t-t time window [default: 0]\n");
  fprintf(stderr,"\t-o outfile [default: 'datafile'.lyap]\n");
  fprintf(stderr,"\t-V verbosity level [default: 3]\n\t\t"
          "0='only panic messages'\n\t\t"
          "1='+ input/output messages'\n\t\t"
          "2='+ plus statistics'\n");
  fprintf(stderr,"\t-h show these options\n");
  exit(0);
}

void scan_options(int n,char **str)
{
  char *out;

  if ((out=check_option(str,n,'l','u')) != NULL)
    sscanf(out,"%lu",&length);
  if ((out=check_option(str,n,'x','u')) != NULL)
    sscanf(out,"%lu",&exclude);
  if ((out=check_option(str,n,'c','u')) != NULL)
    sscanf(out,"%u",&column);
  if ((out=check_option(str,n,'M','u')) != NULL)
```

```
    sscanf(out,"%u",&maxdim);
  if ((out=check_option(str,n,'m','u')) != NULL)
    sscanf(out,"%u",&mindim);
  if ((out=check_option(str,n,'d','u')) != NULL)
    sscanf(out,"%u",&delay);
  if ((out=check_option(str,n,'r','f')) != NULL) {
    eps0set=1;
    sscanf(out,"%lf",&epsmin);
  }
  if ((out=check_option(str,n,'R','f')) != NULL) {
    eps1set=1;
    sscanf(out,"%lf",&epsmax);
  }
  if ((out=check_option(str,n,'#','u')) != NULL)
    sscanf(out,"%u",&epscount);
  if ((out=check_option(str,n,'n','u')) != NULL)
    sscanf(out,"%lu",&reference);
  if ((out=check_option(str,n,'s','u')) != NULL)
    sscanf(out,"%u",&maxiter);
  if ((out=check_option(str,n,'t','u')) != NULL)
    sscanf(out,"%u",&window);
  if ((out=check_option(str,n,'V','u')) != NULL)
    sscanf(out,"%u",&verbosity);
  if ((out=check_option(str,n,'o','o')) != NULL)
    if (strlen(out) > 0)
      outfile=out;
}

void put_in_boxes(double eps)
{
  unsigned long i;
  long j,k;
  static unsigned long blength;

  blength=length-(maxdim-1)*delay-maxiter;

  for (i=0;i<BOX;i++)
    for (j=0;j<BOX;j++)
      box[i][j]= -1;

  for (i=0;i<blength;i++) {
    j=(long)(series[i]/eps)&ibox;
    k=(long)(series[i+delay]/eps)&ibox;
    liste[i]=box[j][k];
    box[j][k]=i;
  }
}

void lfind_neighbors(long act,double eps)
{
```

```
    unsigned int hi,k,k1;
    long i,j,i1,i2,j1,element;
    static long lwindow;
    double dx,eps2=sqr(eps);

    lwindow=(long)window;
    for (hi=0;hi<maxdim-1;hi++)
      found[hi]=0;
    i=(long)(series[act]/eps)&ibox;
    j=(long)(series[act+delay]/eps)&ibox;
    for (i1=i-1;i1<=i+1;i1++) {
      i2=i1&ibox;
      for (j1=j-1;j1<=j+1;j1++) {
        element=box[i2][j1&ibox];
        while (element != -1) {
            if ((element < (act-lwindow)) || (element > (act+lwindow))) {
              dx=sqr(series[act]-series[element]);
              if (dx <= eps2) {
                for (k=1;k<maxdim;k++) {
                  k1=k*delay;
                  dx += sqr(series[act+k1]-series[element+k1]);
                  if (dx <= eps2) {
                      k1=k-1;
                      lfound[k1][found[k1]]=element;
                      found[k1]++;
                  }
                  else
                      break;
                }
              }
            }
            element=liste[element];
        }
      }
    }
}

void iterate_points(long act)
{
  double **lfactor;
  double *dx;
  unsigned int i,j,l,l1;
  long k,element,**lcount;

  check_alloc(lfactor=(double**)malloc(sizeof(double*)*(maxdim-1)));
  check_alloc(lcount=(long**)malloc(sizeof(long*)*(maxdim-1)));
  for (i=0;i<maxdim-1;i++) {
    check_alloc(lfactor[i]=(double*)malloc(sizeof(double)*(maxiter+1)));
    check_alloc(lcount[i]=(long*)malloc(sizeof(long)*(maxiter+1)));
  }
```

```c
    check_alloc(dx=(double*)malloc(sizeof(double)*(maxiter+1)));

  for (i=0;i<=maxiter;i++)
    for (j=0;j<maxdim-1;j++) {
      lfactor[j][i]=0.0;
      lcount[j][i]=0;
    }

  for (j=mindim-2;j<maxdim-1;j++) {
    for (k=0;k<found[j];k++) {
      element=lfound[j][k];
      for (i=0;i<=maxiter;i++)
          dx[i]=sqr(series[act+i]-series[element+i]);
      for (l=1;l<j+2;l++) {
          l1=l*delay;
          for (i=0;i<=maxiter;i++)
            dx[i] += sqr(series[act+i+l1]-series[element+l1+i]);
      }
      for (i=0;i<=maxiter;i++)
          if (dx[i] > 0.0){
            lcount[j][i]++;
            lfactor[j][i] += dx[i];
          }
    }
  }
  for (i=mindim-2;i<maxdim-1;i++)
    for (j=0;j<=maxiter;j++)
      if (lcount[i][j]) {
          count[i][j]++;
          lyap[i][j] += log(lfactor[i][j]/lcount[i][j])/2.0;
      }

  for (i=0;i<maxdim-1;i++){
    free(lfactor[i]);
    free(lcount[i]);
  }
  free(lcount);
  free(lfactor);
  free(dx);
}

int main(int argc,char **argv)
{
  char stdi=0;
  double eps_fak;
  double epsilon;
  unsigned int i,j,l;
  FILE *fout;

  if (scan_help(argc,argv))
```

```
  show_options(argv[0]);

  scan_options(argc,argv);
#ifndef OMIT_WHAT_I_DO
  if (verbosity&VER_INPUT)
    what_i_do(argv[0],WID_STR);
#endif

  infile=search_datafile(argc,argv,&column,verbosity);
  if (infile == NULL)
    stdi=1;

  if (outfile == NULL) {
    if (!stdi) {
      check_alloc(outfile=(char*)calloc(strlen(infile)+6,1));
      sprintf(outfile,"%s.lyap",infile);
    }
    else {
      check_alloc(outfile=(char*)calloc(11,1));
      sprintf(outfile,"stdin.lyap");
    }
  }
  test_outfile(outfile);

  series=get_series(infile,&length,exclude,column,verbosity);
  rescale_data(series,length,&min,&max);

  if (eps0set)
    epsmin /= max;
  if (eps1set)
    epsmax /= max;

  if (epsmin >= epsmax) {
    epsmax=epsmin;
    epscount=1;
  }

  if (reference > (length-maxiter-(maxdim-1)*delay))
    reference=length-maxiter-(maxdim-1)*delay;
  if ((maxiter+(maxdim-1)*delay) >= length) {
    fprintf(stderr,"Too few points to handle these parameters!\n");
    exit(LYAP_K__MAXITER_TOO_LARGE);
  }

  if (maxdim < 2)
    maxdim=2;
  if (mindim < 2)
    mindim=2;
  if (mindim > maxdim)
    maxdim=mindim;
```

```
check_alloc(liste=(long*)malloc(sizeof(long)*(length)));
check_alloc(found=(long*)malloc(sizeof(long)*(maxdim-1)));
check_alloc(lfound=(long**)malloc(sizeof(long*)*(maxdim-1)));
for (i=0;i<maxdim-1;i++)
  check_alloc(lfound[i]=(long*)malloc(sizeof(long)*(length)));
check_alloc(count=(long**)malloc(sizeof(long*)*(maxdim-1)));
for (i=0;i<maxdim-1;i++)
  check_alloc(count[i]=(long*)malloc(sizeof(long)*(maxiter+1)));
check_alloc(lyap=(double**)malloc(sizeof(double*)*(maxdim-1)));
for (i=0;i<maxdim-1;i++)
  check_alloc(lyap[i]=(double*)malloc(sizeof(double)*(maxiter+1)));

if (epscount == 1)
  eps_fak=1.0;
else
  eps_fak=pow(epsmax/epsmin,1.0/(double)(epscount-1));

fout=fopen(outfile,"w");
if (verbosity&VER_INPUT)
  fprintf(stderr,"Opened %s for writing\n",outfile);
for (l=0;l<epscount;l++) {
  epsilon=epsmin*pow(eps_fak,(double)l);
  for (i=0;i<maxdim-1;i++)
    for (j=0;j<=maxiter;j++) {
        count[i][j]=0;
        lyap[i][j]=0.0;
    }
  put_in_boxes(epsilon);
  for (i=0;i<reference;i++) {
   lfind_neighbors(i,epsilon);
   iterate_points(i);
  }
  if (verbosity&VER_USR1)
   fprintf(stderr,"epsilon= %e\n",epsilon*max);
  for (i=mindim-2;i<maxdim-1;i++) {
   fprintf(fout,"#epsilon= %e  dim= %d\n",epsilon*max,i+2);
   for (j=0;j<=maxiter;j++)
       if (count[i][j])
         fprintf(fout,"%d %e %ld\n",j,lyap[i][j]/count[i][j],count[i][j]);
   fprintf(fout,"\n");
  }
  fflush(fout);
}
fclose(fout);
return 0;}
```

For each embedding dimension and each length scale, the file contains a block of data consisting of 3 columns:

1. The number of the iteration,

2. The logarithm of the stretching factor (the slope is the Lyapunov exponent if it is a straight line),

3. The number of points for which a neighborhood with enough points was found.

APPENDIX D: DETRENDED FLUCTUATION ANALYSIS SOURCE CODE

```
/* file: dfa.c     J. Mietus, C-K Peng, and G. Moody      8 February 2001
                   Last revised:                          25 January 2005  v4.9
```

```
-------------------------------------------------------------------------------
dfa: Detrended Fluctuation Analysis (translated from C-K Peng's Fortran code)
Copyright (C) 2001-2005 Joe Mietus, C-K Peng, and George B. Moody

This program is free software; you can redistribute it and/or modify it under
the terms of the GNU General Public License as published by the Free Software
Foundation; either version 2 of the License, or (at your option) any later
version.

This program is distributed in the hope that it will be useful, but WITHOUT ANY
WARRANTY; without even the implied warranty of MERCHANTABILITY or FITNESS
FOR A PARTICULAR PURPOSE.  See the GNU General Public License for more details.

You should have received a copy of the GNU General Public License along with
this program; if not, write to the Free Software Foundation, Inc., 59 Temple
Place - Suite 330, Boston, MA 02111-1307, USA.

You may contact the authors by e-mail (peng@physionet.org) or postal mail
(Beth Israel Deaconess Medical Center, Room KS-B26, 330 Brookline Ave., Boston,
MA 02215 USA).  For updates to this software, please visit PhysioNet
(http://www.physionet.org/).
_____
_____

This method was first proposed in:
  Peng C-K, Buldyrev SV, Havlin S, Simons M, Stanley HE, Goldberger AL. Mosaic
  organization of DNA nucleotides. Phys Rev E 1994;49:1685-1689.  [Available
  on-line at http://prola.aps.org/abstract/PRE/v49/i2/p1685_1]

A detailed description of the algorithm and its application to physiologic
signals can be found in:
  Peng C-K, Havlin S, Stanley HE, Goldberger AL. Quantification of scaling
  exponents and crossover phenomena in nonstationary heartbeat time series.
  Chaos 1995;5:82-87. [Abstract online at http://www.ncbi.nlm.nih.gov/entrez/-
   query.fcgi?cmd=Retrieve&db=PubMed&list_uids=11538314&dopt=Abstract]

If you use this program in support of published research, please include a
citation of at least one of the two references above, as well as the standard
citation for PhysioNet:
  Goldberger AL, Amaral LAN, Glass L, Hausdorff JM, Ivanov PCh, Mark RG,
  Mietus JE, Moody GB, Peng CK, Stanley HE.  PhysioBank, PhysioToolkit, and
```

Physionet: Components of a New Research Resource for Complex Physiologic Signals. Circulation 101(23):e215-e220 [Circulation Electronic Pages; http://circ.ahajournals.org/cgi/content/full/101/23/e215]; 2000 (June 13).
*/

```c
#include <stdio.h>
#include <stdlib.h>
#include <math.h>

#define SWAP(a,b) {temp = (a); (a) = (b); (b) = temp;}

/* Function prototypes. */
long input(void);
int rscale(long minbox, long maxbox, double boxratio);
void dfa(double *seq, long npts, int nfit, long *rs, int nr, int sw);
void setup(void);
void cleanup(void);
void help(void);
double polyfit(double **x, double *y, long ndat, int nfit);
void error(char error_text[]);
double *vector(long nl, long nh);
int *ivector(long nl, long nh);
long *lvector(long nl, long nh);
double **matrix(long nrl, long nrh, long ncl, long nch);
void free_vector(double *v, long nl, long nh);
void free_ivector(int *v, long nl, long nh);
void free_lvector(long *v, long nl, long nh);
void free_matrix(double **m, long nrl, long nrh, long ncl, long nch);

/* Global variables. */
char *pname;    /* this program's name (for use in error messages) */
double *seq;    /* input data buffer; allocated and filled by input() */
long *rs;       /* box size array; allocated and filled by rscale() */
double *mse;    /* fluctuation array; allocated by setup(), filled by dfa() */
int iflag = 1;  /* integrate the input data if non-zero */
int nfit = 2;   /* order of the regression fit, plus 1 */
int nr;         /* number of box sizes */

main(int argc, char **argv)
{
    int i, sw = 0;
    long minbox = 0L, maxbox = 0L, npts, temp;

    /* Read and interpret the command line. */
    pname = argv[0];
    for (i = 1; i < argc && *argv[i] == '-'; i++) {
        switch(argv[i][1]) {
            case 'd':   /* set nfit (the order of the regression fit) */
                if ((nfit = atoi(argv[++i])+1) < 2)
                    error("order must be greater than 0");
```

```
            break;
          case 'i':/* input data are already integrated */
            iflag = 0; break;
          case 'l':/* set minbox (the minimum box size) */
            minbox = atol(argv[++i]); break;
          case 'u':         /* set maxbox (the maximum box size) */
            maxbox = atol(argv[++i]); break;
          case 's':         /* enable sliding window mode */
            sw = 1; break;
        case 'h':   /* print usage information and quit */
        default:
            help();
            exit(1);
      }
    }

    /* Allocate and fill the input data array seq[]. */
    npts = input();

    /* Set minimum and maximum box sizes. */
    if (minbox < 2*nfit) minbox = 2*nfit;
    if (maxbox == 0 || maxbox > npts/4) maxbox = npts/4;
    if (minbox > maxbox) {
        SWAP(minbox, maxbox);
        if (minbox < 2*nfit) minbox = 2*nfit;
    }

    /* Allocate and fill the box size array rs[].  rscale's third argument
       specifies that the ratio between successive box sizes is 2^(1/8). */
    nr = rscale(minbox, maxbox, pow(2.0, 1.0/8.0));

    /* Allocate memory for dfa() and the functions it calls. */
    setup();

    /* Measure the fluctuations of the detrended input data at each box size
       using the DFA algorithm; fill mse[] with these results. */
    dfa(seq, npts, nfit, rs, nr, sw);

    /* Output the results. */
    for (i = 1; i <= nr; i++)
        printf("%g %g\n", log10((double)rs[i]), log10(mse[i])/2.0);

    /* Release allocated memory. */
    cleanup();
    exit(0);
}

/* Read input data, allocating and filling seq[], integrating if iflag != 0.
   Following the convention used for other arrays in this program, seq[0] is
   unused, and the first point is stored in seq[1].  The return value is the
```

number of points read.

This function allows the input buffer to grow as large as necessary, up to the available memory (assuming that a long int is large enough to address any memory location). Note that the integration is done using double precision arithmetic to avoid complete loss of precision when the integrated data reach large amplitudes. */

```c
long input()
{
    long maxdat = 0L, npts = 0L;
    double y, yp = 0.0;

    while (scanf("%lf", &y) == 1) {
        if (++npts >= maxdat) {
            double *s;

            maxdat += 50000;  /* allow the input buffer to grow (the
                                 increment is arbitrary) */
            if ((s = realloc(seq, maxdat * sizeof(double))) == NULL) {
                fprintf(stderr,
                    "%s: insufficient memory, truncating input at row %d\n",
                    pname, npts);
                break;
            }
            seq = s;
        }
        seq[npts] = iflag ? (yp += y) : y;
    }

    if (npts < 1) error("no data read");
    return (npts);
}

int rslen;       /* length of rs[] */

/* rscale() allocates and fills rs[], the array of box sizes used by dfa()
   below.  The box sizes range from (exactly) minbox to (approximately) maxbox,
   and are arranged in a geometric series such that the ratio between
   consecutive box sizes is (approximately) boxratio.  The return value is
   the number of box sizes in rs[].
*/
int rscale(long minbox, long maxbox, double boxratio)
{
    int ir, n;
    long rw;

    /* Determine how many scales are needed. */
    rslen = log10(maxbox / (double)minbox) / log10(boxratio) + 1.5;
    /* Thanks to Peter Domitrovich for pointing out that a previous version
       of the above calculation undercounted the number of scales in some
```

```
    situations. */
  rs = lvector(1, rslen);
  for (ir = 1, n = 2, rs[1] = minbox; n <= rslen && rs[n-1] < maxbox; ir++)
   if ((rw = minbox * pow(boxratio, ir) + 0.5) > rs[n-1])
       rs[n++] = rw;
  if (rs[--n] > maxbox) --n;
  return (n);
}


double **x;    /* matrix of abscissas and their powers, for polyfit(). */


/* Detrended fluctuation analysis
   seq:         input data array
   npts:        number of input points
   nfit:        order of detrending (2: linear, 3: quadratic, etc.)
   rs:          array of box sizes (uniformly distributed on log scale)
   nr:          number of entries in rs[] and mse[]
   sw:          mode (0: non-overlapping windows, 1: sliding window)
  This function returns the mean squared fluctuations in mse[].
*/
void dfa(double *seq, long npts, int nfit, long *rs, int nr, int sw)
{
  long i, boxsize, inc, j;
  double stat;

  for (i = 1; i <= nr; i++) {
    boxsize = rs[i];
    if (sw) { inc = 1; stat = (int)(npts - boxsize + 1) * boxsize; }
       else { inc = boxsize; stat = (int)(npts / boxsize) * boxsize; }
    for (mse[i] = 0.0, j = 0; j <= npts - boxsize; j += inc)
       mse[i] += polyfit(x, seq + j, boxsize, nfit);
    mse[i] /= stat;
  }
}


/* workspace for polyfit() */
double *beta, **covar, **covar0;
int *indxc, *indxr, *ipiv;


/* This function allocates workspace for dfa() and polyfit(), and sets
   x[i][j] = i**(j-1), in preparation for polyfit(). */
void setup()
{
  long i;
  int j, k;

  beta = vector(1, nfit);
  covar = matrix(1, nfit, 1, nfit);
  covar0 = matrix(1, nfit, 1, nfit);
  indxc = ivector(1, nfit);
```

```c
    indxr = ivector(1, nfit);
    ipiv = ivector(1, nfit);
    mse = vector(1, nr);
    x = matrix(1, rs[nr], 1, nfit);
    for (i = 1; i <= rs[nr]; i++) {
        x[i][1] = 1.0;
        x[i][2] = i;
        for (j = 3; j <= nfit; j++)
            x[i][j] = x[i][j-1] * i;
    }
}

/* This function frees all memory previously allocated by this program. */
void cleanup()
{
    free_matrix(x, 1, rs[nr], 1, nfit);
    free_vector(mse, 1, nr);
    free_ivector(ipiv, 1, nfit);
    free_ivector(indxr, 1, nfit);
    free_ivector(indxc, 1, nfit);
    free_matrix(covar0, 1, nfit, 1, nfit);
    free_matrix(covar, 1, nfit, 1, nfit);
    free_vector(beta, 1, nfit);
    free_lvector(rs, 1, rslen);   /* allocated by rscale() */
    free(seq);                    /* allocated by input() */
}

static char *help_strings[] = {
 "usage: %s [OPTIONS ...]\n",
 "where OPTIONS may include:",
 " -d K            detrend using a polynomial of degree K",
 "                   (default: K=1 -- linear detrending)",
 " -h              print this usage summary",
 " -i              input series is already integrated",
 " -l MINBOX       smallest box width (default: 2K+2)",
 " -s              sliding window DFA",
 " -u MAXBOX       largest box width (default: NPTS/4)",
 "The standard input should contain one column of data in text format.",
 "The standard output is two columns: log(n) and log(F) [base 10 logarithms],",
 "where n is the box size and F is the root mean square fluctuation.",
NULL
};

void help(void)
{
    int i;

    (void)fprintf(stderr, help_strings[0], pname);
    for (i = 1; help_strings[i] != NULL; i++)
        (void)fprintf(stderr, "%s\n", help_strings[i]);
```

```c
   }

/* polyfit() is based on lfit() and gaussj() from Numerical Recipes in C
   (Press, Teukolsky, Vetterling, and Flannery; Cambridge U. Press, 1992).  It
   fits a polynomial of degree (nfit-1) to a set of boxsize points given by
   x[1...boxsize][2] and y[1...boxsize].  The return value is the sum of the
   squared errors (chisq) between the (x,y) pairs and the fitted polynomial.
*/
double polyfit(double **x, double *y, long boxsize, int nfit)
{
   int icol, irow, j, k;
   double big, chisq, pivinv, temp;
   long i;
   static long pboxsize = 0L;

   /* This block sets up the covariance matrix.  Provided that boxsize
      never decreases (which is true in this case), covar0 can be calculated
      incrementally from the previous value. */
   if (pboxsize != boxsize) {  /* this will be false most of the time */
         if (pboxsize > boxsize)          /* this should never happen */
            pboxsize = 0L;
         if (pboxsize == 0L)    /* this should be true the first time only */
            for (j = 1; j <= nfit; j++)
                  for (k = 1; k <= nfit; k++)
                     covar0[j][k] = 0.0;
         for (i = pboxsize+1; i <= boxsize; i++)
            for (j = 1; j <= nfit; j++)
                  for (k = 1, temp = x[i][j]; k <= j; k++)
                     covar0[j][k] += temp * x[i][k];
         for (j = 2; j <= nfit; j++)
            for (k = 1; k < j; k++)
                  covar0[k][j] = covar0[j][k];
         pboxsize = boxsize;
   }
   for (j = 1; j <= nfit; j++) {
         beta[j] = ipiv[j] = 0;
         for (k = 1; k <= nfit; k++)
            covar[j][k] = covar0[j][k];
   }
   for (i = 1; i <= boxsize; i++) {
         beta[1] += (temp = y[i]);
         beta[2] += temp * i;
   }
   if (nfit > 2)
         for (i = 1; i <= boxsize; i++)
            for (j = 3, temp = y[i]; j <= nfit; j++)
                  beta[j] += temp * x[i][j];
   for (i = 1; i <= nfit; i++) {
         big = 0.0;
         for (j = 1; j <= nfit; j++)
```

```c
            if (ipiv[j] != 1)
                for (k = 1; k <= nfit; k++) {
                    if (ipiv[k] == 0) {
                        if ((temp = covar[j][k]) >= big ||
                            (temp = -temp) >= big) {
                            big = temp;
                            irow = j;
                            icol = k;
                        }
                    }
                    else if (ipiv[k] > 1)
                        error("singular matrix");
                }
        ++(ipiv[icol]);
        if (irow != icol) {
            for (j = 1; j <= nfit; j++) SWAP(covar[irow][j], covar[icol][j]);
            SWAP(beta[irow], beta[icol]);
        }
        indxr[i] = irow;
        indxc[i] = icol;
        if (covar[icol][icol] == 0.0) error("singular matrix");
        pivinv = 1.0 / covar[icol][icol];
        covar[icol][icol] = 1.0;
        for (j = 1; j <= nfit; j++) covar[icol][j] *= pivinv;
        beta[icol] *= pivinv;
        for (j = 1; j <= nfit; j++)
            if (j != icol) {
                temp = covar[j][icol];
                covar[j][icol] = 0.0;
                for (k = 1; k <= nfit; k++) covar[j][k] -= covar[icol][k]*temp;
                beta[j] -= beta[icol] * temp;
            }
    }
    chisq = 0.0;
    if (nfit <= 2)
        for (i = 1; i <= boxsize; i++) {
            temp = beta[1] + beta[2] * i - y[i];
            chisq += temp * temp;
        }
    else
        for (i = 1; i <= boxsize; i++) {
            temp = beta[1] + beta[2] * i - y[i];
            for (j = 3; j <= nfit; j++) temp += beta[j] * x[i][j];
            chisq += temp * temp;
        }
    return (chisq);
}

/* The functions below are based on those of the same names in Numerical
   Recipes (see above). */
```

```c
void error(char error_text[])
{
   fprintf(stderr, "%s: %s\n", pname, error_text);
   exit(1);
}


double *vector(long nl, long nh)
/* allocate a double vector with subscript range v[nl..nh] */
{
   double *v = (double *)malloc((size_t)((nh-nl+2) * sizeof(double)));
   if (v == NULL) error("allocation failure in vector()");
   return (v-nl+1);
}


int *ivector(long nl, long nh)
/* allocate an int vector with subscript range v[nl..nh] */
{
   int *v = (int *)malloc((size_t)((nh-nl+2) * sizeof(int)));
   if (v == NULL) error("allocation failure in ivector()");
   return (v-nl+1);
}


long *lvector(long nl, long nh)
/* allocate a long int vector with subscript range v[nl..nh] */
{
   long *v = (long *)malloc((size_t)((nh-nl+2) * sizeof(long)));
   if (v == NULL) error("allocation failure in lvector()");
   return (v-nl+1);
}


double **matrix(long nrl, long nrh, long ncl, long nch)
/* allocate a double matrix with subscript range m[nrl..nrh][ncl..nch] */
{
   long i, nrow = nrh-nrl+1, ncol = nch-ncl+1;
   double **m;

   /* allocate pointers to rows */
   m = (double **) malloc((size_t)((nrow+1) * sizeof(double*)));
   if (!m) error("allocation failure 1 in matrix()");
   m += 1;
   m -= nrl;

   /* allocate rows and set pointers to them */
   m[nrl] = (double *) malloc((size_t)((nrow*ncol+1) * sizeof(double)));
   if (!m[nrl]) error("allocation failure 2 in matrix()");
   m[nrl] += 1;
   m[nrl] -= ncl;

   for (i = nrl+1; i <= nrh; i++) m[i] = m[i-1]+ncol;
```

```
   /* return pointer to array of pointers to rows */
   return (m);
}

void free_vector(double *v, long nl, long nh)
/* free a double vector allocated with vector() */
{
   free(v+nl-1);
}

void free_ivector(int *v, long nl, long nh)
/* free an int vector allocated with ivector() */
{
   free(v+nl-1);
}

void free_lvector(long *v, long nl, long nh)
/* free a long int vector allocated with lvector() */
{
   free(v+nl-1);
}

void free_matrix(double **m, long nrl, long nrh, long ncl, long nch)
/* free a double matrix allocated by matrix() */
{
   free(m[nrl]+ncl-1);
   free(m+nrl-1);
}
```

APPENDIX E: EXTENSIVE GRAPHS OF DFA
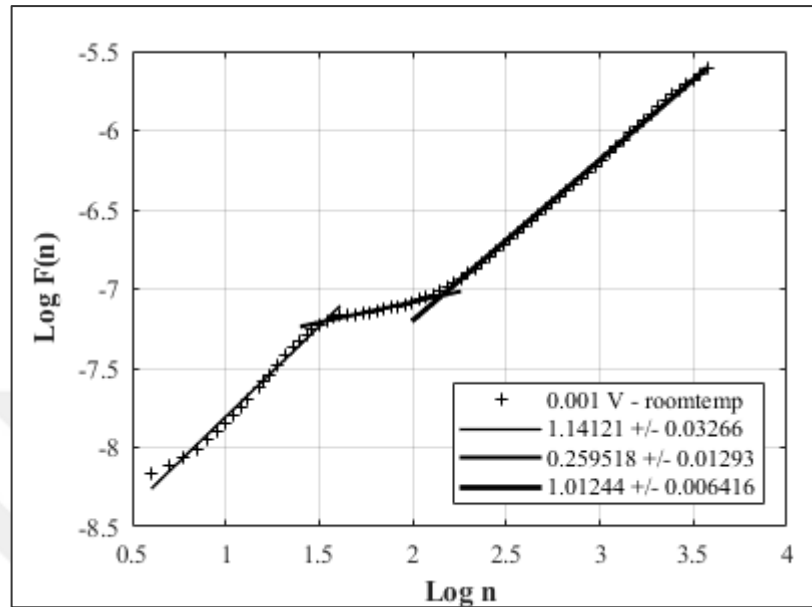
Figure E.1. Log [F(n)] vs. Log (n) with three different scaling exponents
for the measured current values under 0.001 V at room temperature.
The inset shows the scaling exponents for the current.
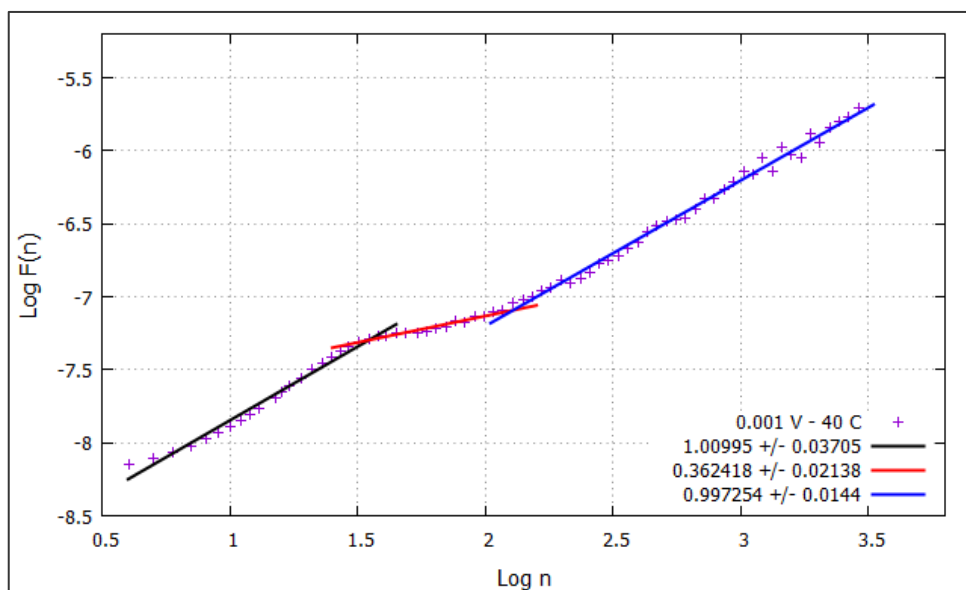
Figure E.2. Log [F(n)] vs. Log (n) with three different scaling exponents
for the measured current values under 0.001 V at 313 K (40 °C).
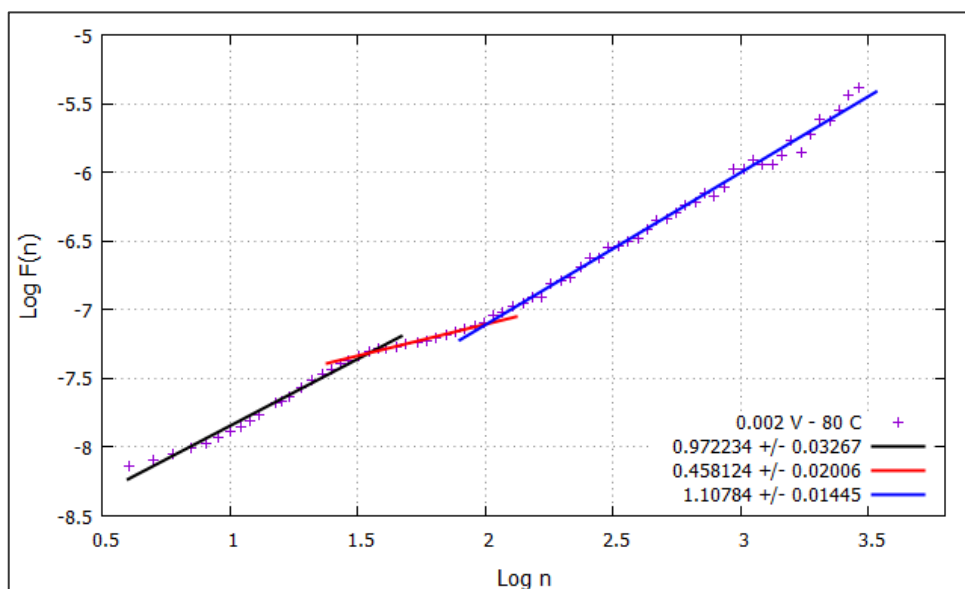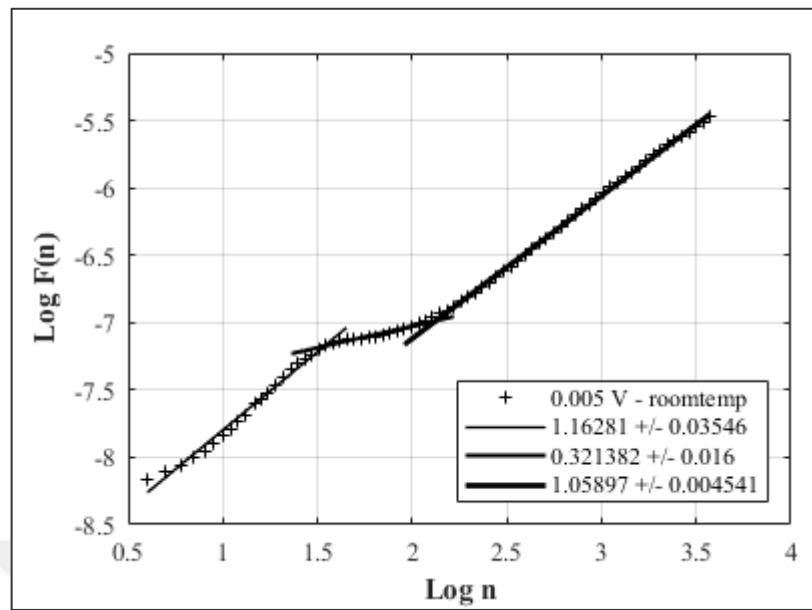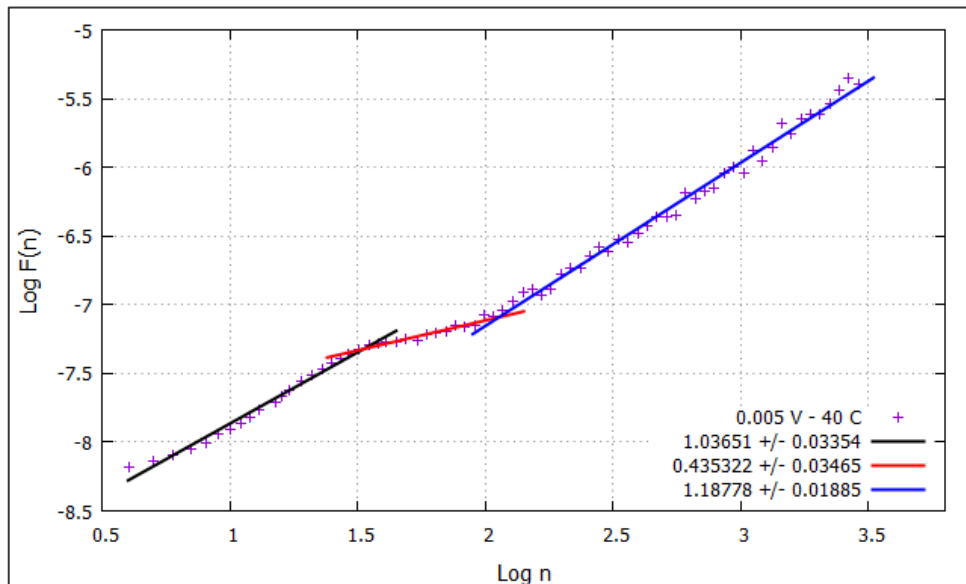The inset shows the scaling exponents for the current.
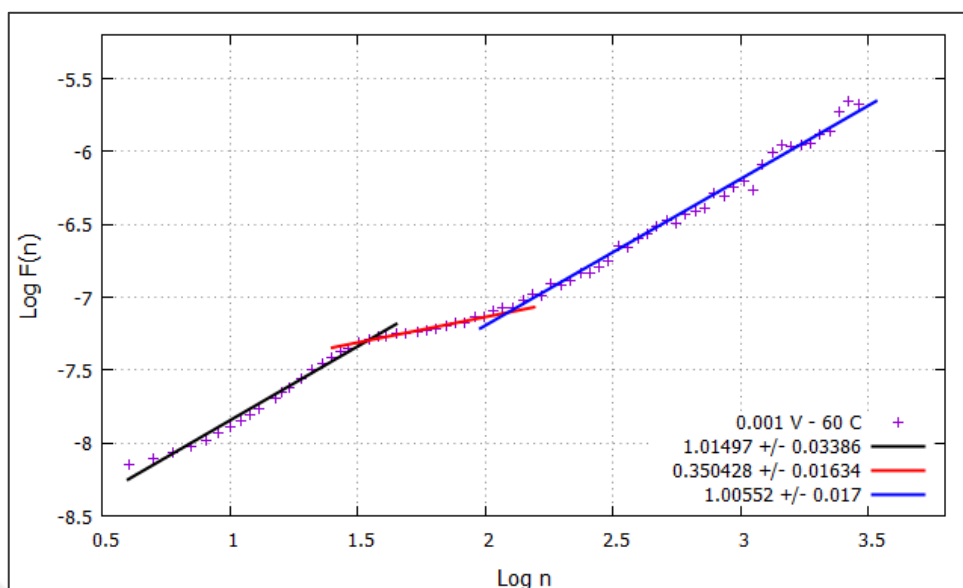
Figure E.3. Log [F(n)] vs. Log (n) with three different scaling exponents for the measured current values under 0.001 V at 333 K (60 °C). The inset shows the scaling exponents for the current.
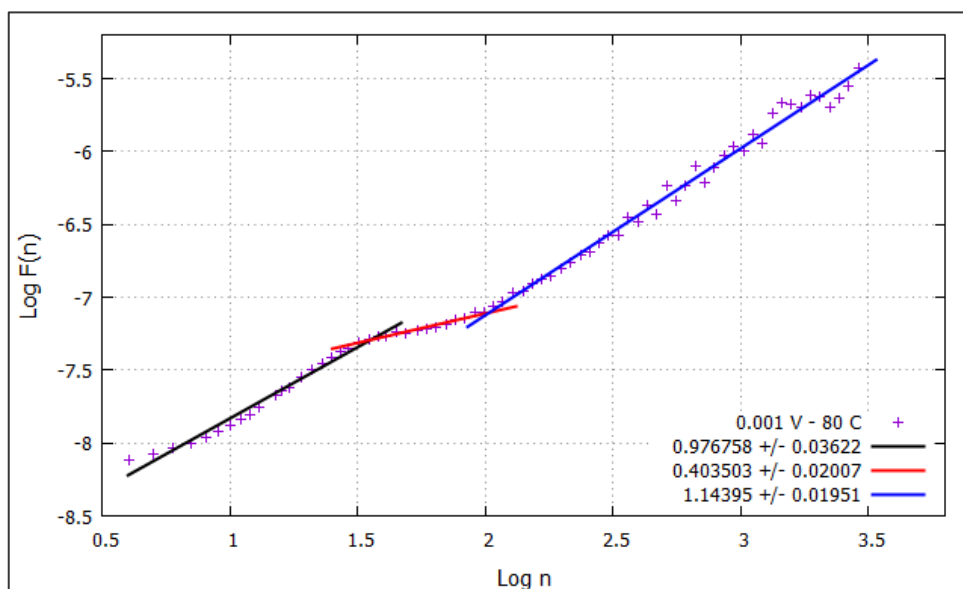
Figure E.4. Log [F(n)] vs. Log (n) with three different scaling exponents for the measured current values under 0.001 V at 353 K (80 °C). The inset shows the scaling exponents for the current.
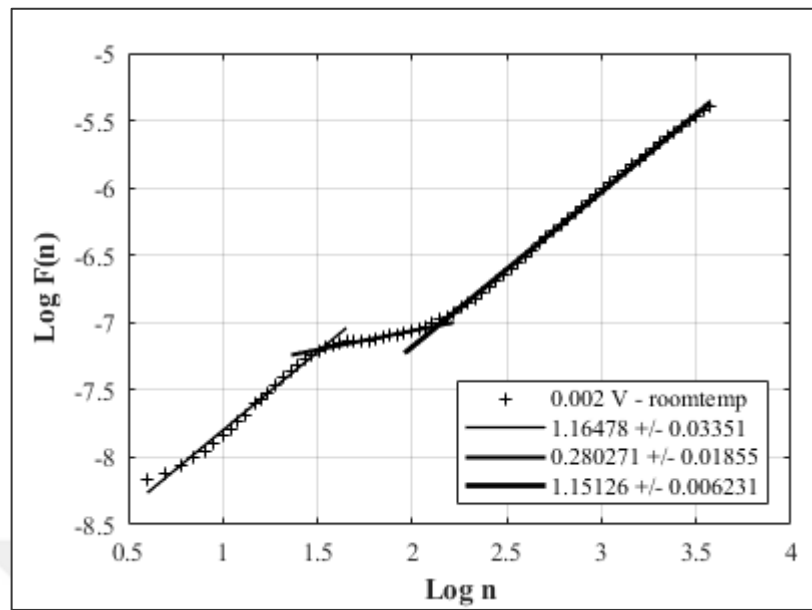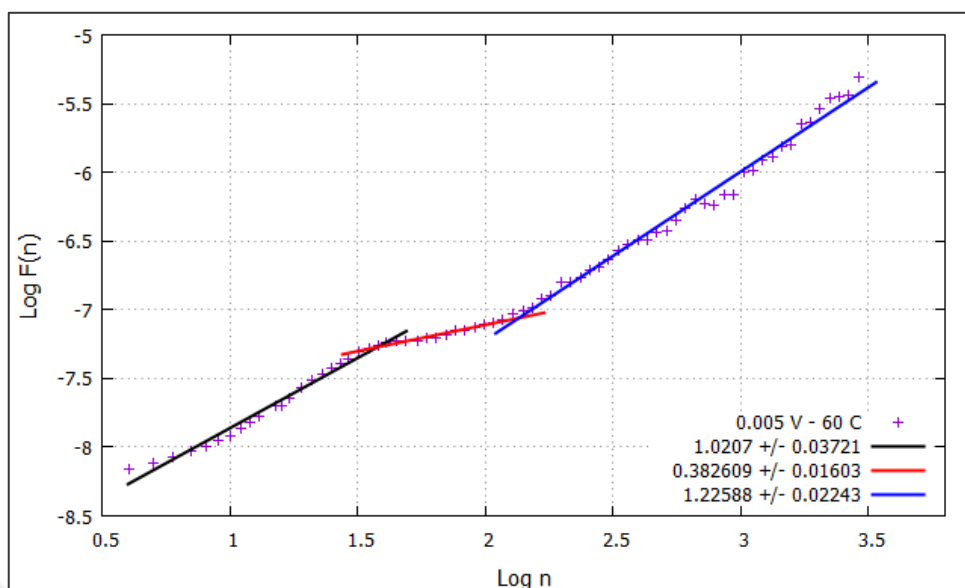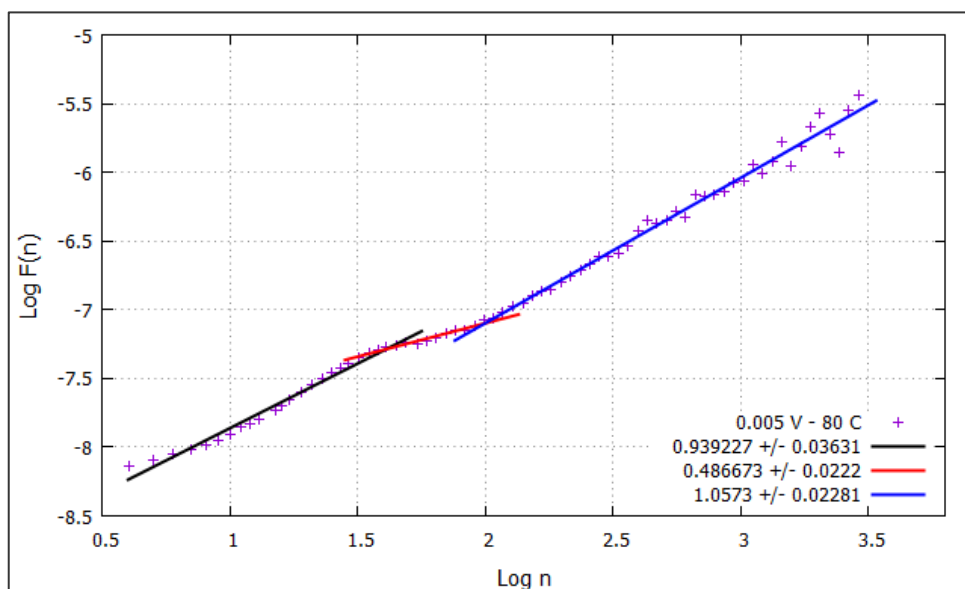
Figure E.5. Log [F(n)] vs. Log (n) with three different scaling exponents for the measured current values under 0.002 V at room temperature. The inset shows the scaling exponents for the current.
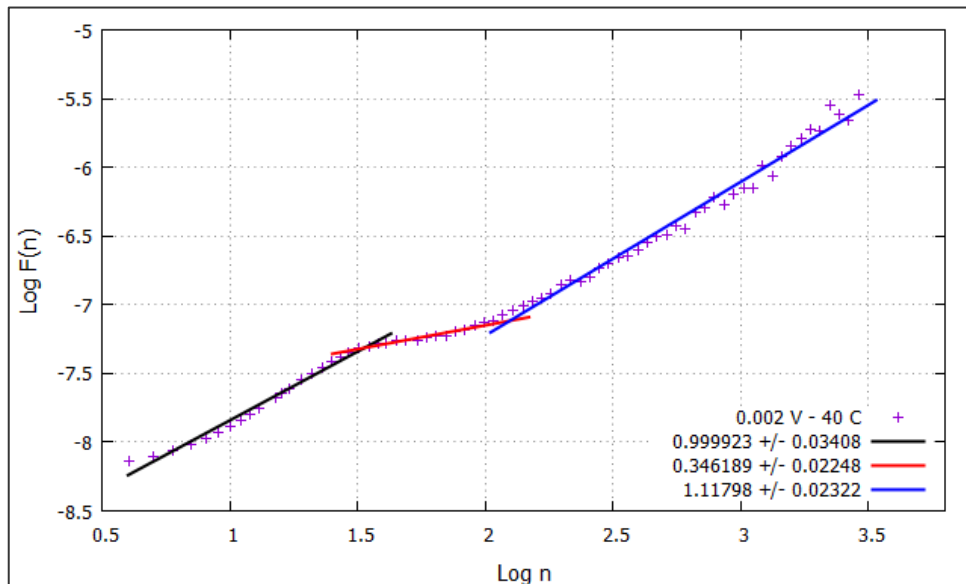
Figure E.6. Log [F(n)] vs. Log (n) with three different scaling exponents for the measured current values under 0.002 V at 313 K (40 °C). The inset shows the scaling exponents for the current.
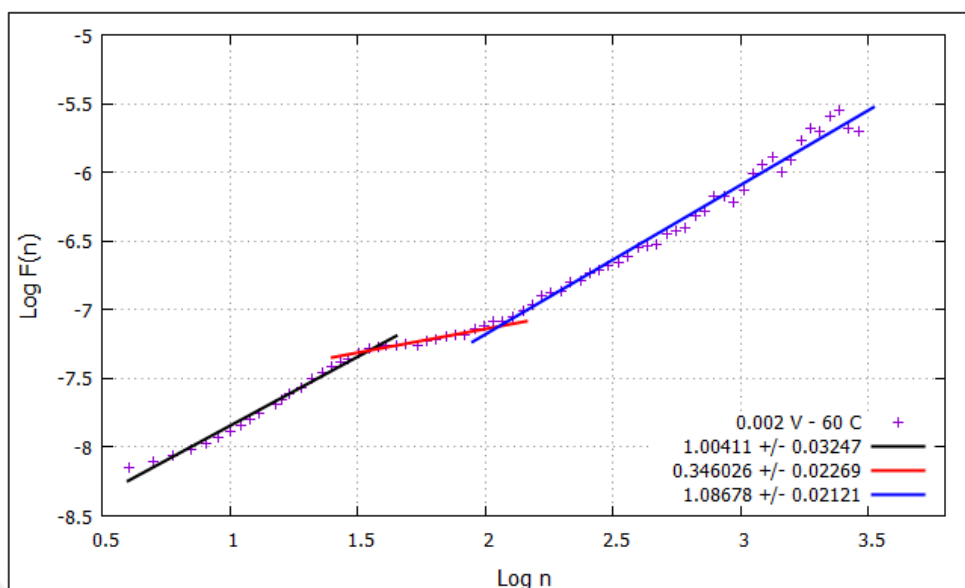
Figure E.7. Log [F(n)] vs. Log (n) with three different scaling exponents
for the measured current values under 0.002 V at 333 K (60 °C).
The inset shows the scaling exponents for the current.

Figure E.8. Log [F(n)] vs. Log (n) with three different scaling exponents
for the measured current values under 0.002 V at 353 K (80 °C).
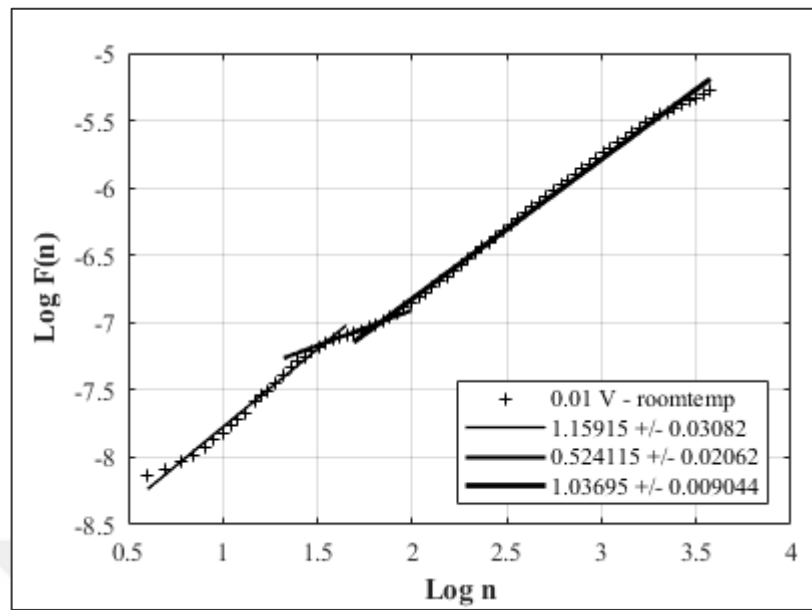The inset shows the scaling exponents for the current.

Figure E.9. Log [F(n)] vs. Log (n) with three different scaling exponents
for the measured current values under 0.005 V at room temperature.
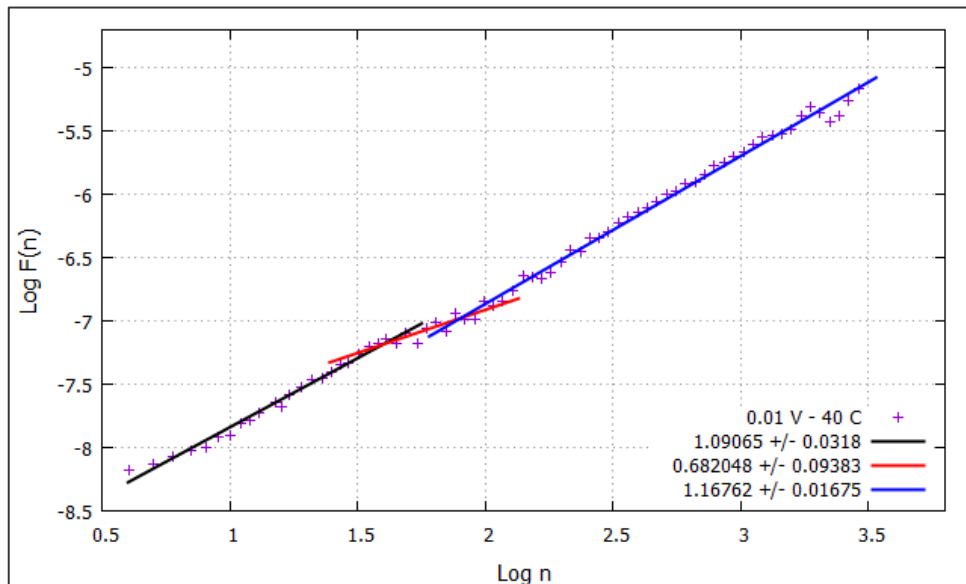The inset shows the scaling exponents for the current.

Figure E.10. Log [F(n)] vs. Log (n) with three different scaling exponents
for the measured current values under 0.005 V at 313 K (40 °C).
The inset shows the scaling exponents for the current.

Figure E.11. Log [F(n)] vs. Log (n) with three different scaling exponents for the measured current values under 0.005 V at 333 K (60 °C). The inset shows the scaling exponents for the current.
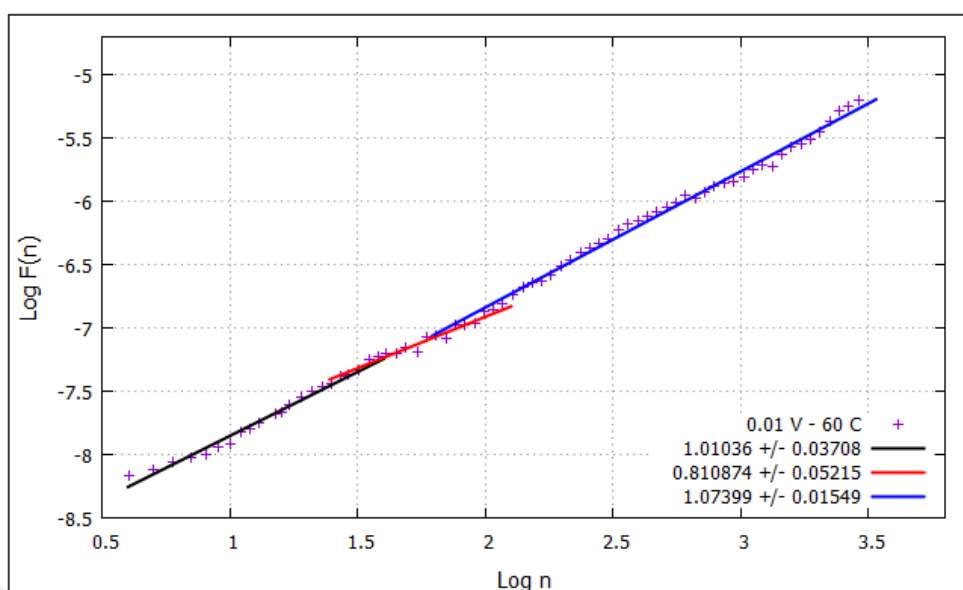

Figure E.12. Log [F(n)] vs. Log (n) with three different scaling exponents for the measured current values under 0.005 V at 353 K (80 °C). The inset shows the scaling exponents for the current.
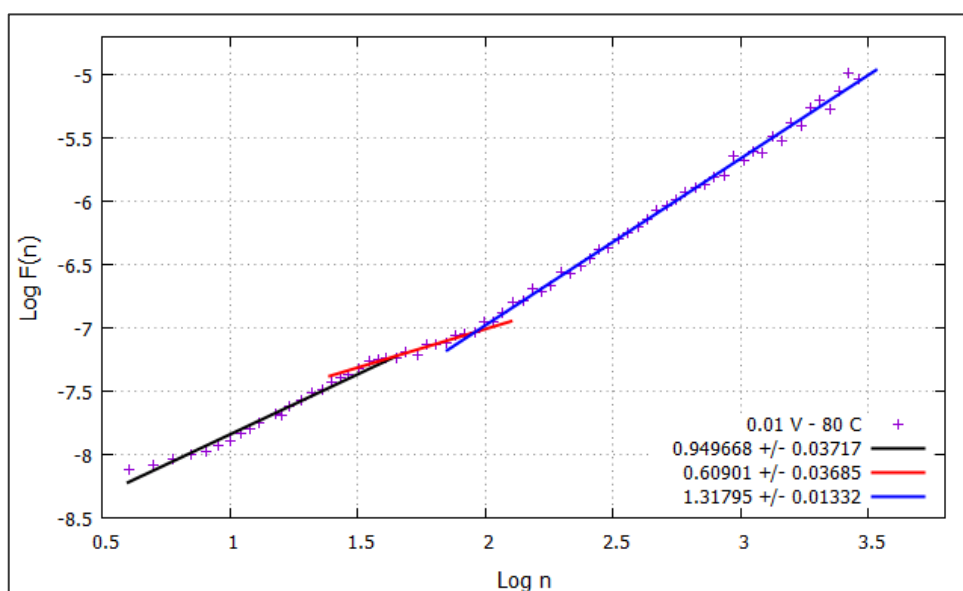
Figure E.13. Log [F(n)] vs. Log (n) with three different scaling exponents
for the measured current values under 0.01 V at room temperature.
The inset shows the scaling exponents for the current.

Figure E.14. Log [F(n)] vs. Log (n) with three different scaling exponents
for the measured current values under 0.01 V at 313 K (40 °C).
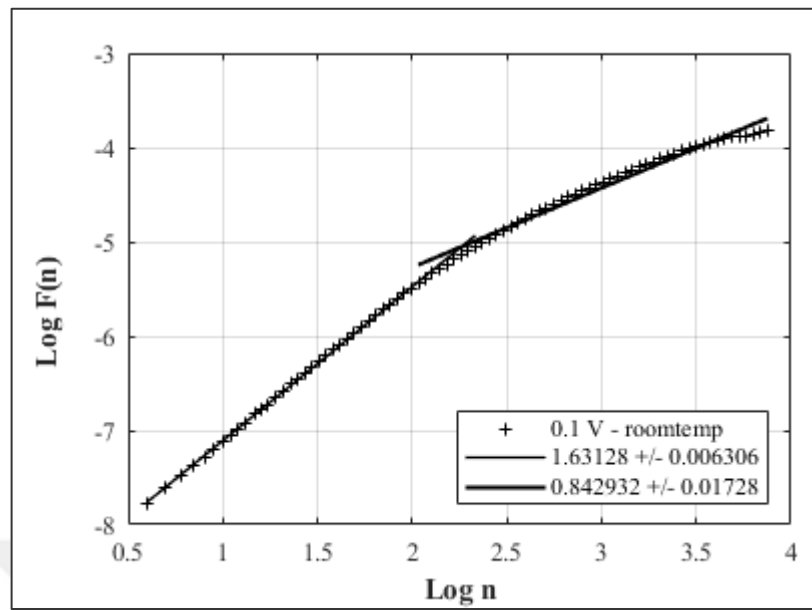The inset shows the scaling exponents for the current.

Figure E.15. Log [F(n)] vs. Log (n) with three different scaling exponents for the measured current values under 0.01 V at 333 K (60 °C). The inset shows the scaling exponents for the current.

Figure E.16. Log [F(n)] vs. Log (n) with three different scaling exponents for the measured current values under 0.01 V at 353 K (80 °C). The inset shows the scaling exponents for the current.

Figure E.17. Log [F(n)] vs. Log (n) with two different scaling exponents
for the measured current values under 0.1 V at room temperature.
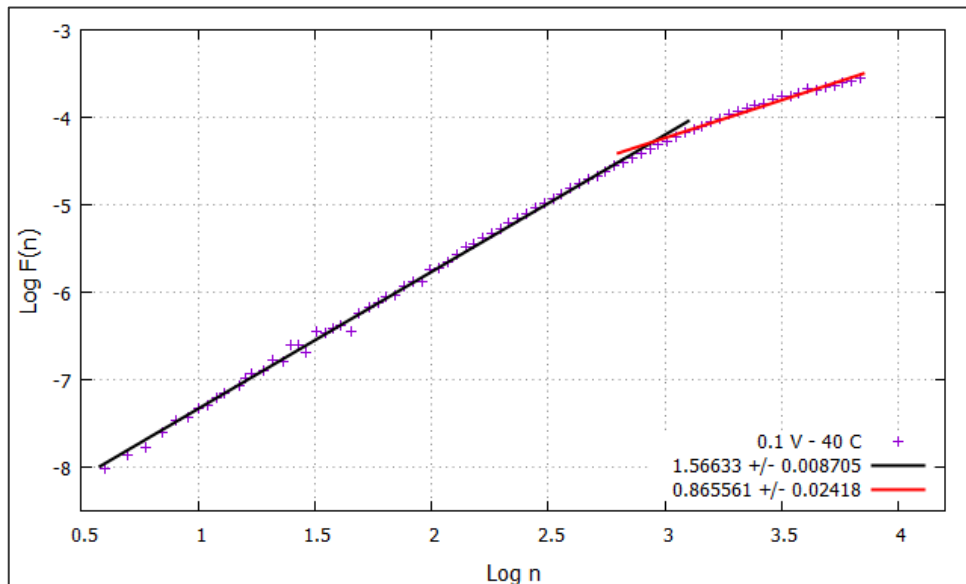The inset shows the scaling exponents for the current.

Figure E.18. Log [F(n)] vs. Log (n) with two different scaling exponents
for the measured current values under 0.1 V at 313 K (40 °C).
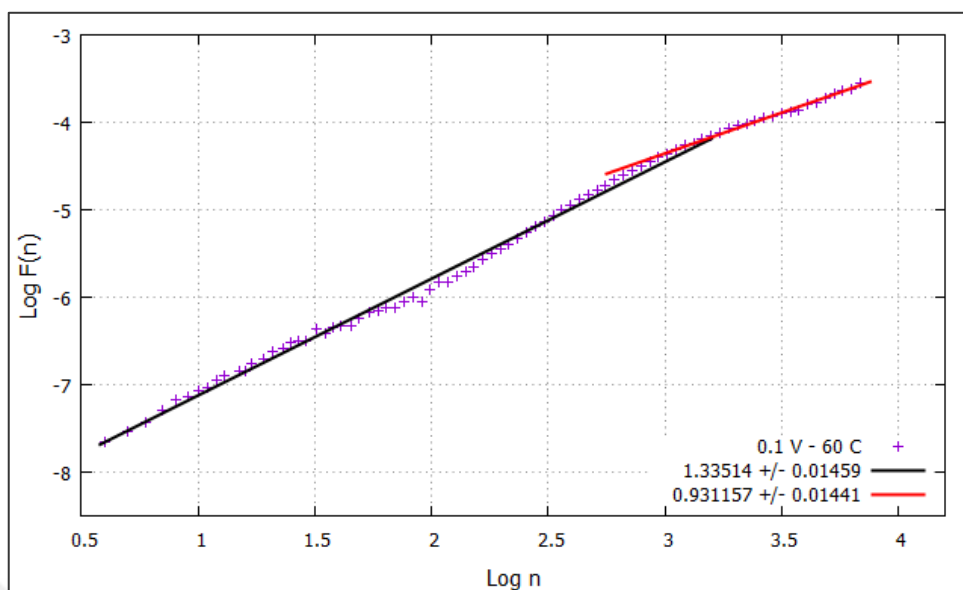The inset shows the scaling exponents for the current.

Figure E.19. Log [F(n)] vs. Log (n) with two different scaling exponents
for the measured current values under 0.1 V at 333 K (60 °C).
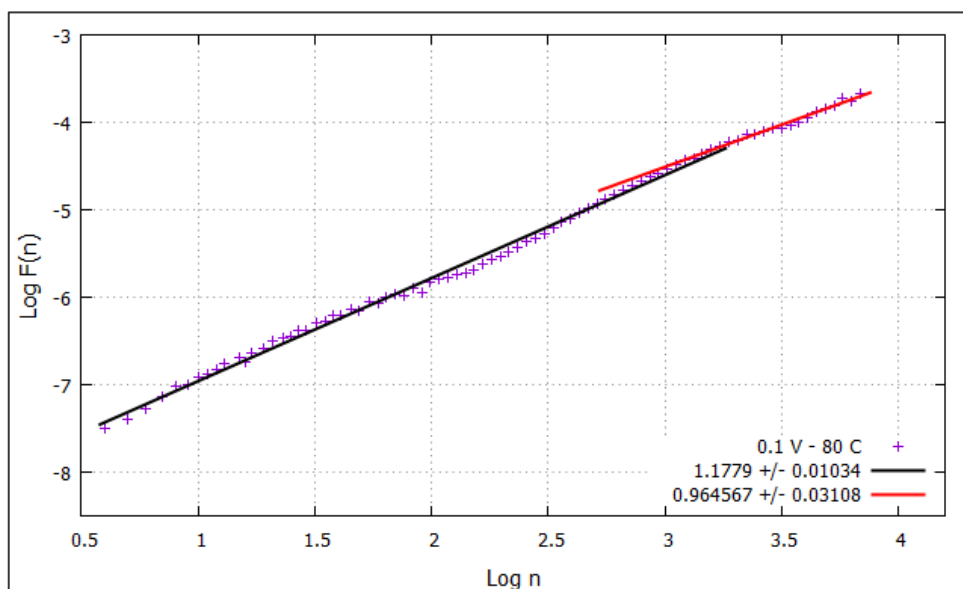The inset shows the scaling exponents for the current.

Figure E.20. Log [F(n)] vs. Log (n) with two different scaling exponents
for the measured current values under 0.1 V at 353 K (80 °C).
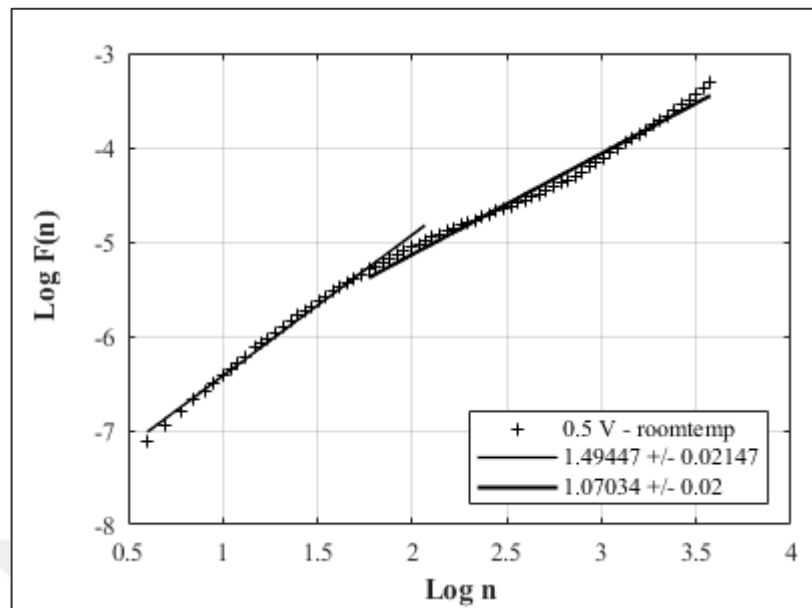The inset shows the scaling exponents for the current.

Figure E.21. Log [F(n)] vs. Log (n) with two different scaling exponents
for the measured current values under 0.5 V at room temperature.
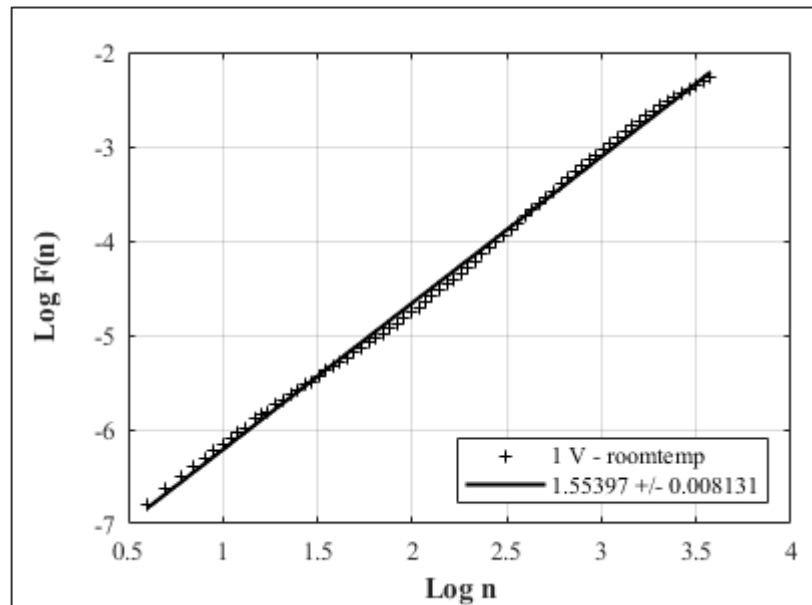The inset shows the scaling exponents for the current.

Figure E.22. Log [F(n)] vs. Log (n) with one different scaling exponent
for the measured current values under 1 V at room temperature.
The inset shows the scaling exponent for the current.

APPENDIX F: MACKEY-GLASS SIMULATION SOURCE CODE

This Matlab source code was modified based on an example which could be found in [104].

```
% data settings
N  = 1000; % number of samples
Nu = 300; % number of learning samples

% Mackay-Glass time series
b   = 0.1;
c   = 0.2;
tau = 17;

Data = importdata ('b.txt');
y = Data (:,2);

% generate Mackay-Glass time series
for n=18:N+299
        y (n+1) = y (n) - b*y (n) + c*y (n-tau)/(1+y (n-tau).^10);
end

% remove initial values
y (1:300) = [];


% plot training and validation data
plot (y,'m-')
grid on, hold on
plot (y (1:Nu),'b')
plot (y,'+k','markersize',2)
legend ('validation data','training data','sampling markers','location','southwest')
xlabel ('time (steps)')
ylabel ('y')
ylim ([-.00025 .00125])
set (gcf,'position',[1 60 800 400])


% prepare training data
yt = con2seq (y (1:Nu)');

% prepare validation data
yv = con2seq (y (Nu+1:end)');


%---------- network parameters -------------
% good parameters (you don't know 'tau' for unknown process)
```

```matlab
inputDelays = 1:6:19;  % input delay vector
hiddenSizes = [6 3];   % network structure (number of neurons)
%------------------------------------

% nonlinear autoregressive neural network
net = narnet (inputDelays, hiddenSizes);

% [Xs,Xi,Ai,Ts,EWs,shift] = preparets (net,Xnf,Tnf,Tf,EW)
%
% This function simplifies the normally complex and error prone task of
% reformatting input and target timeseries. It automatically shifts input
% and target time series as many steps as are needed to fill the initial
% input and layer delay states. If the network has open loop feedback,
% then it copies feedback targets into the inputs as needed to define the
% open loop inputs.
%
%  net : Neural network
%  Xnf : Non-feedback inputs
%  Tnf : Non-feedback targets
%  Tf : Feedback targets
%  EW : Error weights (default = {1})
%
%  Xs : Shifted inputs
%  Xi : Initial input delay states
%  Ai : Initial layer delay states
%  Ts : Shifted targets


[Xs,Xi,Ai,Ts] = preparets (net,{},{},yt);

% train net with prepared training data
net = train (net,Xs,Ts,Xi,Ai);

% view trained net
view (net)

% close feedback for recursive prediction
net = closeloop (net);

% view closeloop version of a net
view (net);

% prepare validation data for network simulation
yini = yt (end-max (inputDelays)+1:end);
% initial values from training data

% combine initial values and validation data 'yv'
[Xs,Xi,Ai] = preparets (net,{},{},[yini yv]);

% predict on validation data
```

```
predict = net (Xs,Xi,Ai);

% validation data
Yv = cell2mat (yv);
% prediction
Yp = cell2mat (predict);

% error
e = Yv - Yp;

% plot results of recursive simulation
figure (1)
plot (Nu+1:N,Yp,'r')
plot (Nu+1:N,e,'g')
legend ('validation data','training data','sampling markers',...
    'prediction','error','location','southwest')
```